Last update: 5 November 2020

A Fast and Scalable Heuristic for the Solution of Large-Scale Capacitated Vehicle Routing Problems

Luca Accorsi[1], Daniele Vigo[1, 2]

[1]*DEI "Guglielmo Marconi", University of Bologna*

[2]*CIRI ICT, University of Bologna*

Research Report OR-20-2

DEI "GUGLIELMO MARCONI", UNIVERSITY OF BOLOGNA

Last update: 5 November 2020

Version history

- 3 August 2020
  First time online
- 5 November 2020
  Fixed average gap columns of FILO and FILO (long) in Appendix B
  Improved notation in Section 2.3.2.1
  Fixed some typos

A Fast and Scalable Heuristic for the Solution of Large-Scale Capacitated Vehicle Routing Problems

Luca Accorsi[1], Daniele Vigo[1,2]
[1]Department of Electrical, Electronic and Information Engineering "G. Marconi", University of Bologna, Viale del Risorgimento 2, 40136 - Bologna, Italy,
[2]CIRI ICT, University of Bologna, via Quinto Bucci, 336, 47521 - Cesena, Italy
{luca.accorsi4, daniele.vigo}@unibo.it

In this paper, we propose a fast and scalable yet effective metaheuristic, called FILO, to solve large-scale instances of the Capacitated Vehicle Routing Problem. Our approach consists of a main iterative part, based on the Iterated Local Search paradigm that employs a carefully designed combination of existing acceleration techniques, as well as novel strategies to keep the optimization localized, controlled and tailored to the current instance and solution. A Simulated Annealing-based neighbor acceptance criterion is used to obtain a continuous diversification, aimed at exploring diversified regions of the search space. Results on extensively studied benchmark instances from the literature, supported by a thorough analysis of the algorithm's main components, show the effectiveness of the proposed design choices making FILO highly competitive with existing state-of-the-art algorithms, both in terms of computing time and solution quality. Finally, guidelines of possible efficient implementations, algorithm source code and a library of reusable components are open sourced to reproduce our results and promote further investigations.

Key words: Capacitated Vehicle Routing Problem, Metaheuristics, Acceleration Techniques, Large-Scale Instances

1. Introduction

The Capacitated Vehicle Routing Problem (CVRP) has been studied for several decades but still remains a challenging problem to solve in practice. In the last years, several new benchmark instances having large ($\mathbb{X}$ dataset, Uchoa et al. (2017)) and very large ($\mathbb{B}$ dataset, Arnold, Gendreau, and Sörensen (2019)) scale made this fundamental problem gaining again the focus in the vehicle routing scene. When dealing with large instances, the careful design and implementation of solution algorithms becomes of primary importance. Failing in finding the best tradeoff between effectiveness and efficiency has dramatic effects, much more noticeable than when dealing with smaller instances. While memory is becoming every year a less pressing problem, a satisfactory solution quality in reasonable computing time still remains the real challenge, as algorithm designers cannot rely anymore on an increment of the working frequency of future processors. Processing units have in fact almost hit their physical maximum speed and new chips are moving towards massive parallelization (see Etiemble (2018)), possibly opening the street to a new age of algorithms making use of concurrent decomposition techniques.

The CVRP can be described by using an undirected graph $G = (V, E)$ where V is the vertex set and E is the edge set. The vertex set V is partitioned into $V = \{0\} \cup V_c$ where 0 is the depot and $V_c = \{1, \ldots, N\}$ is a set of N customers. A cost c_{ij} is associated with each edge $(i, j) \in E$. Moreover, we assume that the cost matrix $\boldsymbol{c}$ satisfies the triangle inequality. For a vertex $i \in V$ and a subset of vertices $V' \in V$, we identify with $\mathcal{N}_i^k(V')$ the set of the k nearest neighbor vertices $j \in V'$ of i with respect to the cost matrix $\boldsymbol{c}$. The set $\mathcal{N}_i^k(V')$ is shortened to $\mathcal{N}_i(V')$ in case $k = |V'|$. Each customer $i \in V_c$ requires an integer quantity $q_i > 0$ from the depot, and $q_0 = 0$. An unlimited fleet of homogeneous vehicles with capacity Q is located at the depot available to serve the customers. Recalling that a Hamiltonian circuit is a closed cycle visiting a set of customers exactly once, a CVRP solution S is composed by a number $|S|$ of Hamiltonian circuits, called *routes*, starting from the depot, visiting a subset of customers and coming back to the depot. We identify with r_i the route of load q_{r_i} serving customer $i \in V_c$. A solution is feasible if all customers are visited exactly once and none of the vehicles exceed its capacity. The cost of a solution S is given by the sum of the edges defining the routes of S. Finally, the CVRP goal is to find the feasible solution with the minimum cost.

A rough analysis of the computing time, normalized to be comparable, of three among the current state-of-the-art CVRP algorithms having a termination criteria based on the number of iterations is shown in Figure 1. Algorithms using a time-based termination criteria are not included because they are not comparable. In fact, even if such an approach would be likely preferred in practice, it may not be the best in comparison settings due to the high variability even occurring within the same hardware configuration that may also harm the reproducibility of final solutions, see Johnson (1999). Moreover, as it is described in Chapter 4 of Toth and Vigo (2003), computing time is just one among other, seldom conflicting, dimensions characterizing heuristic solution approaches. The quality of solutions is often another among the most obvious criteria used to assess algorithms quality. In addition, scalability with respect to the instance size may be another very valuable quality especially when moving to very large-scale instances. Figure 1 includes an estimate of the computing time these algorithms would require to solve instances that are much larger than those for which they were proposed and from which the computing time has been estimated. The quadratic growth they exhibit undermines their applicability on large-scale instances and this turns out to be the main motivation of our research presented in this paper.

The challenge we faced in this research was to design an effective and scalable heuristic solution approach to the CVRP able to solve, in reasonable computing times, very large-scale instances without an explicit instance decomposition. To this end, we reviewed and adapted existing local search acceleration techniques and introduced new strategies to keep the optimization localized, controlled and tailored to the current instance and solution, all this resulted in a well-defined and cohesive solution method.

The study of local search acceleration techniques consists in fact of a very promising direction to design scalable algorithms that are efficient but still retain their effectiveness. Local search, for a local search-based solution method, is typically one among the most time-consuming components. Naive implementations, e.g., those built on full neighbors enumeration, fail to be competitive even on medium-sized instances. Among the most popular acceleration techniques, Granular Neighborhoods (GNs) proposed by Toth and Vigo (2003), define a heuristic filtering of less promising neighbors. This approach experimentally shown to provide an excellent compromise between computing time and solution quality, see, e.g., Toth and Vigo (2003), Zachariadis and Kiranoudis (2010), Schneider, Schwahn, and Vigo (2017), Accorsi and Vigo (2020). Sequential Search proposed by Irnich, Funke, and Grünert (2006), breaks a local search move into basic blocks called partial moves. The execution of those partial moves can be aborted if certain conditions are met thus pruning in advance a non-promising local search move. Finally, Static Move Descriptors (SMD) introduced by Zachariadis and Kiranoudis (2010) and later improved by Beek et al. (2018), provide a data-oriented approach to the local search execution that avoids unnecessary evaluations by exploiting the locality of a local search move application.

Existing successful CVRP algorithms for large-scale instances typically make use of such acceleration techniques and ad-hoc data structures to support their optimization process. In Kytöjoki et al. (2007) the authors devise a Variable Neighborhood Search (VNS, see Mladenović and Hansen (1997)) algorithm combined with the Guided Local Search metaheuristic (GLS, see Voudouris and Tsang (1999)) used to escape from local optima by accepting moves that worsen the solution value according to certain solution features. The proposed method is able to solve problems with up to twenty thousand customers in short computing times by using a number of implementation techniques to reduce memory utilization, e.g., by storing compact representations for the cost matrix, and speed-up the computation with appropriate data structures and smart pre-processing. Zachariadis and Kiranoudis (2010) propose a Tabu Search metaheuristic (TS, see Glover (1989)) based on the SMD concepts in which a penalization strategy is used to diversify the search process. The method is able to solve problems with up to three thousand customers by exploiting the acceleration

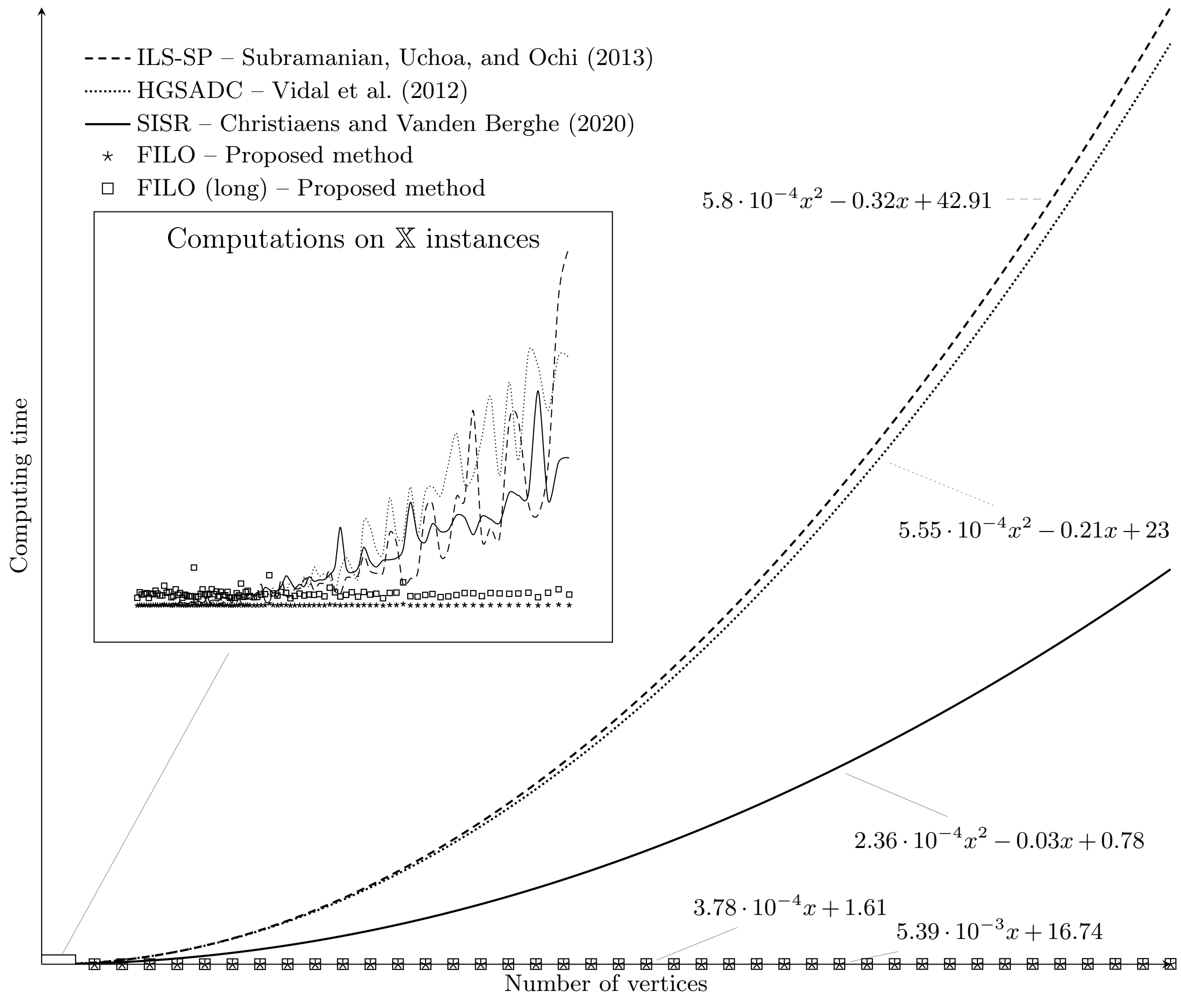

Figure 1 **Computing time growth trends for state-of-the-art CVRP algorithms. The zoomed area provides data on instances actually tested while the main chart compares an estimate of their computing time on much larger instances. The estimated computing time for ILS-SP, HGSADC and SISR is based on the $\mathbb{X}$ dataset for which those algorithm were proposed whereas the estimate for FILO is also based on the additional large-scale datasets considered in this research.**

role of the SMD and a neighborhood reduction policy similar to the GN concept. Finally, Arnold, Gendreau, and Sörensen (2019) propose an adaptation for very large instances, having up to thirty thousand customers, of the algorithm introduced in Arnold and Sörensen (2019) consisting of a local search-based approach using a GLS metaheuristic enhanced by knowledge extracted from previous data mining analyses. The authors reduce the computing time and space requirements by limiting the amount of information stored and using pruning and sequential search techniques.

The algorithm described in this paper, called FILO, consists of a main iterative part based on the Iterated Local Search paradigm, coupled with a Simulated Annealing-based neighbor acceptance criterion to obtain a continuous diversification aimed at exploring diversified regions of the search space. Our approach makes use of GNs and SMDs to speed-up the local search executions together with other newly introduced concepts to keep the optimization localized, controlled and tailored to the current instance and solution. In particular, the main design contributions, embedded into the proposed solution algorithm, are the following:

- We extend the move generator concept introduced in Schneider, Schwahn, and Vigo (2017) to support a dynamic and fine-grained management to specifically intensify the local search only

on areas that are more likely to require a more accurate optimization process, such as parts of the solution that were not improved after several attempts.
- We introduce a selective caching of vertices to identify solution's parts that are more likely to be relevant for forthcoming decisions, e.g., because they were changed more recently. This technique is used to selectively optimize restricted solution areas.
- We illustrate a semi-structured organization of local search operators to achieve the best compromise between diversification and intensification, likelihood of escaping from local optima, and execution time.
- We refine the integration between GNs and SMDs in the light of the above introduced concepts. We also provide guidelines on the implementations of local search operators that to the best of our knowledge were never encoded into the SMD framework, such as the general CROSS-exchange (see Taillard et al. (1997)) and the ejection-chain (see Glover (1996)) operators.
- We detail a strategy to iteratively adapt the strength of a compatible shaking procedure based on the quality and structure of instances and solutions.

Finally, as a result of a thorough analysis we are able to combine the above defined concepts obtaining a fast, scalable and effective CVRP solution algorithm.

The paper is structured as follows. Section 2 describes the details of our solution approach. Section 3 provides the experimental results and Section 4 offers an experimental analysis of the algorithm components. Finally, the Appendix contains support material covering implementation details.

2. Solution Approach

The metaheuristic we propose consists of a *construction* phase, which builds an initial feasible solution by using a restricted version of the savings algorithm (see Clarke and Wright (1964)), followed by an *improvement* phase aimed at further enhancing the initial solution quality. In particular, the improvement phase may first employ a *route minimization* procedure, to possibly reduce the number of routes in the initial solution when it is considered to be using more routes than necessary. Then, a *core optimization* procedure, which is the central part of the algorithm, uses an iterative and localized optimization scheme to further improve the solution quality. Both, route minimization and core optimization, follow the Iterated Local Search paradigm (ILS, see Lourenço, Martin, and Stützle (2003)) in which shakings, performed in a ruin-and-recreate fashion (see Schrimpf et al. (2000)), and local search applications interleave for a prefixed number of iterations. The resulting approach is a Fast ILS Localized Optimization algorithm, shortened to FILO. The following paragraphs provide a detailed description of the algorithm which is the outcome of an iterative design process based on the analyses described in Section 4. In particular, we first describe the construction phase, then the local search engine, which is a pervasive component of the improvement phase, and finally, the section ends with the definition of the improvement procedures.

2.1. Construction

The initial solution is built by using an adaptation of the well-known savings algorithm by Clarke and Wright (1964). As was already shown by other authors, see, e.g., Arnold, Gendreau, and Sörensen (2019), the savings computation, which is quadratic in nature, can be linearized by considering for each customer $i \in V_c$ a restricted number n_{cw} of neighbors $j \in \mathcal{N}_i^{n_{cw}}(V_c)$ for which computing the saving value. By limiting the number of savings one can, especially when working with very large-scale instances, speed-up the construction process without significantly harming the quality and compactness, i.e., number of routes, of initial solutions. Note in addition that, being the construction phase executed once per run, over-optimizing it does not provide any substantial contribution to the efficiency of the whole algorithm. As suggested in Arnold, Gendreau, and Sörensen (2019), we set $n_{cw} = 100$, and we compute the savings values for the arcs connecting each customer i to its n_{cw} neighbor customers j by using a lexicographic order for the customers, so as to avoid symmetries. More precisely, this set is given by the arcs $\{(i,j) : i \in V_c, j \in \mathcal{N}_i^{n_{cw}}(\{j \in V_c : i < j\})\}$. In fact, as reported in the analysis of Section 4.1 we did not found significant differences both in the quality and compactness of solutions generated by using larger n_{cw} values.

2.2. Local Search Engine

Improvement procedures are designed around a complex local search engine making use of a tight integration of GNs, SMDs and selective vertex caching whose details are described in Sections 2.2.2 to 2.2.4. The result is a very fast and extremely localized local search execution exploring neighborhoods induced by the following operators:

- an exchange of a contiguous sequence, called *path*, of n vertices with a path of m vertices belonging to the same or to a different route, see CROSS-exchange, Taillard et al. (1997). In the following it is referred to as nmEX. For example, 21EX identifies the case in which $n = 2$ and $m = 1$. In particular, we implement the neighborhoods associated with $n, m = 0, \ldots, 3$ such that $n \geq m$ and considering nmEX to be equivalent to mnEX.
- a variant for 20EX, 21EX, 22EX, 30EX, 31EX, 32EX and 33EX, called nmREX, in which the first path of n vertices is reversed before being exchanged;
- a variant for 22EX, 32EX and 33EX, called nmREX*, in which both paths are reversed before being exchanged;
- an intra-route 2-opt procedure, called TWOPT, as it is designed for the Traveling Salesman Problem, see Reinelt and Rinaldi (1994);
- two inter-route adaptations of the 2-opt procedure, called TAIL and SPLIT, both working on two different routes at a time. By denoting with head, a path of vertices belonging to the initial part of route, and with tail, a path of vertices belonging to the final part of a route, TAIL swaps the tail of the two involved routes at some point, whereas SPLIT cuts the two routes at some point, then it replaces the tail of the first route with the reversed head of the second route and the head of the second route with the reversed tail of the first route;
- finally, an ejection-chain procedure, called EJCH, implementing the first improving sequence of 10EX found by exploring a restricted number of sequences. In particular, starting from an initial 10EX, a tree of at most n_{EC} nodes representing partial sequences is built. The sequence with the most improving value is always explored first and a number of relocations (10EX) are generated by ejecting customers that restore the feasibility of the current route sequence endpoint. A 10EX may visit the same route more than once and no limit on the length of a sequence is imposed. As soon as a sequence is found to restore the feasibility of the target route, the associated 10EX are implemented. For more details, we refer the reader to Appendix A.3.8.

The above operators are structured into a Hierarchical Randomized Neighborhood Descent, see Section 2.2.1, whose aim is to define a balanced combination of intensification-diversification, likelihood of escaping from local optima, and execution efficiency.

The next paragraphs provide a detailed description of the local search engine individual components that are pervasively used in both improvement procedures. Finally, the section ends with the route minimization and core optimization characterization.

2.2.1. Hierarchical Randomized Variable Neighborhood Descent. We propose a local search architecture based on the combination of the Variable Neighborhood Descent (VND, see, e.g., Duarte et al. (2018)) and the Randomized VND (RVND, see, e.g., Subramanian, Uchoa, and Ochi (2013)) principles. Both, VND and RVND, consider a set of local search operators that are sequentially applied to a solution S generating a so called neighborhood of S containing a number of neighbor solutions, or simply neighbors, of S. The key difference between VND and RVND is on the criteria defining the order in which those operators are applied.

In the VND, operators a generally sorted in increasing neighborhood cardinality with larger neighborhoods possibly including smaller ones. A typical example is a sequence of k-opt operators, with $k = 2, 3, \ldots, \ell$. This order has both an efficiency purpose, because smaller neighborhoods are faster to explore, and a functional purpose, because larger neighborhoods are used to escape from the local optima of smaller ones. Whenever an improving neighbor is found, the search is restarted from the initial smallest neighborhood.

On the contrary, in the RVND, the sequence of operators is shuffled before each local search execution. This approach is used when neighborhoods induced by local search operators are not related one to the other or have the same cardinality. In this case, there are not well-defined guidelines providing hints about the order that will eventually lead to the best possible outcome. Relying on randomness is thus a reasonable approach that does not bias the search towards any operator, provides a natural diversification still improving the objective function, and relieves the designers from enforcing a possibly not ideal neighborhood exploration order. When an improvement is found, all the operators are re-considered after being possibly re-shuffled.

The Hierarchical RVND (HRVND) we propose mixes the two approaches by defining a slightly more structured neighborhood exploration strategy in which the operators order is neither completely random nor fixed a priori. More precisely, local search operators are arranged in *tiers* containing a subset of the available operators. Each tier is a compound operator that applies its subset of local search operators by following the RVND principles. The overall HRVND is defined by linking the tiers together once they have been ordered according to the same criteria defined by the VND, such as the overall computational complexity of the operators involved in the tier. The HRVND can thus be seen as a standard VND in which each tier is a compound local search operator and where subsequent more expensive tiers are used to escape from the local optima of the previous ones.

The proposed HRVND local search applies operators described in Section 2.2 organized in the following two tiers: (i) 10EX, 11EX, SPLIT, TAILS, TWOPT, 20EX, 21EX, 22EX, 20REX, 21REX, 22REX, 22REX*, 30EX, 31EX, 32EX, 33EX, 30REX, 31REX, 32REX, 33REX, 32REX* and 33REX*, and (ii) EJCH. The first tier contains operators defining neighborhoods of quadratic cardinality and with a very similar execution time, whereas the second tier contains the most expensive operator employed by the local search engine. More details about computing times and improving power are provided in the analysis of Section 4.2.

Each tier stores its operators in a circular list which is shuffled before the application (see Algorithm 1). The neighborhood associated with an operator is completely explored and all the improvements applied before moving to the next operator in the list. More details about the neighborhood exploration are given in Section 2.2.3 and in Section A.2 of the Appendix. The next tier is only applied when the solution is a local optima for the previous tiers. Moreover, as in the standard VND setting, after a complete tier execution, if the solution was improved, the search is restarted from the initial tier.

Algorithm 1 HRVND tier application

```
1: procedure TIERAPPLICATION($S, \mathcal{O}, \mathcal{R}$)
2:     $\mathcal{O} \leftarrow$ SHUFFLE($\mathcal{O}, \mathcal{R}$)
3:     $e \leftarrow 0, c \leftarrow 0$
4:     repeat
5:         $S' \leftarrow$ APPLY($\mathcal{O}_c, S$)
6:         if COST($S'$) $<$ COST($S$) then $S \leftarrow S', e \leftarrow c$
7:         $c \leftarrow (c+1)$ mod LENGTH($\mathcal{O}$)
8:     until $c \neq e$
9:     return $S$
10: end procedure
```

Notation: $\mathcal{O}$ list of tier operators, $\mathcal{O}_c$ operator in position c, $\mathcal{R}$ random engine.

2.2.2. Move Generators and Granular Neighborhoods. A *move generator* $(i, j) \in E$ is an arc that, as the name suggests, is used to generate and identify a *unique* move in a local search context. In particular, in Toth and Vigo (2003), a set T of move generators is used to define a restricted local search neighborhood, also known as *granular neighborhood*, containing a subset of the possible moves associated with a local search operator.

A way to select those arcs of interest is by using a so called *sparsification rule*. For example, in Toth and Vigo (2003) and Accorsi and Vigo (2020), arcs are chosen if their cost is below a given threshold, while in Schneider, Schwahn, and Vigo (2017), the reduced cost coming from a simple relaxation is used for the same purpose. Performing a local search by considering moves induced by move generators in T only, allows to linearize the search time to $O(|T|)$.

In our approach, to speed-up the local search execution, all neighborhoods induced by local search operators are implemented as GNs.

In particular, we define the set T of move generators to contain all arcs connecting a vertex $i \in V$ to its $n_{gs} = 25$ nearest vertices. More precisely, the set $T = \cup_{i \in V} \{(i,j),(j,i) \in E : j \in \mathcal{N}_i^{n_{gs}}(V \setminus \{i\})\}$. Note that move generators are described by arcs instead of edges. In fact, a GN is said to be asymmetric if the move induced by (i,j) is different from that induced by (j,i), and symmetric otherwise. All the local search operators we considered, with the exception of TWOPT and SPLIT, identify an asymmetric GN. The defined sparsification rule comes directly from the original GNs definition found in Toth and Vigo (2003), where the emphasis was on trying to replace long edges with short ones. However, contrarily to Toth and Vigo (2003) in which the sparsification is based on a cost rule selecting all edges having a cost lower than a given threshold, we adopt a nearest-neighbor rule that ensures a minimum number of move generators involving any vertex. A cost rule may in fact not be well suited when the standard deviation among arc costs is high, e.g., in clustered instances, and may cause several vertices not to have any move generator associated with when the threshold is very low.

As it is described in previous works such as Schneider, Schwahn, and Vigo (2017) and Accorsi and Vigo (2020), by using an additional value called *sparsification factor*, one could further filter the set of move generators according to some criteria, typically based on the arc cost, resulting in a dynamic GN based on a dynamic set of *active* move generators. In the following, a move generator is said to be active when selected by the current sparsification factor.

In our implementation, instead of using a single sparsification factor, we propose a more fine-grained management of dynamic move generators by means of a *vertex-wise* sparsification factor $\gamma_i \in [0,1]$ for each vertex $i \in V$. The dynamic set of active move generators for a *sparsification vector* $\boldsymbol{\gamma} = (\gamma_0, \gamma_1, \dots, \gamma_N)$ is identified by $T^{\boldsymbol{\gamma}} = \cup_{i \in V} \{(i,j),(j,i) \in E : j \in \mathcal{N}_i^{k_i}(V \setminus \{i\})\}$ and $k_i = \lfloor \gamma_i \cdot n_{gs} \rceil$, where $\lfloor x \rceil$ denotes the nearest integer to x. Being the local search indeed local, a precise control over move generators may allow to tailor the search towards specific areas in which it is more needed. For example, the number of move generators may be increased for a part of the solution in which no (local) improvement happened after several search attempts. Because GNs are used in both improvement procedures, the precise description of the sparsification vector $\boldsymbol{\gamma}$ management is detailed in their respective section.

Finally, several papers (see, e.g., Schneider, Schwahn, and Vigo (2017)), support the inclusion in the set of move generators of all the edges connecting the depot to customers. However, when scaling to large-scale instances, we experienced that, even a dynamic management of such move generators becomes very challenging causing a significant increase in the computing time without any guarantees on improvements to the solution quality. More details are given in Section 4.4.

2.2.3. Static Move Descriptors. Static move descriptors (SMDs), introduced for compound neighborhoods in Zachariadis and Kiranoudis (2010) and later adapted to the VND setting in Beek et al. (2018), enable the efficient execution of local search procedures by replacing the classical for-loop exploration of neighborhoods with a structured inspection of the moves associated with a local search operator through the careful design of specialized data structures and procedures.

SMDs can be used to thoroughly describe a neighborhood of a solution. Every SMD identifies a *unique* local search move generating a neighbor solution and the associated change in the objective function value, called δ-tag. The combination of GNs and SMDs arises very naturally. In fact, a move generator uniquely defines a move within a GN and thus unambiguously identifies an SMD. On the other hand, an SMD uniquely describes a move (and its effect on the objective function) and thus unambiguously identifies the move generator inducing that move. For this reason, in the rest of the paper we will use SMD and move generator interchangeably.

A local search operator whose neighborhood is designed according to the SMD principles requires the definition of four stages. First, an *initialization* stage, executed once at the beginning of the neighborhood exploration, computes the δ-tag for the available SMDs. Then, a sequence of *search*, *execution* and *update* stages is performed until no more improving solutions are available in the neighborhood. The search stage examines the SMDs looking for a *feasible and improving* SMD, that is an SMD associated with a move that generates a feasible and improving neighbor solution. Moreover, the search process might be required to meet some additional criteria, e.g., the SMD associated with the most improving feasible move might be sought. Once found, the move associated with the feasible and improving SMD is executed during the execution stage. Because a local search application causes only a local change in a solution, most of the SMDs will still hold a correct δ-tag even after (part of) the solution is changed. An operator-specific list of SMDs requiring an update to their δ-tag can thus be considered during the update stage. Finally, the neighborhood exploration ends when the search stage is no longer able to identify a feasible and improving SMD.

In our implementation, all (granular) neighborhoods are designed according to the SMD principles and a binary heap is used to store the SMDs, corresponding to active move generators, organized according to their δ-tag. During the initialization stage, only improving SMDs are inserted into the heap to keep the computational complexity of its management to the minimum. As in Beek et al. (2018), during the search stage instead of retrieving the most improving SMD by removing infeasible SMDs until a feasible one is found, we linearly scan the vector representing the heap data structure searching for a feasible SMD. This approach does not require the re-insertion of removed SMDs once a feasible move is found but it no longer guarantees the execution of the most improving move. However, being the SMDs roughly sorted by the heap internal procedures, linear scan provides a so called *rough-best-improvement* move acceptance strategy. Note that the heap data structure is not unique for a set of entries and linear scan is highly affected by the order in which heap management operations are executed. For more details we refer the reader to Sections A.2 and A.3 of the Appendix.

Finally, to speed-up the initialization stage we coupled it with the selective vertex caching strategy described in Section 2.2.4 that forces the local search to focus on recently changed areas of the solution.

2.2.4. Selective Vertex Caching. Sparsification rules describing GNs are complemented by the identification of a set of vertices of interest by means of a *selective vertex caching* strategy. In particular, every solution S keeps track of a subset of vertices $\bar{V}_S \subseteq V$ that, at the current algorithm state, is considered to be highly relevant.

In our implementation, $\bar{V}_S$ consists of the set of vertices directly belonging to solution areas that recently underwent some changes. Without loss of generality, changes in a solution S, seen from a vertex perspective, can be subdivided into insertions and removals. For example consider the relocation of vertex i from its original position to another one between vertex j and its predecessor π_j. The removal *directly* affects vertex i itself, its successor σ_i and its predecessor π_i, while the subsequent insertion affects vertices i, j and π_j. Within this settings, after the move execution, we say that i, π_i, σ_i, j and π_j are *cached* for S, i.e. they are inserted into $\bar{V}_S$. This strategy allows to easily keep track of solution areas that were recently changed. However, not all changes have the same importance but most recent ones are more likely to be relevant for a forthcoming decision. This aspect is captured by limiting, for a solution S, the maximum number of vertices that can be cached at the same time to a constant value C by imposing $|\bar{V}_S| \leq C$ and adopting a *least recently used* strategy to maintain $\bar{V}_S$.

2.2.4.1. *Selective Vertex Caching to Restrict Local Search Execution.* The selective caching of vertices can be employed to identify a kernel of relevant vertices to be used in local search procedures. In particular, as mentioned at the end of Section 2.2.3, we used it as an heuristic acceleration and filtering technique for the initialization stage of the SMDs that, as shown in the analysis of Section 4.5, may also have a significant influence on subsequent SMD stages and ultimately on the overall local search execution.

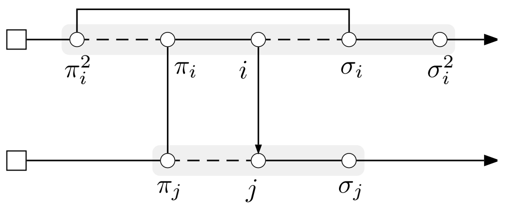

Figure 2 **A 20ex application induced by move generator (i, j) relocating path $(\pi_i - i)$ between π_j and j. SMDs involving vertices in the gray area require an update to their δ-tag after the move execution.**

During the optimization of a solution S, the SMD initialization stage considers, for the heap insertion, the restricted subset of move generators $(i, j) \in \bar{T}^\gamma(S) \subseteq T^\gamma$, such that, at least one of the endpoints i or j belongs to the subset of cached vertices $\bar{V}_S$. More precisely, $\bar{T}^\gamma(S) = \cup_{i \in \bar{V}_S}\{(i, j), (j, i) \in E : j \in \mathcal{N}_i^{k_i}(V \setminus \{i\})\}$ with $k_i = \lfloor \gamma_i \cdot n_{gs} \rceil$. During subsequent SMD update stages, additional move generators might, however, be added to the heap due to the search incrementally extending to vertices not belonging to the selective cache and whose SMDs require an update but that have not been directly involved in a change of the solution. To better understand this, consider the scenario shown in Figure 2 in which during a 20EX neighborhood exploration a move induced by move generator (i, j) is executed, causing the relocation of path $(\pi_i - i)$ between π_j and j. Once the move is executed, vertices $\pi_i^2, \pi_i, i, \sigma_i, \pi_j$ and j will be marked as cached. However, as shown by the gray overlay, two additional vertices, namely σ_i^2 and σ_j are also (indirectly) affected by the move execution. In particular, active move generators involving σ_i^2, i.e. $\{(\sigma_i^2, j) : j \in V\} \cap T^{\bar{\gamma}}$, require to be updated because the predecessor of σ_i changes from i to π_i^2. A similar reasoning applies to some move generators involving σ_j. More details about update lists associated with different local search operators are given in Section A.3 of the Appendix. Note that σ_i^2 and σ_j do not belong to the cache but their move generators will be updated and, if improving, inserted into the heap and considered during subsequent SMD search stages.

Move generators evaluated during the SMD search stage can hence have been considered because involving vertices belonging to the selective vertex cache or because involving vertices indirectly affected by a previous move application. This highlights that the cache dimension C actually imposes a soft constraint on the SMDs considered during the local search execution that, starting from the restricted kernel of cached vertices, may potentially extend to include move generators involving all instance vertices.

A possible scenario happening in any of the improvement procedures, analyzed from the perspective of the number of distinct of vertices either cached or (directly and indirectly) reached by the local search execution is depicted in Figure 3. Improvement procedures, at the beginning of each iteration, work with solutions S having no cached vertices, i.e. $\bar{V}_S = \emptyset$. As mentioned in Section 2.2, both procedures make use of a shaking performed in a ruin (R^-) and recreate (R^+) fashion. The vertices involved in the disruptive effects of the shaking applied to solution S are added to the set $\bar{V}_S$. This is the kernel of vertices used to identify the area on which focusing the optimization of the subsequent local search execution. In particular, each SMD initialization stage (I) considers the current kernel of cached vertices. Then, a sequence of SMD search (S) and execution and update (X) stages might cause the search to reach far more vertices than those cached (dashed line) potentially covering all vertices. However, as it is discussed in Section 4.5, the maximum size C of this kernel indirectly affects the exploration power as well as the computing time of the local search. The overall result is an implicit dynamic instance decomposition induced by a very focused and localized neighborhood exploration strategy mainly considering those areas of the solution that are more likely to require some further optimization because more recently changed.

2.3. Improvement

Improvement procedures are iterative randomized local search-based procedures aimed at further enhancing the initial solution quality. Both, route minimization and core optimization, work by

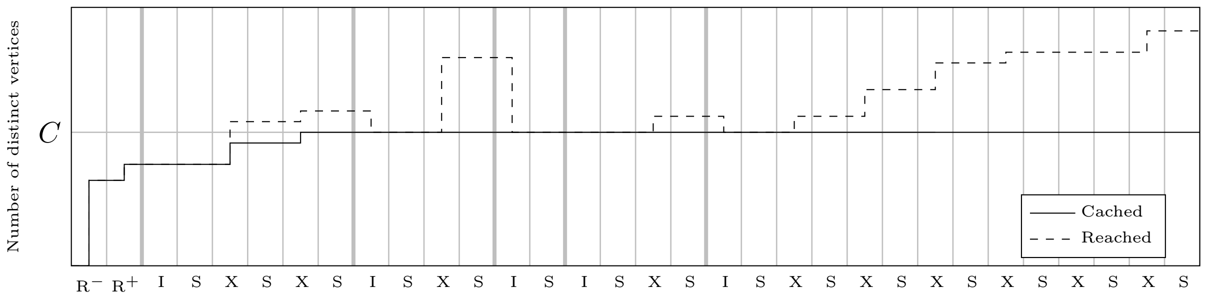

Figure 3 **Evolution of an improvement procedure iteration in terms of number of distinct vertices simultaneously cached and considered during a neighborhood exploration (Reached). The number of vertices is analyzed after the ruin (R^-) and recreate (R^+) application, and local search application. Each local search operator application is partitioned into an SMD initialization (I) and a sequence of search (S) and execute and update (X) stages.**

re-optimizing, through the local search engine, a restricted area disrupted by a ruin-and-recreate application. This area is identified by a number of vertices stored in the selective vertex cache. At the beginning of each improvement procedure iteration the cache is thus emptied to perform an optimization only focused on the very limited solution area identified by the upcoming shaking application. The route minimization procedure may visit infeasible solutions to perform its routes compacting action while the core optimization procedure only moves in the feasible space and achieves its diversification by means of an effective simulated annealing strategy.

2.3.1. Route Minimization. The CVRP typically does not impose any limit on the number of routes that solutions may have. However, there is often a positive correlation between the number of routes in a solution and its cost. Moreover, many simple construction algorithms, as the one we use, usually produce solutions using far more routes than those found in good quality solutions. We thus include an optional route minimization procedure that may be executed right after the initial solution construction.

This procedure is applied to a solution S built by the initial construction phase whenever the number $|S|$ of its routes is found to be greater than an ideal estimated number of routes k. The value k is computed by heuristically solving a bin-packing problem with items of weight q_i for each customer $i \in V_c$ and bins of capacity Q through a simple greedy first-fit algorithm (see, e.g., Chapter 8 of Martello and Toth (1990)).

The route minimization procedure, whose pseudocode is shown in Algorithm 2, starts by setting the best found solution S^* to be equal to the initial solution S generated by the construction phase. During each iteration a pair (r_i, r_j) of routes belonging to S is selected and their customers removed from the solution and placed into a list of unrouted customers L. In particular, the first route r_i is chosen as the route containing a random customer seed i. The second route r_j is identified by considering customer neighbors $j \in \mathcal{N}_i$ in increasing c_{ij} cost until a customer j belonging to a route $r_j \neq r_i$ is found. Customers in L are, with equal probability, either randomly shuffled or sorted according to their demand, in decreasing order. Then, for each unrouted customer $i \in L$ a position in the current set of existing routes is searched, such that the insertion of i keeps the target route feasible and the insertion cost is minimized. When such a position cannot be found, i.e., when inserting i violates the capacity constraints of all existing routes, and consequently a new route should be created to accommodate customer i, an action is selected according to the current number of routes $|S|$. If $|S|$ is lower than the estimate k, a new single-customer route with i is created. Otherwise, the single-customer route serving i is created only when a random number drawn from a uniform real distribution in the interval $[0, 1]$ results greater than a threshold $\mathcal{P}$ that at the beginning of the route minimization procedure was set to $\mathcal{P} = 1$. When this is not the case, i is inserted into an additional list $\bar{L}$. Once all customers in L have been considered, the list L is

Algorithm 2 Route minimization procedure

```
1: procedure RouteMin($S, \mathcal{R}$)
2:     $S^* \leftarrow S, \mathcal{P} \leftarrow \mathcal{P}_0, L \leftarrow [\,]$
3:     for $n \leftarrow 1$ to $\Delta_{RM}$ do
4:         $\bar{V}_S \leftarrow \emptyset$
5:         $(r_i, r_j) \leftarrow$ PickPairOfRoutes($S, \mathcal{R}$)
6:         $L \leftarrow [L,$ CustomersOf($r_i$), CustomersOf($r_j$)$]$
7:         $S \leftarrow S \setminus r_i \setminus r_j$
8:         $L \leftarrow$ DefineOrder($L, \mathcal{R}$)
9:         $\bar{L} = [\,]$
10:        for $i \in L$ do
11:            $p \leftarrow$ BestInsertionPositionInExistingRoutes($S$)
12:            if $p \neq none$ then
13:                $S \leftarrow$ Insert($i, p, S$)
14:            else
15:                if $|S| < k \vee U(0,1) > \mathcal{P}$ then
16:                    $S \leftarrow$ BuildSingleCustomerRoute($i, S$)
17:                else
18:                    $\bar{L} \leftarrow [\bar{L}, i]$
19:                end if
20:            end if
21:        end for
22:        $L \leftarrow \bar{L}$
23:        $S \leftarrow$ hrvnd.tier1($S, \mathcal{R}$)
24:        if $|L| = 0 \wedge (\text{Cost}(S) < \text{Cost}(S^*) \vee (\text{Cost}(S) = \text{Cost}(S^*) \wedge |S| < |S^*|))$ then
25:            $S^* \leftarrow S$
26:            if $|S^*| \leq k$ then return $S^*$
27:        end if
28:        $\mathcal{P} \leftarrow z \cdot \mathcal{P}$
29:        if $\text{Cost}(S) > \text{Cost}(S^*)$ then $S \leftarrow S^*$
30:    end for
31:    return $S^*$
32: end procedure
```

set to $L = \bar{L}$ and the threshold $\mathcal{P}$ is lowered according to an exponential schedule $\mathcal{P} = z \cdot \mathcal{P}$ with $z = (\mathcal{P}_f/\mathcal{P}_0)^{(1/\Delta_{RM})}$ and $\mathcal{P}_f = 0.01$ and $\mathcal{P}_0 = 1$, the final and initial probability of not creating an additional single-customer route respectively.

Afterward, a restricted HRVND consisting of the first tier only but using all the available move generators, i.e., $\gamma_i = 1, i \in V$, is applied to the possibly partial current solution. We restrict the HRVND to the first tier because we noticed it was already sufficient to obtain good quality solutions with a considerable computing time saving. Moreover, we set $\gamma_i = 1, i \in V$ to avoid a complex management of move generators in this secondary improvement phase that as shown in the parameters Table 1 is executed for a small number $\Delta_{RM} = 1000$ of iterations.

When a solution S in which all customers are routed is found, the best solution S^* is replaced with S if the latter has a better cost or it has the same cost but a lower number of routes. Moreover, we impose an early stopping condition such that if S^* has a number of routes lower or equal than k, the route minimization procedure prematurely ends returning S^*.

Before proceeding to the next iteration, a partial or feasible solution S having a cost greater than the current best found solution S^* is reset to the latter, i.e., $S = S^*$.

Finally, solution S^* is returned after Δ_{RM} iterations in case the early stopping condition is not verified throughout the route minimization execution.

2.3.2. Core Optimization. The core optimization, whose pseudocode is shown in Algorithm 3, is an iterative randomized optimization procedure that, by making use of an adaptive shaking strategy and the local search engine, implements a powerful localized solution improvement.

First, the best solution S^* is set to be equal to solution S generated by the construction phase and possibly improved by the route minimization procedure. A shaking application performs a ruin step, in which by means of a random walk in the customer sub-graph, a number of customers are removed. Then, a simple greedy recreate step defines the new position for the previously removed customers. More precisely, the ruin step, starting from a randomly selected seed customer $i \in V_c$, identifies a random walk of length ω_i in the sub-graph $G' = (V'_c, E'_c)$ where $V'_c = V_c$ and $E'_c = \{(i,j) : i,j \in V'_c\}$ is the set of arcs connecting customers. When a customer i is visited, it is removed from the solution and the sub-graph G' is updated accordingly by setting $V'_c = V'_c \setminus \{i\}$ and $E'_c = E'_c \setminus \{(i,j),(j,i) : j \in V'_c\}$. A partial walk ending at customer i is extended by either moving within the same route r_i, forward or backward, or by jumping to a neighbor route, which can be any or a not yet visited one. First, whether to move in the same route or jump to another route is selected, then the possible options associated with the first choice are considered. At every step, the choices are considered with equal probability. When a jump to a neighbor route is selected to extend a walk ending at $i \in V'_c$, customers $j \in \mathcal{N}_i(V'_c)$ are considered in increasing c_{ij} cost until a route r_j satisfying the appropriate requirements, i.e. a not yet visited route or any, is found. In the unlikely case that such a route cannot be found, the ruin procedure is prematurely aborted. Note that a jump to a neighbor route is always selected when the current route r_i contains i only.

The recreate step greedily inserts the removed customers in the position minimizing the insertion cost after they have, with equal probability, either been randomly shuffled or sorted by decreasing demand, or by increasing or decreasing distance from the depot.

The ruin intensity is controlled by the meta procedure described in Paragraph 2.3.2.1 that iteratively adapts the random walk length ω_i from a seed customer $i \in V_c$ to identify a disruptive action that best suits the instance and solution under examination.

The HRVND is then applied to the shaken solution S to identify a local optimum S'. Whether to accept S' as the next point in the search trajectory is determined by a simulated annealing acceptance strategy, see Kirkpatrick, Gelatt, and Vecchi (1983). In particular, S' is accepted if $c(S') < c(S) + \mathcal{T} \cdot \ln U(0,1)$. The value of $\mathcal{T}$ is initially set to $\mathcal{T} = \mathcal{T}_0$ and lowered at the end of each core optimization iteration by performing $\mathcal{T} = c \cdot \mathcal{T}$ with $c = (\mathcal{T}_f / \mathcal{T}_0)^{(1/\Delta_{CO})}$ and Δ_{CO} is the number of core optimization iterations.

The core optimization makes full use of vertex-wise dynamic move generators. In particular, at the beginning of the procedure sparsification parameters γ_i are set to a base value γ_{base}. Whenever $(\delta \cdot \Delta_{CO} \cdot \text{AVERAGE}(|\bar{V}_S|))/|V|$ nonimproving iterations involving a vertex i are performed, the value is updated as $\gamma_i = \min\{\gamma_i \cdot \lambda, 1\}$ where $\delta \in [0,1]$ is a reduction factor, $\text{AVERAGE}(|\bar{V}_S|)$ denotes the average number of vertices cached after previous local search executions, and λ is an increment factor. However, the value of γ_i is reset to γ_{base}, whenever a solution S improving S^* is found during the execution of a local search involving i, i.e., $i \in \bar{V}_S$ after the HRVND application. This update rule is a possible vertex-wise implementation of the standard way of handling dynamic move generators described in Schneider, Schwahn, and Vigo (2017) in which the total number of core optimization iterations is partitioned over restricted working areas identified by cached vertices. Note that, when the cache size C is smaller than the total number of instance vertices, i.e. $C < |V|$, some vertex i may not be considered for the γ_i update even if involved in a change during the HRVND execution because, due to the limit imposed by C, it is no longer cached after the optimization. However, as shown in the analysis of Section 4.5, an accurate selection of C, that may heuristically filter out some vertices from the update, does not prevent the finding of good solutions in a much more limited computing time compared the scenario in which $C = |V|$ and the selective vertex caching is completely disabled.

2.3.2.1. *Structure Aware and Quality Oriented Shaking Meta Strategy.* We propose a declarative approach to the selection of the shaking intensity that, if coupled with a shaking procedure able to take advantage of it, allows for an improved flexibility and adaptability compared to a random or a fixed intensity. This strategy makes use of a number of integer *shaking parameters* $\omega_i, i \in V_c$ defining the intensity of a shaking application seeded at customer i.

The idea is to iteratively adapt the parameters ω_i so that solution S', obtained by re-optimizing the disrupted area of solution S, meets some quality criteria with respect to S. On the one hand,

Algorithm 3 Core optimization procedure

```
 1: procedure CoreOptimization($S, \mathcal{R}$)
 2:     $\bar{\omega} \leftarrow (\omega_0, \omega_1, \dots, \omega_{|V_c|}), \omega_i \leftarrow \omega_{base}\ \forall i \in V$
 3:     $\bar{\gamma} \leftarrow (\gamma_0, \gamma_1, \dots, \gamma_{|V_c|}), \gamma_i \leftarrow \gamma_{base}\ \forall i \in V$
 4:     $S^* \leftarrow S, \mathcal{T} \leftarrow \mathcal{T}_0$
 5:     for $n \leftarrow 1$ to $\Delta_{CO}$ do
 6:         $\bar{V}_S \leftarrow \emptyset$
 7:         $\hat{S}, i' \leftarrow$ Shake($S, \mathcal{R}, \bar{\omega}$), $\mathcal{S} \leftarrow \bar{V}_{\hat{S}} \setminus \{0\}$
 8:         $S' \leftarrow$ hrvnd($\hat{S}, \mathcal{R}$), $\mathcal{L} \leftarrow \bar{V}_{S'}$
 9:         if cost($S'$) $<$ cost($S^*$) then
10:             $S^* \leftarrow S'$
11:             ResetSparsificationFactors($\bar{\gamma}, \mathcal{L}$)
12:         else
13:             UpdateSparsificationFactors($\bar{\gamma}, \mathcal{L}$)
14:         end if
15:         UpdateShakingParameters($\bar{\omega}, S', S, i', \mathcal{S}, \mathcal{R}$)
16:         if AcceptNeighbor($S, S', \mathcal{T}$) then $S \leftarrow S'$
17:         $\mathcal{T} \leftarrow c \cdot \mathcal{T}$
18:     end for
19:     return $S^*$
20: end procedure
```

S' could be of lower quality compared to S or, more precisely, the distance in terms of cost between S' and S is greater than a *intensification upper bound* threshold Ω_{UB}, i.e. $\text{Cost}(S') - \text{Cost}(S) > \Omega_{UB}$. From a simplified perspective, we may assume this happened because the initial disruption produced by the ruin was too strong and caused too much turbulence on the original solution S that subsequent local search procedures were not able to successfully correct and improve. On the other hand, S' and S may be of comparable quality and in particular, $0 \leq \text{Cost}(S') - \text{Cost}(S) < \Omega_{LB}$ with Ω_{LB} an *intensification lower bound* threshold. In this case, the disruptive effect of the ruin was probably not strong enough to jump to a different search space area and the subsequent local search procedures were able to partially undo the changes. Finally, S' may be better than S showing that the combination of shaking and subsequent re-optimization was appropriate. In our implementation, we define $\Omega_{LB} = \bar{c}_S \cdot I_{LB}$ and $\Omega_{UB} = \bar{c}_S \cdot I_{UB}$, where $\bar{c}_S$ is the average cost of an arc in solution S computed as $\bar{c}_S = \text{Cost}(S)/(N + 2 \cdot |S|)$ and $I_{LB}, I_{UB} \in \mathbb{R}$ are shaking factors.

From the above observations, we can derive a simple update rule for the shaking parameters ω_i that is executed at every core optimization iteration. Denoting by $\tilde{w} = w_{i'}$ the shaking parameter value associated with the current customer seed i'

$$\omega_i = \begin{cases} \omega_i + 1, \text{ if } 0 \leq \text{Cost}(S') - \text{Cost}(S) < \Omega_{LB} \wedge \omega_i < \tilde{\omega} + 1 & (i) \\ \omega_i - 1, \text{ if } \text{Cost}(S') - \text{Cost}(S) > \Omega_{UB} \wedge \omega_i > \tilde{\omega} - 1 & (ii) \\ \text{randomly select between } (i) \text{ and } (ii), \text{ otherwise} & (iii) \end{cases} \qquad i \in \mathcal{S}$$

where $\mathcal{S} = \bar{V}_{\hat{S}} \setminus \{0\}$ is the set of vertices cached in the shaken solution $\hat{S}$ right after the shaking execution excluding the depot, which is never considered in the ruin execution, see line 7 of Algorithm 3. Shaking parameters $\omega_i, i \in \mathcal{S}$ are moved towards the new value for $\tilde{\omega}$ but without exceeding it. This prevents situations in which a single vertex j surrounded by a number of vertices $\tilde{V}$ all having a very small (respectively, large) shaking parameter value has its w_j indirectly incremented (respectively, decremented) to very large (respectively, small) values due to updates involving some $i \in \tilde{V}$. Furthermore, update rule (iii) describes the scenario in which S' is improving with respect to S. We found experimentally beneficial to perform limited random variations of the involved shaking parameter values to avoid they stagnate to minimum values satisfying rules (i) and (ii) and explore possibly promising combinations of values. Finally, The update depends on the specific area where the shaking was executed and the parameters are iteratively adjusted according to the

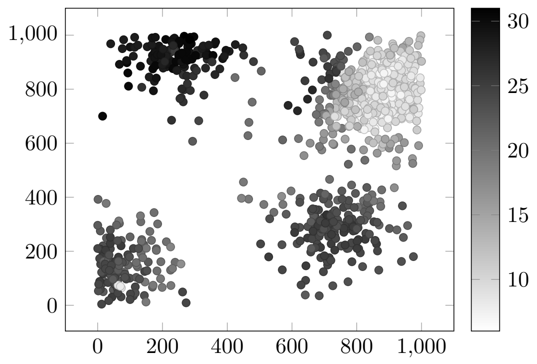

Figure 4 **Shaking parameters values at the end of the core optimization procedure for instance X-n979-k58 of the $\mathbb{X}$ dataset. Each circle represent a customer i in its x_i and y_i coordinates and the color denotes the shaking parameter ω_i value.**

effects previous shaking applications caused on nearby areas. This adaptive procedure thus makes the shaking both aware of the structure of the instance and of the solution under examination.

As an example, consider Figure 4 showing shaking parameter values $\omega_i, i \in V$ for instance X-n979-k58 of the $\mathbb{X}$ benchmark after the core optimization procedure. As can be seen from the figure, very dense areas of customers typically require lower values for the shaking parameters, whereas customers in sparse areas are associated with stronger shaking applications.

Note that set $\mathcal{S}$ also contains vertices involved in the recreate step. An ideal update rule should consider only customers involved in the ruin step or even better the only seed customer i, however, especially for large-scale instances, this would require an enormous amount of iterations for the procedure to converge to reasonably effective shaking parameter values that would still likely require an update as the algorithm evolves. We thus found that updating the shaking parameters for all vertices that are in the selective cache after the shaking application is a reasonable strategy to identify a number of vertices that are somehow related and can be thought as belonging to the same area.

Finally, the initial value for the shaking parameters is not relevant for small-sized instances in which an initial value of $\omega_{base} = 1$ may be used. On the contrary, it becomes quite relevant when moving to very large instances if the total number of core optimization iterations remains constant. In fact, on the one hand, using a small value might cause several unfruitful shaking iterations in which ω_i values are slowly increased to more effective values wasting precious computing resources with insufficient disruptions. On the other hand, a value that is too high might dramatically slow-down the overall algorithm execution with the risk of an excessively powerful ruin activity. We experimentally found a reasonable compromise by setting $\omega_{base} = \lceil \ln |V| \rceil$ as initial shaking intensity that is then automatically adjusted by the above update rules.

3. Computational Results

The computational testing has the main objective of assessing the performance of the proposed algorithm. To accomplish this, we first show its effectiveness on the $\mathbb{X}$ dataset proposed by Uchoa et al. (2017) on which state-of-the-art CVRP algorithms are typically evaluated. Then, we proceed to the real target of the paper, that is showing how the designed components allow the overall algorithm to easily scale to very large-scale instances still retaining its effectiveness. To this end, we focus on the increasingly popular $\mathbb{B}$ instances recently proposed by Arnold, Gendreau, and Sörensen (2019) and on two less studied large-scale datasets, namely $\mathbb{K}$ and $\mathbb{Z}$ proposed by Kytöjoki et al. (2007) and Zachariadis and Kiranoudis (2010), respectively.

3.1. Implementation and Experimental Environment

The algorithm was implemented in C++ and compiled using g++ 8.3.0. The experiments were performed on a 64-bit desktop computer with an Intel Xeon CPU E3-1245 v5 central processing

Table 1 Parameters.

Initial solution definition – Described in Sections 2.1 and 2.3.1 – Analyzed in Section 4.1	
$n_{cw} = 50$	Number of neighbors considered in the savings computation.
$\Delta_{RM} = 10^3$	Maximum number of route minimization iterations.
Granular neighborhood – Described in Section 2.2.2 – Analyzed in Section 4.4	
$n_{gs} = 25$	Number of neighbors considered by the sparsification rule.
$\gamma_{base} = 0.25$	Base sparsification factor.
$\delta = 0.5$	Reduction factor used in the definition of the fraction of non-improving iterations performed before increasing a sparsification parameter.
$\lambda = 2$	Sparsification increment factor.
Core optimization – Described in Sections 2.2, 2.2.4, 2.3.2, and 2.3.2.1 – Analyzed in Sections 4.2, 4.5 and 4.3	
$\Delta_{CO} = 10^5, 10^6$	Number of core optimization iterations for a short and a long run.
$\mathcal{T}_0$, $\mathcal{T}_f$	Initial and final simulated annealing temperature.
$C = 50$	Maximum number of recently accessed vertices.
$\omega_{base} = \lceil \ln \lvert V \rvert \rceil$	Initial shaking intensity.
$n_{EC} = 25$	Maximum number of sequences explored by EJCH for each move generator.
$I_{LB} = 0.375, I_{UB} = 0.85$	Shaking factors.

unit (CPU), running at 3.5 GHz and with 16 GB of RAM on a GNU/Linux Ubuntu 18.04 operating system. The algorithm source code together with a library of reusable components can be downloaded from `https://acco93.github.io/filo/` and detailed instructions are given to accurately reproduce our results. In all the computational testing we considered a standard version of FILO and a long version, called FILO (long), having ten times the number of core optimization iterations compared to the standard version. Because of the randomized nature of the algorithm, for every experiment, we performed a symbolic number of fifty runs for each instance defining the seed of the pseudorandom engine (the Mersenne twister of Matsumoto and Nishimura (1998)) equal to the run counter minus one. Moreover, to mitigate the impact of small time variations due to overhead of the operating system, we used a clock function that reports running times with a precision set to one second as the minimum recordable time.

To better compare our results with other algorithms, for which no source code was available, that were executed on different hardware configurations, we used the single-thread rating defined by PassMark® Software (2020), that, at the time of writing, assigns a score of 2285 to our CPU. Competing methods CPU times are scaled to match our CPU score and their normalized time is identified by $\hat{t} = t \cdot (P_A/P_B)$, where P_A is the competing method CPU single-thread rating, P_B is our CPU rating and t is the raw computing time. All times refer to an average run and are reported in minutes. For randomized algorithms we report, when available, the best (Best), the average (Avg) and the worst (Worst) gap of the solution found by the algorithm with respect to the best known solution value (BKS). Gaps are computed as $100 \cdot (\textsc{cost}(S) - BKS)/BKS$ where S is the final solution. For deterministic algorithms we report the gap (Gap) of the solution found by a single run.

3.2. Parameters Tuning

The crafting of the FILO as well as the tuning of its parameters followed an iterative process whose key decisions are detailed in Section 4. Parameters are summarized in Table 1 and their tuning, whose hidden interactions and interconnected effects might be very complex to analyze, followed a straightforward sequential strategy aimed at keeping the tuning effort low but still able to identify good performing values for each parameter when considered individually. First, reasonable values were identified by using the authors sensibility, experience, and a trial-and-error approach. Then, we evaluated the algorithm behavior while changing the value of one parameter at a time and keeping the others fixed. A new value was kept when it allowed an improvement in quality while decreasing or keeping similar the computing time. This process was iterated several times until satisfactory results were obtained. In fact, we noticed that the iterated sequential tuning of individual parameters, without a prefixed order, was enough to reach good local optima without exploring all possible combination of values. The parameters tuning, as well as the algorithm design, was mainly performed by considering the largest $\mathbb{X}$ instances and in particular those with more than five hundred vertices. However, the resulting tuned algorithm was then used for all our computational testing.

We briefly summarize in the following the key choices performed during the parameters tuning procedure referring to Section 4 for more details.

The number of customers n_{cw} for which computing the savings in the construction phase and the maximum number of route minimization iterations Δ_{RM} are low impact parameters. Once set to a reasonable value, small variations do not significantly change the outcome of the procedures in which they are employed. In particular, we set them approximately to one of the smallest values able to provide results of a quality comparable to greater values that may however have required an higher computing time.

Conversely, the value of n_{gs}, γ_{base}, δ and λ heavily affect the algorithm performance. The number of neighbors n_{gs}, the base sparsification factor γ_{base} and the reduction factor δ were set so as to identify the best trade-off between computing time and solution quality, see Section 4.4. In particular, we noticed that a milder sparsification, obtained, e.g., by increasing n_{gs}, γ_{base} or both; or by decreasing δ, may sometimes provide slightly better solutions but with an unacceptable increment in the computing time. This is particularly noticeable in instances for which very good quality (or near-optimal) solutions are early found in the search and for which the sparsification is just steadily decreased by increasing the $\gamma_i, i \in V$ and never reset, see, e.g., the computing time for instance X-n219-k73 of the $\mathbb{X}$ dataset in Table 9 (Section B of the Appendix) and the outliers associated with FILO in Figure 1. We set the the value for λ as in the original proposal of Toth and Vigo (2003) leaving the other granular parameters depending on it. In average, we found a very aggressive sparsification associated with an large number of optimization iterations to be preferable compared to a very accurate local search execution performed in fewer iterations.

The number of core optimization iterations Δ_{CO} was set to properly suit all the medium to very-large instances we considered. However, to alleviate the above-mentioned indiscriminate increment for γ_i values in small-sized instances, that typically converge to the final value faster, a number of iterations defined as a function of the instance size might be more appropriate. Nonetheless, we preferred not to use that approach to better highlight the scalability properties of FILO.

The simulated annealing initial and final temperatures $\mathcal{T}_0$ and $\mathcal{T}_f$ were defined to be proportional to the average cost of an arc in an instance. In particular, the value of $\mathcal{T}_0$ is defined as 0.1 times the average instance arc cost, i.e. $\mathcal{T}_0 = 0.1 \cdot \sum_{i,j \in V : i<j} c_{ij} / (|V| \cdot (|V|-1)/2)$ and $\mathcal{T}_f$ is 0.01 times $\mathcal{T}_0$. In fact, we found this strategy better than defining a fixed range, when applied to different datasets with completely unrelated arc costs. For example, the average arc cost for the $\mathbb{K}$ dataset is about 3500% larger than that of the $\mathbb{X}$ dataset and 164100% larger than that of the $\mathbb{Z}$ dataset.

The size of the selective cache C was chosen as the value that identified a good trade-off between computing time and solution quality, see Section 4.5.

As mentioned in Section 2.2.4, small to large instances are not significantly affected by the choice of the initial shaking intensity ω_{base}, in fact, comparable quality and computing time is obtained by setting $\omega_{base} = 1$. However, when scaling to very large-scale instances, the difference in the final outcome is much more noticeable. We found that setting ω_{base} as a logarithmic function of the number of vertices provides a reasonable starting point for the shaking procedure to actually perform some fruitful iterations in such large instances before reaching better performing values for the shaking parameters $\omega_i, i \in V_c$.

We set the number n_{EC} of EJCH sequences explored from every move generator to the minimum value able to provide reasonably good improvements in a much more limited computing time variability compared to larger values, see Section 4.2.

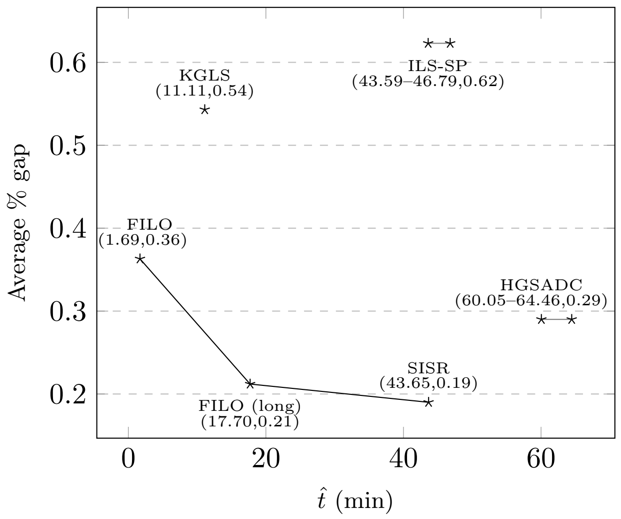

Figure 5 State-of-the-art CVRP algorithms performance comparison over the $\mathbb{X}$ instances of Uchoa et al. (2017). A tuple describing the computing time and the average percentage gap is reported below each algorithm name. For ILS-SP and HGSADC we report a range of times since the exact CPU model is not specified.

Finally, the shaking factors I_{LB} and I_{UB} can have a major impact on the overall algorithm execution. In fact, moving both to large values allows the guiding meta strategy to increment the ω_i values inducing a stronger shaking effect that will eventually require a longer local search re-optimization. On the other hand, values that are too low, does not allow to disrupt the current solution in a way that the re-optimization might perform some improvements. The identified values, coming from a limited random search analysis (see Bergstra and Bengio (2012)) described in Section 4.3, resulting in an associated shaking which is neither too disruptive nor too gentle, are again a compromise between computing time and final solution quality.

3.3. Testing on $\mathbb{X}$ Instances

The $\mathbb{X}$ instances introduced in Uchoa et al. (2017) are the current standard benchmark for the CVRP. They are a hundred small- to large-sized instances, containing up to one thousand customers and covering a wide range of demand distributions and vertices layouts. The performance of FILO is compared with current state-of-the-art algorithms on this dataset.

- The *iterated local search matheuristic* (ILS-SP), proposed by Subramanian, Uchoa, and Ochi (2013) consisting of an ILS interacting with a mixed integer programming (MIP) solver. The MIP solver is used to define new solutions as a combination of routes belonging to previously found local optima through the time-limited solution of a set partitioning model.
- The *Hybrid Genetic Search with Adaptive Diversity Control* (HGSADC), proposed by Vidal et al. (2012), which is a population-based method with an advanced and continuous diversification procedure;
- The *Knowledge-Guided Local Search* (KGLS), proposed by Arnold and Sörensen (2019) in which a GLS metaheuristic is enhanced by knowledge extracted from previous data mining analyses;
- Finally, the *Slack Induction by String Removal* (SISR) recently introduced by Christiaens and Vanden Berghe (2020), which is a sophisticated, yet easily reproducible, ruin-and-recreate-based approach combined with a simulated annealing metaheuristic.

ILS-SP, HGSADC and SISR are general methods able to solve a broad class of VRP variants while KGLS also supports the Multi-Depot VRP and the Multi-Trip VRP. ILS-SP, HGSADC and KGLS are local search-based methods, whereas SISR performs its improvement action through a ruin-and-recreate approach. Finally, KGLS defines a time-based termination condition of three minutes every 100 customers, while all the other methods fix a maximum number of iterations.

Table 2 **Aggregate computations on $\mathbb{X}$ instances.**

		ILS-SP		HGSADC		KGLS		SISR		FILO		FILO (long)	
Size	Vertices	Avg	$\hat{t}^1$	Avg	$\hat{t}^1$	Avg	$\hat{t}$	Avg	$\hat{t}$	Avg	t	Avg	t
S	101 – 247	0.31	1.52	0.07	3.79	0.28	4.66	0.11	3.78	0.18	1.69	0.09	18.06
M	251 – 491	0.59	14.57	0.30	19.09	0.64	9.40	0.25	19.64	0.40	1.66	0.25	17.51
L	502 – 1001	0.98	123.32	0.50	169.28	0.69	19.47	0.21	110.54	0.50	1.72	0.30	17.56

[1] obtained by averaging normalized times associated with the fastest and the slowest compatible CPUs.

Figure 5 shows a graphic comparison of the algorithms performance in terms of efficacy and efficiency. More precisely, it reports the average behavior over 50 runs for ILS-SP, HGSADC, SISR and FILO, and over a single run for KGLS, which is a deterministic algorithm. The best known solution values (BKS) used to compute gaps are taken, at the time of writing, from CVRPLIB (2020). FILO favorably compares with the best existing ones, achieving an excellent compromise between solution quality and computing time. In particular, FILO finds average solutions significantly better than ILS-SP and KGLS, and similar to those found by HGSADC. However, SISR outperforms FILO. FILO (long), on the other hand, finds average solutions significantly better than ILS-SP, HGSADC and KGLS, and similar to those found by SISR. We refer to Section B of the Appendix for full details.

As mentioned in Section 3.1, the average computing time for a single run $\hat{t}$ has been roughly normalized to match our CPU score by using the single-thread rating of PassMark® Software (2020), which assigns a score in the range 1389 – 1491 to compatible Intel Xeon CPUs used by ILS-SP and HGSADC for which the precise model is not specified in Uchoa et al. (2017), a score of 2052 to the AMD Ryzen 3 1300X CPU used by KGLS, and finally a score of 1662 to the Intel Xeon E5-2650 v2 CPU used by SISR.

Table 2 provides aggregate computations, grouped by instance size. The table highlights the scalability properties of FILO, by showing that the computing time for the largest instances is very similar compared to that obtained for smaller ones, yet the solution quality remains comparable to that achieved by other state-of-the-art algorithms. The computing time of FILO, as also suggested by the regression coefficients shown in Figure 1, is thus more related to the number of core optimization iterations rather than to the instance size. Moreover, by comparing the computing times of FILO and FILO (long), which differ by a factor 10 on the core optimization iterations, the increase in the computing time seems to be quite predictable with the increase in the number of iterations. More experiments can be found in the analysis Section 4.7 in which we studied, for a limited set of instances, the effects of further increasing the number of core optimization iterations.

3.4. Testing on Very Large-Scale Instances

Having assessed the performance of FILO on the standard $\mathbb{X}$ instances, we now examine the real target of the proposed approach, consisting of very large-scale instances. To this end, we tested FILO on three challenging datasets containing instances with several thousands of customers.

The $\mathbb{B}$ instances proposed by Arnold, Gendreau, and Sörensen (2019) are a set of ten very large-scale instances containing up to thirty thousand customers and reflecting real-world parcel distribution problems in Belgium. They include a first scenario in which the depot is located centrally with respect to the customers and relatively short routes are performed, and a second one in which the depot is eccentric with respect to the service zone, thus, much longer routes are required to visit the customers. We mainly compared FILO with KGLS$^{\text{XXL}}$ proposed in Arnold, Gendreau, and Sörensen (2019), that is an adaptation for very large-scale instances of the KGLS algorithm introduced in Section 3.3. As for KGLS, also KGLS$^{\text{XXL}}$ defines a time-based termination condition of three (respectively, twelve) minutes every 1000 customers for the short (respectively, long) version. KGLS$^{\text{XXL}}$ was executed on the same hardware configuration described for the $\mathbb{X}$ dataset. Moreover, for the sake of completeness, we include results obtained by the LKH-3 algorithm proposed

Table 3 Computations on $\mathbb{B}$ instances.

		KGLS$^{\text{XXL}}$		KGLS$^{\text{XXL}}$(long)		LKH-3	FILO				FILO (long)			
ID ($\lvert V_c \rvert$)	BKS	Gap	$\hat{t}$	Gap	$\hat{t}$	Gap	Best	Avg	Worst	t	Best	Avg	Worst	t
L1 (3000)	193092	0.74	13.47	0.71	53.88	0.67	0.26	0.38	0.50	2.13	-0.02	0.12	0.20	21.50
L2 (4000)	111810	4.18	17.96	2.69	71.84	1.50	0.43	0.62	0.86	3.28	-0.13	0.07	0.29	36.20
A1 (6000)	478091	0.83	26.94	0.73	107.76	0.68	0.35	0.43	0.55	2.76	0.04	0.10	0.17	28.00
A2 (7000)	292597	2.62	31.43	1.18	125.72	1.67	0.53	0.68	0.87	3.11	-0.10	0.00	0.14	33.66
G1 (10000)	470329	0.86	44.90	0.69	179.61	0.82	0.51	0.59	0.67	3.63	0.08	0.14	0.19	36.57
G2 (11000)	259712	2.94	49.39	1.85	197.57	2.33	0.50	0.72	1.06	4.62	-0.39	-0.31	-0.20	59.34
B1 (15000)	503407	1.35	67.35	0.73	269.41	1.20	0.66	0.75	0.82	4.67	0.03	0.09	0.14	47.83
B2 (16000)	349602	3.49	71.84	1.77	287.37	2.23	0.58	0.80	1.08	5.34	-0.72	-0.60	-0.45	62.70
F1 (20000)	7256529	0.97	89.80	0.54	359.21	0.61	0.52	0.56	0.62	7.22	0.08	0.12	0.18	78.44
F2 (30000)	4405678	3.65	134.70	2.24	538.82	2.13	1.21	1.40	1.57	10.99	-0.12	-0.02	0.12	150.93
Mean		2.16	54.78	1.31	219.12	1.38	0.56	0.69	0.86	4.78	-0.12	-0.03	0.08	55.52

New best solutions: (L1, 193052);(L2, 111661);(A2, 292303);(G2, 258700);(B2, 347092);(F2, 4400188).

by Helsgaun (2017) in very long computing sessions (up to several days). The best known solution values (BKS) used to compute gaps are taken, at the time of writing, from CVRPLIB (2020). We note that for many of those BKS, no citable publication is available, and the results are typically the outcome either of very long runs, or the methods are warm-started with previously-known best solutions. As can be seen from Table 3, FILO is able to successfully find very good quality solutions in relatively short computing time compared to KGLS$^{\text{XXL}}$. In particular, we note that the average gap of FILO is almost half of that of KGLS$^{\text{XXL}}$ (long) in just about five minutes of computing time. Furthermore, FILO (long) is able to find several new best known solution in less than three hours of computing time. Moreover, computing times remain consistent across instances with different structures. We again note the scalability of FILO by observing that, to solve an instance with ten times more customers, the computing time increases of about five times.

The $\mathbb{K}$ dataset proposed in Kytöjoki et al. (2007) contains eight very large-scale instances with up to twelve thousand customers. The first four instances (W, E, S, and M) are derived from real-life waste collection problems in Finland, while the remaining instances contain customers randomly and uniformly distributed. Again, we mainly compared with KGLS$^{\text{XXL}}$ proposed in Arnold, Gendreau, and Sörensen (2019) but we included results of the GVNS algorithm introduced in Kytöjoki et al. (2007) that was the first method used to solve the $\mathbb{K}$ instances. GVNS was run on an AMD Athlon 64 3000+ having a single thread score of 554 while KGLS$^{\text{XXL}}$ was run on the same hardware configuration as for the $\mathbb{B}$ dataset. As can be seen from Table 4, FILO is able to successfully find very good quality solutions in relatively short computing time when compared to KGLS$^{\text{XXL}}$. In

Table 4 Computations on $\mathbb{K}$ instances.

		GVNS		KGLS$^{\text{XXL}}$		KGLS$^{\text{XXL}}$ (long)		FILO				FILO (long)			
ID ($\lvert V_c \rvert$)	BKS*	Gap	$\hat{t}$	Gap	$\hat{t}$	Gap	$\hat{t}$	Best	Avg	Worst	t	Best	Mean	Worst	t
W (7798)	4481423	1.75	8.36	0.39	7.72	0.00	35.02	-7.35	-5.71	-3.31	9.59	-8.47	-7.74	-6.23	145.23
E (9516)	4507948	5.54	20.34	0.33	18.86	0.00	42.66	-2.87	-2.01	-0.58	14.10	-4.06	-3.41	-2.49	248.11
S (8454)	3189850	4.51	13.63	0.46	12.66	0.00	38.17	-5.04	-3.85	-1.90	9.30	-6.07	-5.48	-4.07	146.82
M (10217)	3071090	3.25	18.81	0.78	17.42	0.00	45.80	-2.54	-1.82	0.44	15.86	-3.46	-3.13	-2.74	263.56
R3 (3000)	182206	2.20	1.16	0.50	1.08	0.00	13.47	-0.50	-0.39	-0.25	2.25	-0.88	-0.81	-0.70	21.09
R6 (6000)	347224	1.58	5.92	0.19	5.48	0.00	26.94	-0.35	-0.27	-0.19	2.97	-0.81	-0.74	-0.68	27.70
R9 (9000)	511378	1.19	13.99	0.05	12.93	0.00	40.41	-0.25	-0.17	-0.09	3.70	-0.70	-0.66	-0.61	33.48
R12 (12000)	672456	1.25	26.28	0.06	24.34	0.00	53.88	-0.09	-0.01	0.07	4.47	-0.60	-0.54	-0.50	39.76
Mean		2.66	13.56	0.35	12.56	0.00	37.04	-2.37	-1.78	-0.73	7.78	-3.13	-2.81	-2.25	115.72

* taken from Arnold, Gendreau, and Sörensen (2019).
New best solutions: (W, 4101686.00);(E, 4324802.50);(S, 2996254.00);(M, 2964867.25);(R3, 180597.91);(R6, 344407.00);(R9, 507787.66);(R12, 668435.00).

Table 5 Computations on $\mathbb{Z}$ instances.

		PSMDA			FILO				FILO (long)			
ID ($\|V_c\|$)	BKS	Best	Avg	$\hat{t}$[1]	Best	Mean	Worst	t	Best	Avg	Worst	t
ZK1 (3000)	13666.36	0.00	0.94	60.18	-1.45	-1.31	-1.14	2.50	-1.81	-1.71	-1.54	22.68
ZK2 (3000)	3536.25	0.00	1.32	60.18	-2.14	-1.97	-1.76	2.30	-2.68	-2.55	-2.36	20.81
ZK3 (3000)	1170.33	0.00	1.55	60.18	-2.67	-2.53	-2.39	1.97	-3.24	-3.09	-2.96	18.60
ZK4 (3000)	1139.08	0.00	1.32	60.18	-2.23	-2.08	-1.91	1.86	-2.76	-2.65	-2.55	16.84
Mean		0.00	1.28	60.18	-2.12	-1.97	-1.80	2.16	-2.62	-2.50	-2.35	19.73

[1] max (normalized) time per run.
New best solutions: (ZK1, 13419.44);(ZK2, 3441.54);(ZK3, 1132.47);(ZK4, 1107.62).

particular, both FILO and FILO (long) find new best solutions for all instances. The computing time associated with random instances follows the same trend seen for the $\mathbb{B}$ instances. On the other hand, instances derived from real-life problems require a much larger computing time. By analyzing the structure of the final solutions obtained by FILO (long), we note that they are composed of few very long routes with several hundreds of customers. Moreover, by observing the average shaking intensity at the end of a run $\bar{\omega} = \sum_{i \in V_c} \omega_i / |V_c|$, averaged over the W, E S and M instances, we note that this value (91.37 ± 28.86) is four times larger compared to that associated with the $\mathbb{B}$ dataset (22.42 ± 4.40). The reason of such a large average value may be related to the shaking procedure behavior. In particular, given the very low number of routes for those instances, which is in average 15.00 ± 1.83, when the shaking procedure select to jump to a not yet visited neighbor route, this may not be available. In such cases, the ruin is prematurely aborted possibly causing a mismatch between the actual shaking intensity and the required one identified by $\omega_i, i \in V_c$ values. Such a mismatch may cause the average shaking intensity to increase to abnormally large values. In many cases, this won't really affect the ruin activity because it will be prematurely aborted. However, in many other, in which the early stop comes after that several customers have already been removed, the ruin activity will be in average stronger than required, causing a more time-consuming re-optimization.

Finally, the $\mathbb{Z}$ dataset was proposed in Zachariadis and Kiranoudis (2010). The dataset contains four large-scale instances, representing the actual distribution of customers locations within Greek cities. All instances have three thousand customers whose demand is uniformly distributed in 1–100. The vehicle capacity is set to 1000. We compared FILO with the *Penalized Static Move Descriptors Algorithm* (PSMDA) described in Zachariadis and Kiranoudis (2010) consisting of a Tabu Search metaheuristic in which the local search is executed by means of SMDs considering compound operators and a neighborhood pruning technique similar to that of GNs. The algorithm was run for a prefixed amount of time on an Intel Core2 Duo T5500 CPU having a single-thread score of 573. As can be seen from Table 5, FILO successfully solved the $\mathbb{Z}$ dataset finding new best solutions for all the four instances in a very limited computing time, which remains comparable to that associated with instances of similar size of the $\mathbb{B}$ and $\mathbb{K}$ dataset.

To conclude, we refer to Section C of the Appendix for the statistical significance of the above reported results. To summarize, FILO and FILO (long) obtain, in short computing time, average solutions that are generally significantly better than those found by the competing algorithms.

4. Algorithmic Components Analysis

The design of FILO followed an iterative process, whose core decisions were driven by the analyses detailed in this section. In particular, we review (i) the definition of the initial solution by means of the construction phase, possibly followed by the route minimization procedure, (ii) the acceleration and pruning techniques employed by the local search engine, and (iii) the guiding of the shaking strategy. As for the parameters tuning, and if not stated otherwise, the analyses reported here refer to the set of large size $\mathbb{X}$ instances with more than five hundred vertices. Finally, when analyzing components involving some randomization, we performed ten runs by setting the pseudorandom

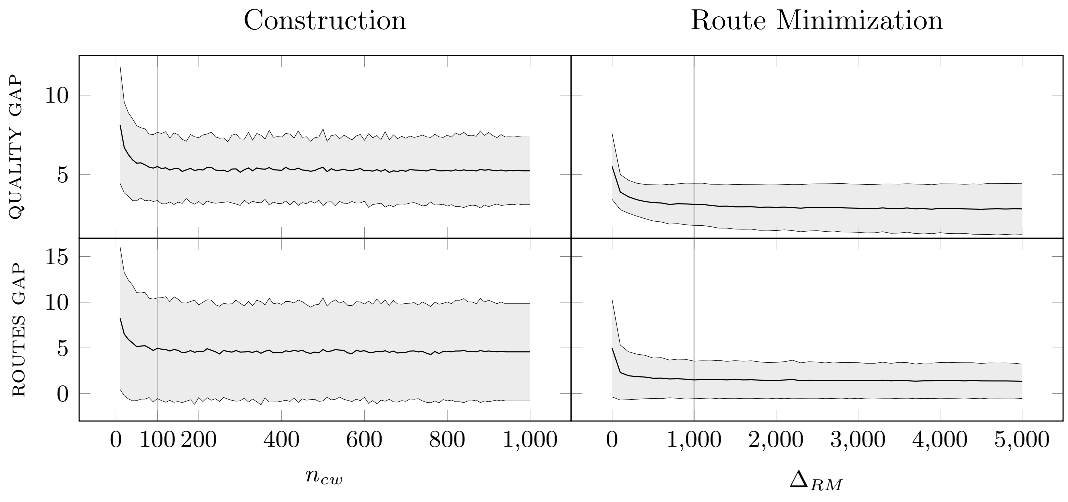

Figure 6 **Tuning of the n_{cw} and Δ_{RM} parameters based on instances listed in Table 6 for which initial solutions have a large gap and use more route than suggested by the heuristic estimate. For each diagram, the middle line represent the average and the grayed area identifies the standard deviation. Selected values for n_{cw} and Δ_{RM} are marked with a vertical line.**

engine seed equal to the run counter minus one, and reporting aggregated results averaged over seeds and instances.

4.1. Initial Solution Definition

The construction phase depends on parameter n_{cw} to identify, for each customer $i \in V_c$, the number of neighbors $j \in \mathcal{N}_i^{n_{cw}}(\{j \in V_c : i < j\})\}$ involved in the savings computation. Figure 6 (left) shows the variation of the solution quality (QUALITY GAP) and compactness (ROUTES GAP) when varying n_{cw}. In particular, we focused on the subset of instances, listed in Table 6, for which computing an initial solution of good quality is difficult, i.e., instances for which initial solutions have a large gap and use more routes than suggested by the heuristic estimate. Our findings validate and support what was already proposed in Arnold, Gendreau, and Sörensen (2019). A value of n_{cw} around 100 provides initial solutions of quality comparable to that of larger values but in slightly shorter computing times (which are, however, in the order of a few tens of milliseconds for the largest n_{cw} values we considered). As in Section 3.1, the QUALITY GAP is defined as $100 \cdot (\text{COST}(S) - BKS)/BKS$, where S is the solution resulting from the procedure, and similarly ROUTES GAP is defined as $100 \cdot (|S| - k)/k$, where k is the heuristically found ideal estimated number of routes described in Section 2.3.1.

Not surprisingly, using larger n_{cw} values is not sufficient to increase the compactness of solutions. Indeed, the route minimization procedure faces this strategic aspect of the CVRP, which is more concerned with the assignment of customers rather than with their routing. Note, however, that, contrarily to most existing route minimization procedures, the proposed one is still quality-oriented. In fact, a solution with a better objective function is always preferred over a solution with a lower number of routes, but the procedure structure is more specifically aimed at reducing the number of routes while often also obtaining the desirable effect of improving the objective function. Figure 6 (right) shows the results of this procedure when applied, for different number of iterations Δ_{RM}, to a solution S built by the construction phase with $n_{cw} = 100$. The diagrams highlight the procedure effectiveness both in improving low quality initial solutions and in quickly compacting them by often significantly reducing the number of their routes. As a result, we selected $n_{cw} = 100$ and $\Delta_{RM} = 1000$. The average computing time for largest values of Δ_{RM} is around ten seconds.

In addition, Table 6 compares the final algorithm outcome when the route minimization procedure is disabled, i.e., $\Delta_{RM} = 0$. Despite not always been crucial for the final solution quality, because

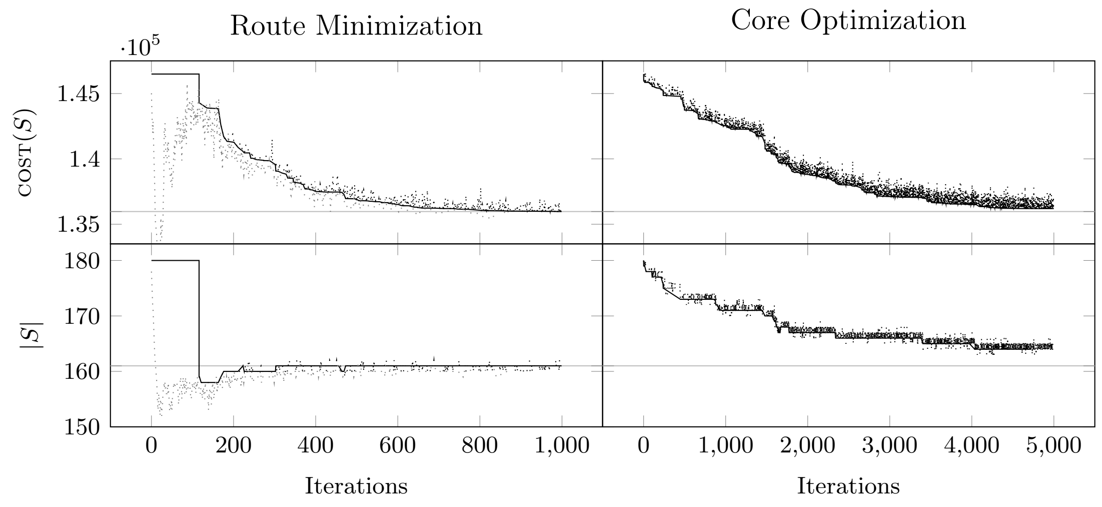

Figure 7 **Example of improvement procedures evolution when applied to the same initial solution for instance X-n936-k151. The continuous line shows the cost (top) and number of routes (bottom) associated with the best solution (in terms of cost) found up to that iteration, while dots represents the current search trajectory. In particular, gray and black dots are associated with infeasible and feasible solutions respectively.**

of the complex interactions among all the algorithm's components, the route minimization procedure provides substantial improvement for those instances containing several customers with small demand and a few customers with relatively large demand, such as X-n670-k130 and X-n936-k151. We can conclude that, in average, the route minimization positively affects the final algorithm's outcome without any relevant time impact on the computing time.

Finally, as an illustrative example we consider the scenario depicted in Figure 7, showing a single run for instance X-n936-k136, that represents the evolution of the route minimization procedure with $\Delta_{RM} = 1000$ on the left, and of the core optimization procedure with $\Delta_{CO} = 5000$ on the right. Both procedures run for a similar computing time of about three seconds and were applied to the same starting solution generated by the construction phase. By moving into the infeasible space, the

Table 6 **Computations with and without route minimization procedure (RM).**

	FILO no RM ($\Delta_{RM} = 0, \Delta_{CO} = 10^5$)				FILO with RM ($\Delta_{RM} = 10^3, \Delta_{CO} = 10^5$)			
ID[1]	Best	Avg	Worst	t	Best	Avg	Worst	t
X-n524-k153	0.29	0.57	0.81	1.37	0.08	0.39	0.68	1.34
X-n536-k96	0.69	0.80	0.89	1.51	0.71	0.80	0.87	1.60
X-n586-k159	0.46	0.65	0.79	1.73	0.57	0.73	0.87	1.65
X-n599-k92	0.37	0.47	0.60	1.54	0.37	0.47	0.69	1.57
X-n613-k62	0.51	0.68	0.84	1.12	0.39	0.66	0.96	1.16
X-n670-k130	1.32	1.95	2.38	1.36	0.83	1.08	1.32	1.41
X-n685-k75	0.35	0.55	0.67	1.34	0.47	0.63	0.82	1.42
X-n733-k159	0.32	0.38	0.45	1.25	0.25	0.34	0.45	1.25
X-n749-k98	0.57	0.75	0.88	1.40	0.54	0.68	0.85	1.46
X-n766-k71	0.59	0.73	0.93	1.59	0.46	0.59	0.66	1.60
X-n783-k48	0.52	0.60	0.72	1.74	0.34	0.62	0.87	1.75
X-n819-k171	0.60	0.76	0.93	1.37	0.83	0.90	1.03	1.43
X-n936-k151	0.90	1.26	1.52	1.29	0.39	0.83	1.23	1.31
X-n979-k58	0.27	0.36	0.48	2.24	0.26	0.35	0.44	2.37
Mean	0.55	0.75	0.92	1.49	0.47	0.65	0.84	1.52

[1] for which the route minimization procedure is executed.

route minimization procedure is very effective in quickly improving and compacting trivially bad initial solutions. However, being its structure specifically designed to reduce the number of routes, its improving effect vanishes after a few hundred iterations.

4.2. Local Search

We analyzed the local search operators described in Section 2.2 in the context of the core optimization procedure, where all features we propose are fully employed. The effect of a local search operator application is tightly linked to the state of the algorithm in that specific instant. In particular, in our approach randomization plays a major role in selecting the area that, once disrupted by the shaking procedure, is re-optimized, and the evolution of the algorithm affects shaking intensity and sparsification factors. We thus believe that the evaluation of a local search operator cannot be done "in vacuum", but needs to be performed within the algorithm execution. Therefore, we studied the effectiveness of individual operators by sampling the algorithm state throughout the core optimization phase. More specifically, a sample consists of a shaken solution S and its subset of cached vertices $\bar{V}_S$, the shaking vector $\boldsymbol{\omega}$, and the sparsification vector $\boldsymbol{\gamma}$. Each sample, being derived from the actual algorithm execution, is a relevant snapshot describing the algorithm evolution. Moreover, according to when the sample is taken, it could describe initial or final algorithm states associated with lower and higher quality solutions.

We tested every local search operator on each sample for a total number of $\Delta_{CO} = 10^5$ core optimization iterations. In addition, we considered seven variants for the EJCH operator, named EJCH(n_{EC}), where n_{EC} defines the maximum number of sequences explored from each move generator, when searching for a feasible sequence of relocations.

Figure 8 shows, for each local search operator applied to a shaken solution, the gap improvement when successfully applied, the application time in 10^{-6} seconds, and the success ratio computed as the number of improving applications over the total number of attempts.

As expected, EJCH($\cdot$) are the most effective, yet time consuming, operators. Their success ratio also suggest that in most shaken solutions, finding an improving ejection-chain is relatively easy. However, when this is not the case, the consequences are quite dramatic, as shown by the large variance in the application time reported by EJCH with the highest n_{EC}. By observing Figure 8 we note that simpler operators, such as 10EX, 11EX, TAILS, and SPLIT, have both a large success ratio, meaning that are more likely to be applied, and provide larger gap improvements compared to all other operators with quadratic cardinality. This may happen because their feasibility requirements are more easily met and thus they are more frequently applied. On the other hand, we found that all the remaining operators, despite having a lower success ratio, still do allow to find better final solutions compared to scenarios in which they are disabled. Surprisingly, TWOPT is seldom useful, meaning that the shaking procedure typically generates routes that are almost two-optimal. However we kept it thanks to its very short application time.

When structuring the HRVND, we grouped in the first tier all the operators with a comparable application time, i.e., all the operators but EJCH($\cdot$).

The selection of which EJCH to include, was guided by the results of Figure 9, showing the effect of EJCH($\cdot$), when applied to solutions that are already a local optima for the first HRVND tier. As can be seen from the diagrams, by applying the EJCH($\cdot$) operator on first tier local optima, the application time as well as its variability is dramatically reduced to a magnitude similar to that of other simpler operators. Moreover, the success ratio, the gap improvement and experiments with an HRVND without EJCH($\cdot$), suggest that its application may be relevant to obtain very good quality final solutions. In our implementation, we selected EJCH(25), shortened to EJCH in the rest of the paper, because it is more compatible with the scalability objectives of our approach still retaining its effectiveness when compared to EJCH($\cdot$) with greater n_{EC}.

Finally, as we apply the operators of each tier in an RVND fashion, especially for the first tier, we may expect a lower success ratio and gap improvement, as well as a shorter application time when they are applied on solutions that are already local optima for a number of other operators of the same tier.

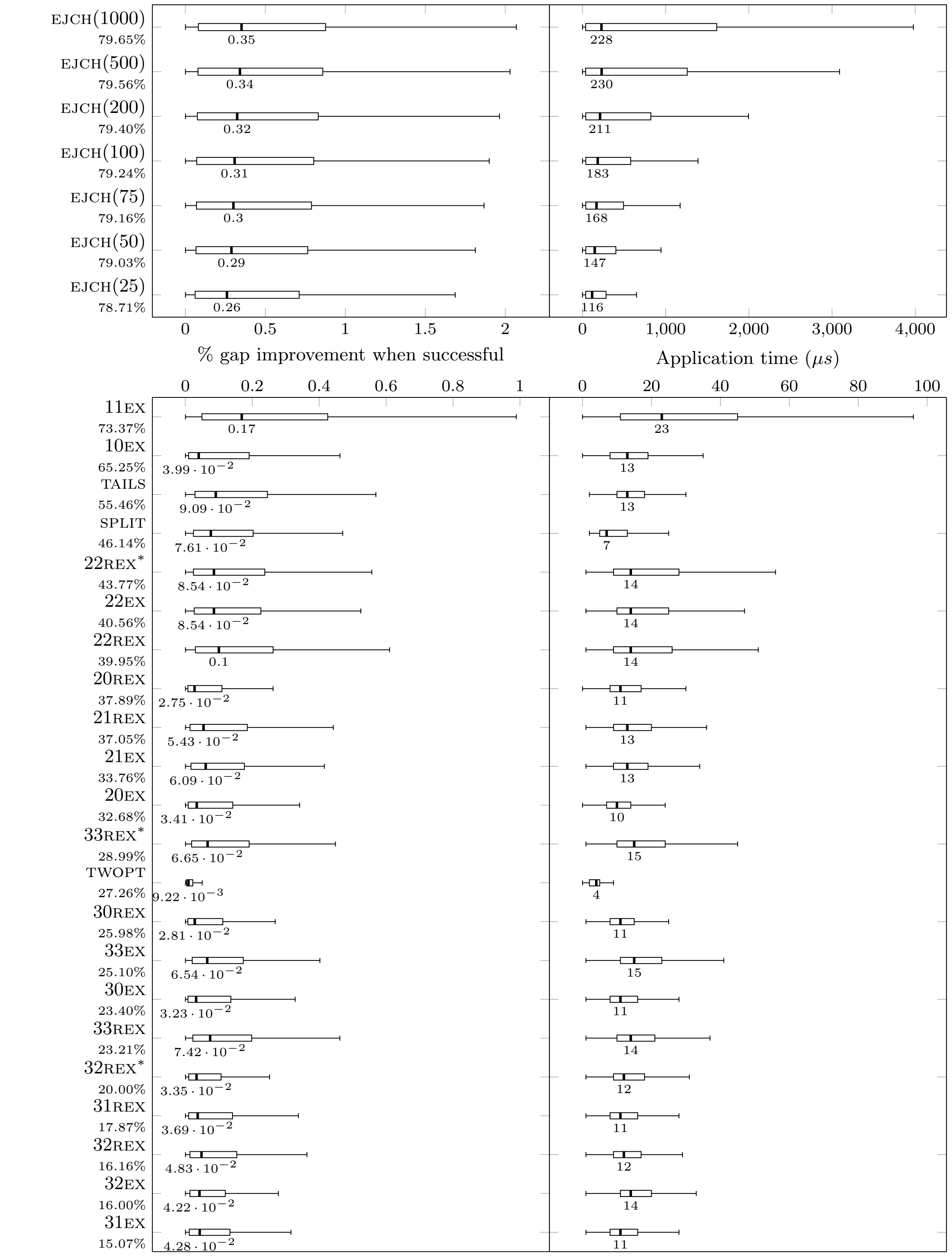

Figure 8 Statistics for local search operators when applied to shaken solutions. In particular, for each operator we report the expected gap improvement when successfully applied (left), the total exploration time (right) and the success ratio (below each operator's name). The median value is shown below each boxplot.

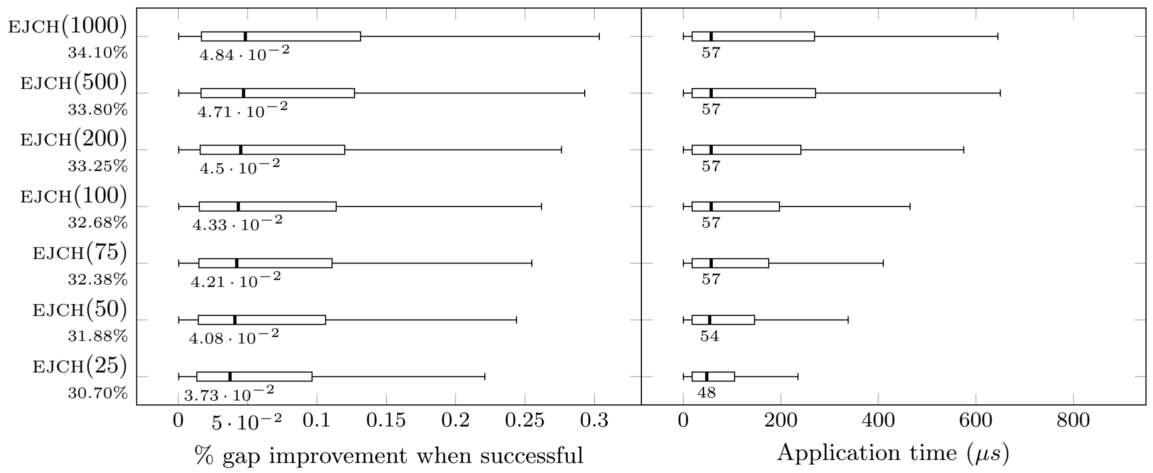

Figure 9 Statistics for local search operators when applied to HRVND first tier local optima. In particular, for each operator we report the expected gap improvement when successfully applied (left), the total exploration time (right) and the success ratio (below each operator's name). The median value is shown below each boxplot.

We can now study in more detail how each operator contributes to the total improvement of the defined HRVND structure. In particular, denoting with $\mathbb{O}$ the set of local search operators we employ, for each operator $O \in \mathbb{O}$ we stored the total gap improvement $D(O)$ achieved in a number of $I(O)$ successful applications. Note that a single application consists of a full neighborhood exploration. The ratio $R(O) = D(O)/I(O)$ thus identifies the expected improvement a successful exploration of O would produce on an average solution. We can compute the percentage *Relative Neighborhood Improvement* index of O with respect to the set of the available operators $\mathbb{O}$ as $\text{RNI}(O, \mathbb{O}) = 100 \cdot R(O) / \sum_{O' \in \mathbb{O}} R(O')$, which is shown in Figure 10. By observing the figure, we note that all the operators positively contribute to the overall improvement process.

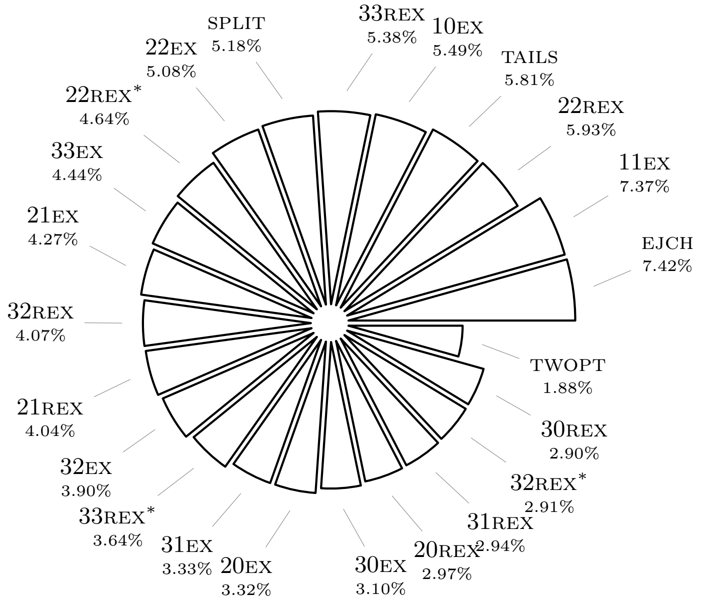

Figure 10 Percentage relative neighborhood improvement index for each local search operator in the engine. The index summarizes the contribution of each operator to the total improvement.

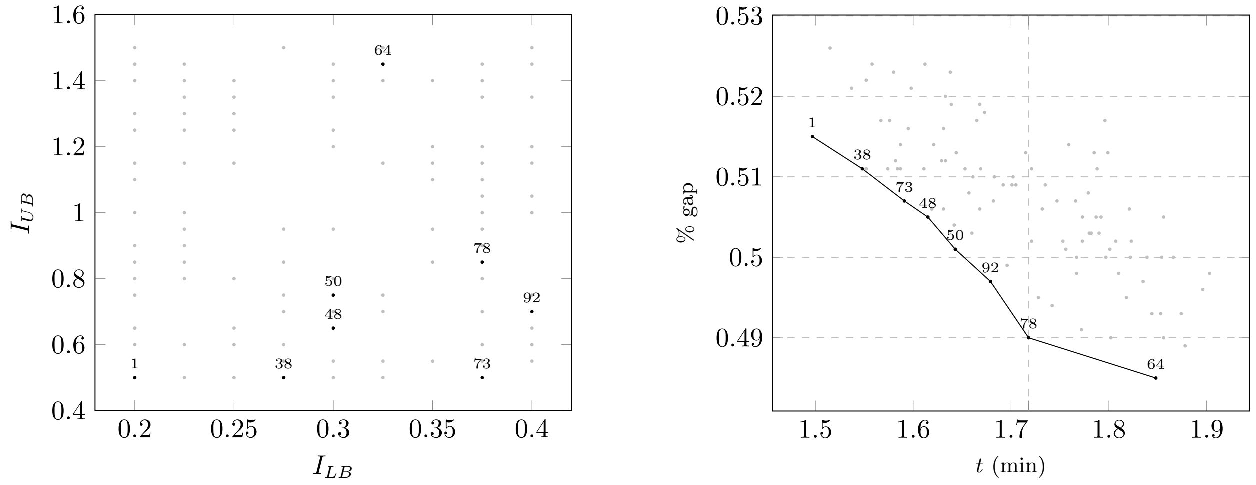

Figure 11 **Tuning of I_{LB} and I_{UB}. In the left diagram, the configurations we considered in the random search. In the right, the performance associated with each configuration obtained by running FILO with the ones we plot on the left diagram. Only the best configurations are numbered.**

4.3. Shaking Guiding Strategy

The structure-aware and quality-oriented strategy employed by the core optimization procedure to guide the shaking intensity uses two factors to determine whether to increment, reduce or randomly change the parameters $\omega_i, i \in V_c$ of customers involved in a shaking application. More precisely, I_{LB} determines when shaking parameters are increased, while I_{UB} defines when they are decreased. Together, they identify the range in which the guiding strategy actively operates. To determine reasonably effective values for I_{LB} and I_{UB} we performed a limited random search testing a hundred unique combinations for $I_{LB} \in [0.2, 0.4]$ discretized with a step of 0.025 and $I_{UB} \in [0.5, 1.5]$ discretized with a step of 0.05. A graphic representation for the different configurations and their performances is depicted in Figure 11. The proposed ranges are the outcome of an iterative process in which larger ones have been narrowed down to focus on combinations producing good quality solutions in short computing time. As shown in Figure 11, the values in the selected ranges have a minor impact on the solution quality and a slightly more relevant one on the computing time.

In our implementation we selected configuration 78, corresponding to $I_{LB} = 0.375$ and $I_{UB} = 0.85$. We noticed that slightly better solutions can be obtained when using moderately larger values in particular for I_{UB}. However, by letting shaking parameters reach larger values, we may expect the associated re-optimization time to increase. As an example, we analyzed the average shaking intensity at the end of a run, defined as $\bar{\omega} = \sum_{i \in V_c} \omega_i / |V_c|$, for three representative configurations, namely 1, 50 and 64, corresponding to values for I_{LB} and I_{UB} in the lower, middle and high part of the range; the tested configurations have $\bar{\omega}$ equal to 13.33, 14.70 and 16.56, respectively. The tuning of I_{LB} and I_{UB} requires a little care, in fact, by selecting values that are too large the risk is an increase in computing time with poor quality final solutions. Finally, being the factors used in combination with the average cost of a solution arc, see Section 2.3.2.1, once set to reasonable values, the procedure can generalize fairly well to solutions and instances with a very different structure as shown by our computational results.

4.4. Move Generators and Granular Neighborhoods

The benefits of GNs are well documented in several papers, such as Toth and Vigo (2003) and Schneider, Schwahn, and Vigo (2017). However, a careful tuning is necessary to get the best out of them. In fact, different values for the number of neighbors considered in the sparsification rule n_{gs}, the base sparsification factor γ_{base} and the reduction factor δ affecting the number of nonimproving iterations before increasing a sparsification factor, can dramatically alter the performance of the algorithm and, more specifically, its computing time. The sparsification increment factor λ may also

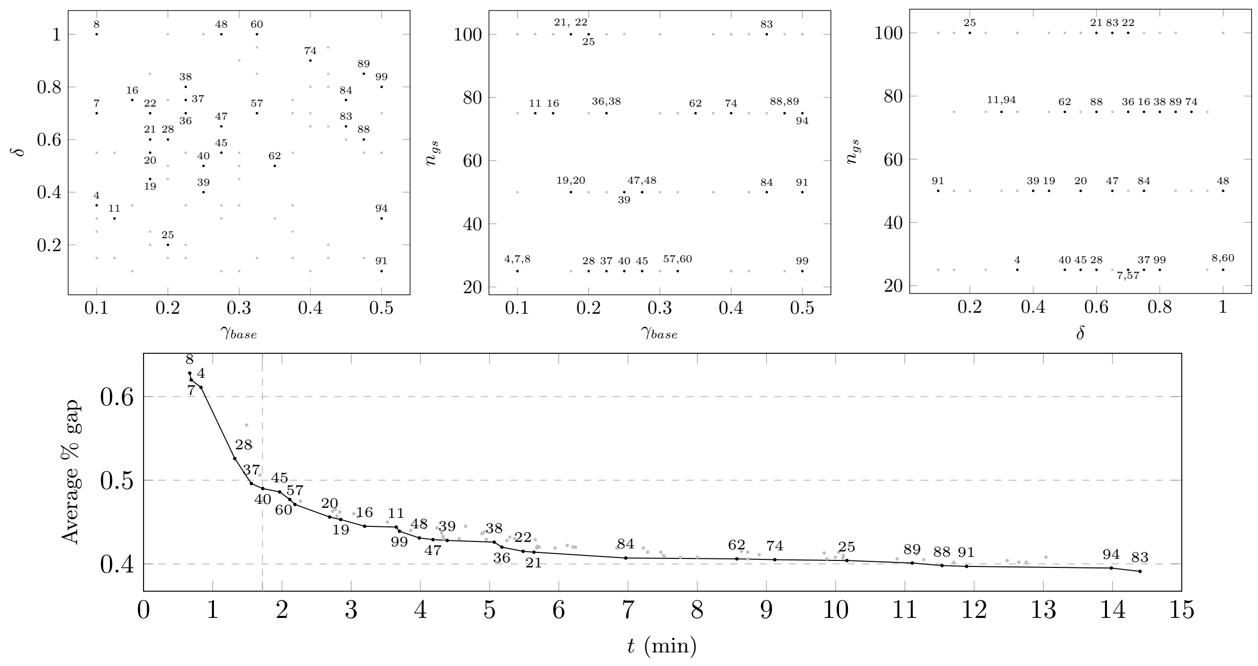

Figure 12 **Tuning of n_{gs}, γ_{base}, and δ. On the top, the configurations we considered in the random search. On the bottom, the performance associated with each configuration obtained by running FILO with the configuration values. Only the best configurations are numbered and seven suboptimal ones, with a computing time greater that 15 minutes, are omitted.**

play a role, however, we fixed it to $\lambda = 2$, as in the original GNs definition, and made the others parameter depend on its value.

As for the shaking parameters, we adopted the same procedure of the previous section. More precisely, we studied the effect of varying n_{gs}, γ_{base} and δ by performing a limited random search among reasonable ranges of values. The selected configurations, and the associated performances can be seen in Figure 12. In particular, we drawn a hundred unique combinations for $n_{gs} \in \{25, 50, 75, 100\}$, $\gamma_{base} \in [0.1, 0.5]$, discretized with step 0.025, and $\delta \in [0.1, 1]$, discretized with step 0.05. As expected a larger value for n_{gs} is generally associated with a better final solution quality, however, the associated computing time increment just provide an extremely limited gap improvement.

In our implementation, we selected configuration 40, corresponding to $n_{gs} = 25$, $\gamma_{base} = 0.25$, and $\delta = 0.5$, because it allows to get very good quality solutions in a relatively short computing time. By classifying as high-performing Pareto optimal configurations, those producing an average gap lower or equal than 0.55% within a computing time not larger than 5 minutes, and low-performing the remaining Pareto optimal configurations, we obtain a dataset of 14 high-performing configurations and 16 low-performing ones. We gained some insights about granular-related characteristics of these configurations by analyzing a simple J48 decision tree trained with WEKA 3.8 (Frank, Hall, and Witten (2016)) on the above dataset. A configuration can be classified as high-performing with an accuracy of about 97% if $n_{gs} \leq 50 \wedge 0.12 < \gamma_{base} \leq 0.35$ or $n_{gs} > 50 \wedge \gamma_{base} \leq 0.15$. Apparently, δ does not provide useful insights to discriminate between configuration performances. These rules suggest that a very aggressive sparsification is preferable to obtain reasonably good results in short computing times. The reason may be related to the metaheuristic approach we used to guide the search. In particular, the neighbor acceptance strategy used in FILO is based on a simulated annealing rule. The current search trajectory may thus be far worse than the current best found solution thus making additional core optimization iterations more convenient compared to very accurate neighborhood explorations.

We then studied, as suggested in several papers, the effect of including in the sparsified set the arcs incident into the depot. More precisely, we considered the set $T_0 = \cup_{i \in V_c}\{(i, 0)(0, i)\}$ and we

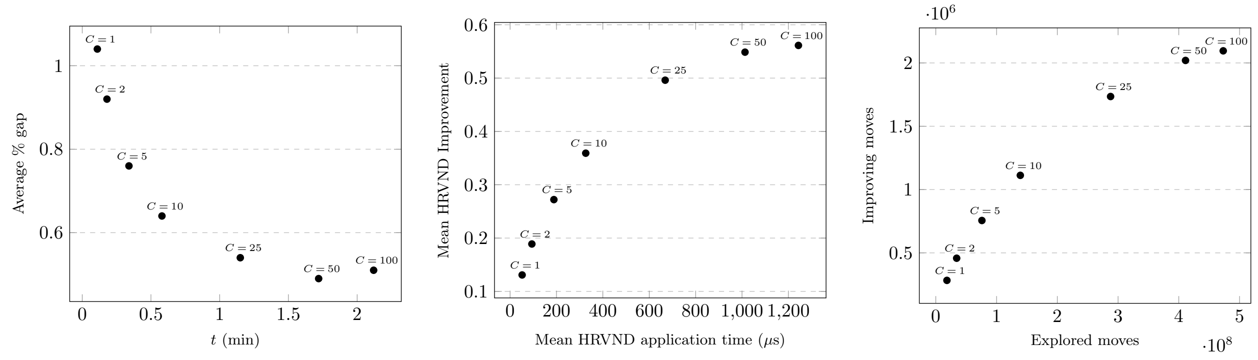

Figure 13 **Tuning of C. Computational results (left) and local search statistics (center, right) obtained by running FILO with the associated C value.**

defined $T' = T \cup T_0$, where T is the set of move generators defined in Section 2.2.2. Moreover, we defined the dynamic set of move generator $T_0^{\gamma_0} = \{(i,0),(0,i) \in i \in \mathcal{N}^k(V_c)\} \subseteq T_0$ with $k = \lfloor \gamma_0 \cdot |V_c| \rfloor$. The new complete set of dynamic move generators is thus $T'^{\gamma} = T^{\gamma} \cup T_0^{\gamma_0}$. Note that, by filtering each set separately, we avoid one set to completely overshadow the other in case it considers shorter arcs. The average gap by running FILO with this new set of move generators was 0.51% compared to the 0.49% obtained with move generators defined by the rule of Section 2.2.2 only. However, the computing time was of about 115% larger, i.e. 3.70 minutes compared to 1.72. In the light of this results, including all arcs incident into the depot may not be ideal when moving to very large-scale instances.

Finally, we compared the vertex-wise management of move generators with the more standard one in which after a number of $\delta \cdot \Delta_{CO}$ nonimproving iterations the total number of active move generators is doubled, i.e. $\gamma_i = \min\{\gamma_i \cdot \lambda, 1\}, i \in V$, and when a solution improving the current best found solution is identified, all sparsification factors are reset, i.e. $\gamma_i = \gamma_{base}, i \in V$. In particular, by running FILO with move generators managed in the standard way we obtained a gap of 0.51% compared to 0.49% of the vertex-wise management in a similar computing time. However, we believe both strategies to be equally effective when properly tuned. To conclude, the proposed vertex-wise management of move generators might be a reasonable and effective alternative generalization of the standard one that better fits the localized optimization design of FILO.

4.5. Selective Vertex Caching

The dimension of the cache C may considerably affect the overall algorithm outcome by indirectly acting on the different components employed. As an example, a small C value will promote a milder shaking intensity. In fact, most of the customers involved in stronger shakings would not be considered by subsequent local search application because not cached due to the limit imposed by C. Furthermore, a low C value would cause the local search to perform less improvements per iteration, reducing the likelihood of improving the best found solution S^*. As a result, sparsification factors $\gamma_i, i \in V$ might reach larger values compared to scenarios using a larger C. Figure 13 compares the average performance of FILO and statistics related to the local search execution while varying C. In our implementation, we selected $C = 50$ because it produces solutions of a quality comparable to larger values but within shorter computing times. Note, however, that the selective vertex caching and shaking guiding strategy are highly interconnected components. In fact, even by setting $C >> 100$, results and statistics remain comparable to those with $C \approx 100$, because of the limits on the number of ruined customers imposed by the shaking guiding strategy.

Figure 14 provides a number of hints about the scalability properties of FILO. In fact, we observed that the number of moves explored by the local search as well as its average application time does not depend on the instance size. There is, however, a positive correlation between the number of routes and the number of explored moves.

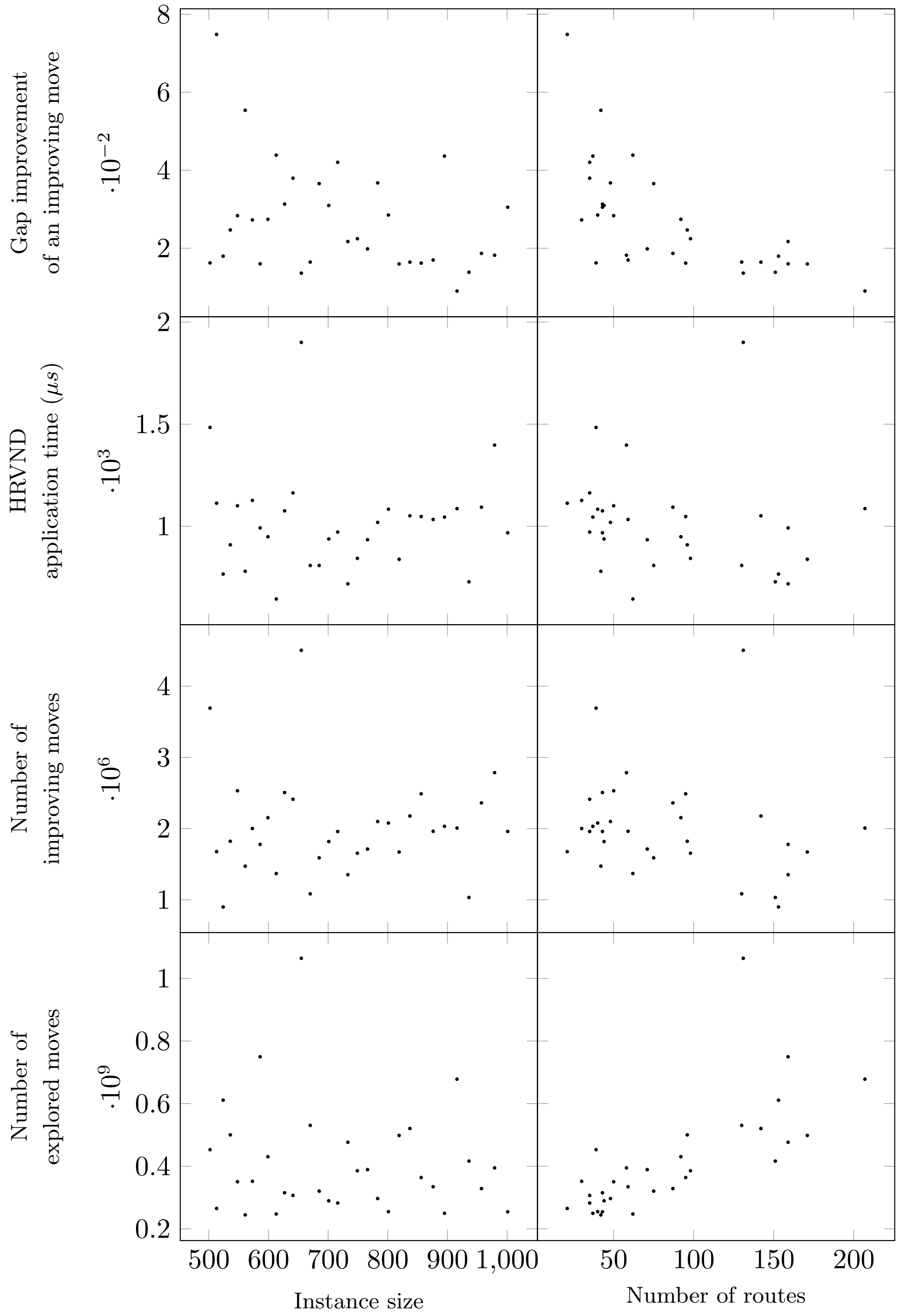

Figure 14 **Statistics for local search operators while varying the instance size and the nominal number of routes, i.e. defined in the $\mathbb{X}$ instance name.**

Finally, we tested FILO without the selective vertex caching. In particular, we set $C = |V|$ and we included all vertices into the cache never removing them. Remember that, the normal cache behavior requires that it is emptied at the beginning of each improvement iteration. Several components make use of the cache to identify interesting areas where it is considered worth working. As an example, the update of the shaking parameters in this scenario will try to identify a set of values that are globally good. The average results were comparable with those with $C = 50$ and the cache

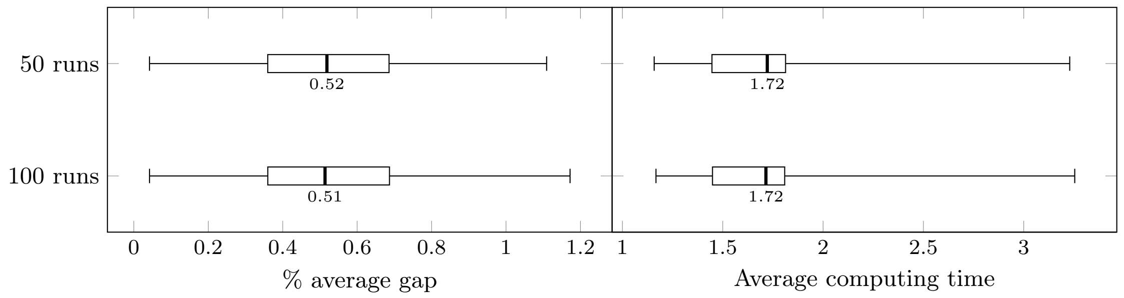

Figure 15 **Average gap and computing time comparison while varying the number of runs per instance. The median value is shown below each boxplot.**

is enabled. In particular, the average gap was 0.50%, but the computing time increased by a factor of ten, raising to 20.15 minutes.

4.6. Computations with Limited Memory Footprint

Random access memory (RAM) is nowadays relatively cheap and large amount of it is easily supported even by low-cost laptops. Time, on the other hand, is much more valuable and new chips are moving to massive parallelization rather than to an increase of their working frequency. Solution methods, however, seldom make use of parallel processing to solve a single instance even if this might be a very interesting, yet challenging, research direction when moving to very large-scale instances. We can thus state that nowadays the real bottleneck is not the amount of available RAM but more likely the computing time used to solve an instance. Indeed, the largest instance we considered having thirty thousand vertices, F2 from the $\mathbb{B}$ dataset, can be easily processed on a laptop with 16GB of RAM by using, during the main core optimization procedure, about 66% of the available RAM. Despite this premise, in this section we investigate the behavior of FILO when the cost matrix, which is one of the most RAM consuming data structure we use, is not stored but arc costs are computed on-demand. In this case, the computing time increases by about 52%, i.e., from 1.72 minutes to 2.60 minutes. As an example, without storing the cost matrix the F2 instance RAM requirements drops from 10.56 GB to 3.68GB. This may allow the algorithm to be applicable to even larger instances compared to the one we considered. An alternative more sophisticated method proposed in Arnold, Gendreau, and Sörensen (2019) consists in storing into a hashmap a number of arcs connecting close vertices that are supposed to be used more frequently than others.

4.7. Extreme Runs

In this section we investigate whether allowing longer computations is enough to improve the quality of final solutions. This is partially answered by the FILO (long) version we considered in the computational results of Section 3. In addition, Table 7 shows the results we obtained by setting $\Delta_{CO} = 10^7$. The average gap for the subset of large instances of the $\mathbb{X}$ decreased from the 0.30% of FILO (long) to 0.19%, see Table 2. Moreover, we found three new best solutions. The increment of the computing time remains quite constant, i.e., by increasing the number of iteration of a factor ten, the computing time increases of about ten times.

Finally, we study whether performing a larger number of run per instance drastically changes the average result and computing time. To this end, we compared the results obtained on the large scale $\mathbb{X}$ instances in 50 runs, and described in Section 3.3, with the results obtained by performing 100 runs. Seeds were selected as described in Section 3.1. The average results (rounded to two decimal places) when performing a 100 runs increased to 0.51% and the computing time remained the same, see Figure 15.

To better assess whether there was a statistically significant difference among the averages between runs with seeds 0–49 and runs with seeds 0–99, we performed a Wilcoxon signed-rank test (Wilcoxon (1945)) by using the R software (R Core Team (2020)). The null hypothesis states that the two

Table 7 Long computations on large-sized $\mathbb{X}$ instances.

ID	BKS	Best	Avg	Worst	t
X-n502-k39	69226	0.00	0.01	0.04	262.65
X-n513-k21	24201	0.00	0.07	0.16	222.27
X-n524-k153	154593	0.01	0.14	0.27	146.99
X-n536-k96	94868	0.50	0.60	0.71	161.76
X-n548-k50	86700	0.01	0.02	0.09	207.85
X-n561-k42	42717	0.08	0.20	0.28	138.73
X-n573-k30	50673	0.12	0.22	0.26	205.74
X-n586-k159	190316	0.20	0.25	0.31	181.93
X-n599-k92	108451	0.15	0.22	0.33	189.87
X-n613-k62	59545	0.12	0.20	0.39	121.34
X-n627-k43	62173	0.03	0.12	0.32	198.31
X-n641-k35	63705	0.05	0.11	0.18	206.51
X-n655-k131	106780	0.00	0.02	0.03	378.73
X-n670-k130	146332	0.50	0.64	0.90	136.33
X-n685-k75	68225	0.17	0.34	0.52	142.94
X-n701-k44	81923	0.03	0.11	0.35	163.87
X-n716-k35	43387	0.09	0.16	0.29	176.98
X-n733-k159	136190	0.06	0.13	0.20	135.04
X-n749-k98	77314	0.15	0.25	0.38	141.90
X-n766-k71	114456	0.16	0.27	0.34	156.24
X-n783-k48	72394	0.10	0.17	0.26	191.01
X-n801-k40	73331	-0.03	0.09	0.15	188.16
X-n819-k171	158121	0.39	0.44	0.53	141.35
X-n837-k142	193737	0.12	0.21	0.26	191.22
X-n856-k95	88990	0.01	0.07	0.13	188.52
X-n876-k59	99303	0.11	0.16	0.24	176.58
X-n895-k37	53928	-0.04	0.13	0.31	189.72
X-n916-k207	329179	0.19	0.23	0.31	200.72
X-n936-k151	132812	0.16	0.26	0.38	127.16
X-n957-k87	85469	-0.00	0.06	0.11	195.38
X-n979-k58	118988	0.05	0.16	0.24	244.49
X-n1001-k43	72369	0.06	0.17	0.27	169.54
Mean		0.11	0.19	0.30	183.74

New best solutions: (X-n801-k40, 73311);(X-n895-k37, 53906);(X-n957-k87, 85467).

samples of averages are identical, that is, they have the same median. Both, the average gap and computing time, do not statistically differ when performing 50 or 100 runs. In fact, by assuming a confidence level $\alpha = 0.025$, the p-values are 0.977935 and 0.500047 for the average solution quality and computing time, respectively. In both cases, the p-value is greater than α and thus we cannot reject the null hypothesis stating that the samples are not statistically different.

5. Conclusions

In this paper, we presented FILO, an effective and scalable algorithm for the CVRP. FILO performs its main improving action by re-optimizing a very limited area that was previously disrupted by a localized shaking application. The shaking is performed in ruin-and-recreate fashion and it is guided by a meta strategy that iteratively tailors the ruin intensity to the current instance and solution. A sophisticated local search engine is then used to re-optimize the disrupted area by means of a number of interconnected novel and revisited components, which characterize both the effectiveness and scalability of the proposed algorithm. In particular, a selective vertex caching strategy is used to focus the optimization process on solution areas that were recently changed, dynamic Granular Neighborhoods managed in a more general way are used to identify a number of promising neighbor solutions by intensifying the search only where it is more necessary, and finally, a number of local search operators based on the Static Move Descriptor concept are structured into a Hierarchical

Randomized Variable Neighborhood Descent to actually perform the improvements. Despite the exploration of several neighborhoods, the method is very fast thanks to an accurate design, and greatly benefits from the above mentioned acceleration and pruning techniques. Moreover, FILO exhibits a computing time that is linear with respect to the instance size, making it very suitable to solve very large-scale instances without sacrificing the quality of the final solutions. In fact, it is able to find several new best solutions for very large-scale instances and two new best solutions for the well-studied $\mathbb{X}$ dataset proposed by Uchoa et al. (2017).

Acknowledgments

We gratefully thanks Birger Raa for initial discussions on Static Move Descriptors and Granular Neighborhoods, Luca Ghedini for managing the cluster of machines we used for the experiments, and Florian Arnold for sharing the $\mathbb{K}$ dataset. This research was partially funded by the U.S. Air Force Office of Scientific Research [Award FA9550-17-1-0234].

Appendix A: Move Generators and Static Move Descriptors

Efficiently managing move generators is crucial for any local search-based algorithm making use of GNs. In addition, flexibility might be required when experimenting different sparsification rules and composition of them, as we did in the analysis proposed in Section 4.4. In the following sections, we first discuss a flexible but still efficient implementation of move generators for the symmetric CVRP, supporting the union of different sparsification rules and a vertex-wise dynamic management. Then, we show how it can be used to efficiently implement SMD-based local search operators.

A.1. Move Generators Storage and Management

Given a set R of sparsification rules, the complete set of move generators T is defined by the union of a number of move generator sets T_r, each one defined by a sparsification rule $r \in R$. More precisely, $T = \bigcup_{r \in R} T_r$. Each set T_r may be filtered according to a sparsification vector $\boldsymbol{\gamma} = (\gamma_0, \gamma_1, \ldots, \gamma_N)$ defining, for each vertex $i \in V$, a percentage $\gamma_i \in [0,1]$ of move generators in T_r to be considered as active. More precisely, the dynamic set of move generators $T_r^{\boldsymbol{\gamma}}$ filtered according to $\boldsymbol{\gamma}$ is defined as $T_r^{\boldsymbol{\gamma}} = \bigcup_{i \in V} \{(i,j),(j,i) : j \in V \wedge \textsc{condition}(i,j,\gamma_i)\}$, where $\textsc{condition}(i,j,\gamma_i)$ is a criterion defining whether (i,j) and (j,i) are active based on the value of γ_i.

In the following, we describe a possible implementation of the above defined general move generators framework. An illustrative example, representing the implementation of a set of move generators T defined by the union of two sparsification rules r_0 and r_1, is shown in Figure 16.

A list of move generators $L(T)$ is built by considering unique move generators defined by the different sparsification rules $r \in R$. By denoting with $L(T)_\ell$ the move generator $(i,j)_\ell$ indexed by ℓ in $L(T)$, we structured the list $L(T)$ so as to satisfy:

1. $L(T)_\ell = (i,j)_\ell \wedge L(T)_{\ell+1} = (j,i)_{\ell+1}$ for each even index ℓ;
2. $L(T) \not\ni (i,i), \forall i \in V$.

Condition 1 asks that both (i,j) and (j,i) are considered. This ensures the evaluation of a consistent set of moves when exploring asymmetric neighborhoods. Moreover, (i,j) and (j,i) are stored contiguously into $L(T)$ so that given a move generator indexed by ℓ, its reversed counterpart can be efficiently retrieved, when necessary. Finally, Condition 2 discards self-moves which are typically not used in local search procedures.

A number of lists $L(T_r, v)$, one for each vertex $v \in V$, is associated with each sparsification rule $r \in R$. Those lists identify a portion of $L(T)$ consisting of move generators $(i,j) \in T_r$. In particular, each list $L(T_r, v)$ keeps track of the even indices ℓ of move generators $(i,j)_\ell$ such that $v = i$ or $v = j$. Because of Condition 1 on $L(T)$, it is not necessary to store the index of the counterpart of (i,j) that can be found accessing $L(T)_{\ell+1}$.

In addition, each list $L(T_r, i)$, along with indices ℓ, stores an inclusion percentage value $p_{ri\ell}$ used to define whether move generators $(i,j)_\ell$ and $(j,i)_{\ell+1}$ are active according to the current sparsification factor γ_i. More precisely, the above defined $\textsc{condition}(i,j,\gamma_i)$ is implemented as $\textsc{condition}(i,j,\gamma_i) = p_{ri\ell} \le \gamma_i$ where ℓ is the even index pointing to move generator T_ℓ having i and j as endpoints.

Depending on how the inclusion percentage values are defined we can model the classical or the vertex-wise management of the dynamic move generators for a sparsification rule $r \in R$. In the classical management $\sum_{i \in V} \sum_{\ell \in L(T_r,i)} p_{ri\ell} = 1$ whereas in the vertex-wise management $\sum_{\ell \in L(T_r,i)} p^i_{r\ell} = 1$ for each $i \in V$.

The complete dynamic set of move generators can thus be addressed by iterating over each sparsification rule $r \in R$, each vertex $i \in V$, each list $L(T_r, i)$, and considering move generators $(i,j)_\ell$ and $(j,i)_{\ell+1}$ such that $p_{ri\ell} \le \gamma_i$.

Note that by storing indices instead of move generators, different sparsification rules identifying the same subset of move generators would point to the same entry of $L(T)$.

In our implementation, the Sparsification Rule r_0 described in Section 2.2.2 is implemented by defining $p_{r_0 v\ell} = n/|L(T_{r_0}, v)|$, where n is the index of move generator ℓ in a list of move generators $(i,j) \in L(T_{r_0}, i)$ sorted in increasing c_{ij} cost. The additional Sparsification Rule r_1 employed in the analysis of Section 4.4 defines instead $p_{r_1 v\ell} = n/|T_{r_1}|$, where n is the index of move generator ℓ in a list of move generators $(i,j) \in L(T_{r_1})$ sorted in increasing c_{ij} cost.

A.2. An Abstract SMD-based Local Search Operator

The general structure of all SMD-based local search operator we used is shown in Algorithm 4. Note that, as mentioned in Section 2.2.3, we use SMD and move generator interchangeably.

First, during a *pre-processing* step, if necessary, additional computation useful for the actual neighborhood exploration may be executed. As an example, $\textsc{tails}$ and $\textsc{split}$ benefits from pre-computing routes cumulative load.

A heap data structure $\mathcal{H}$ is initialized with currently active move generators according to the sparsification vector $\boldsymbol{\gamma}$ and such that one of the endpoint belongs to the set $\bar{V}_S$ of cached vertices for the solution S under

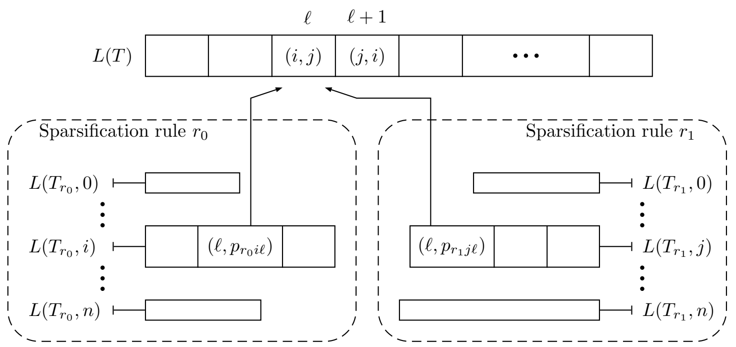

Figure 16 **Implementation of the list $L(T)$ of move generators defined by two sparsification rules r_0 and r_1. Two move generators (i,j) and (j,i) indexed ℓ and $\ell+1$ respectively, are explicitly shown. As can be seen, those move generators are defined by both sparsification rules and their associated lists point to the same shared entries in $L(T)$. The inclusion percentages $p_{r_0 i\ell}$ and $p_{r_1 j\ell}$ might however cause those move generators to be active at different times according to the value of γ_i and γ_j.**

examination. In particular, those move generators, denoted by $T^\gamma(S)$, can be easily retrieved by using the data structures defined in Section A.1 of the Appendix and more specifically, $T^\gamma(S) = \bigcup_{r\in R, i\in \bar{V}_S}\{(i,j)_\ell : p_{ri\ell} \leq \gamma_i, \ell \in L(T_r,i)\}$. When dealing with local search operators defining asymmetric neighborhoods, both $(i,j)_\ell$ and $(j,i)_{\ell+1}$ have to be included. Given condition 1 on list $L(T)$ defined in Section A.1 of the Appendix, this can be done by extending $T^\gamma(S) = T^\gamma(S) \cup \bigcup_{r\in R, i\in \bar{V}_S}\{(i,j)_{\ell+1} : p_{ri\ell} \leq \gamma_i, \ell \in L(T_r,i)\}$.

For each move generator $(i,j) \in T^\gamma(S)$, the δ-tag $\delta(i,j)$, identifying the effect of the application of the move induced by (i,j) on S, is computed. Every (i,j) inducing an improving move, i.e. $\delta(i,j) < 0$, is inserted into the heap data structure $\mathcal{H}$. By only inserting improving move generators the heap computational complexity is kept at its minimum.

The heap $\mathcal{H}$ is linearly scanned until a feasible move is found. If such a move cannot be found, then S is considered to be a local optimum with respect to the local search operator under examination. Note that by heuristically restricting the initialization stage to only consider move generators involving vertices in $\bar{V}_S$, some improvement may be overlooked, but as shown by the experiments in Section 4.5, this does not typically affect the final solution quality.

Once a move generator (i,j) inducing a feasible and improving change to S is found, a list A of operator-dependant affected vertices is assembled. The application of (i,j) during the execute stage will change some of the δ-tag of move generators involving vertices in A.

The update stage recomputes the δ-tag for active move generators $U_{(i,j)} = \bigcup_{r\in R}\bigcup_{i\in A}\{(v_1,v_2)_\ell : \ell \in L(T_r,i) \wedge (v_1 = i \vee v_2 = i) \wedge p_{ri\ell} \leq \gamma_i\}$. In case of an asymmetric neighborhood, the updates are extended to $U_{(i,j)} = U_{(i,j)} \cup \bigcup_{r\in R}\bigcup_{i\in A}\{(v_1,v_2)_{\ell+1} : \ell \in L(T_r,i) \wedge (v_1 = i \vee v_2 = i) \wedge p_{ri\ell} \leq \gamma_i\}$. For each move generator requiring an update $(v_1,v_2) \in U_{(i,j)}$ the following cases are possible:

- (v_1,v_2) is removed from the heap $\mathcal{H}$ if $(v_1,v_1) \in \mathcal{H}$ and $\delta(v_1,v_2) \geq 0$;

Algorithm 4 Abstract SMD-Based Local Search Operator

```
1: procedure Apply($S, T^\gamma$)
2:     preprocess($S$)
3:     $\mathcal{H} \leftarrow$ initialization($S, T^\gamma$)
4:     $n \leftarrow 0$
5:     while $n < len(\mathcal{H})$ do
6:         $(i,j) \leftarrow$ peek($\mathcal{H}, n$)
7:         $n \leftarrow n+1$
8:         if $\neg$isFeasible($S, (i,j)$) then continue
9:         $A \leftarrow$ affectedVertices($S, (i,j)$)
10:        $S \leftarrow$ execute($S, (i,j)$)
11:        update($\mathcal{H}, T^\gamma, A$)
12:        $n \leftarrow 0$
13:    end while
14: end procedure
```

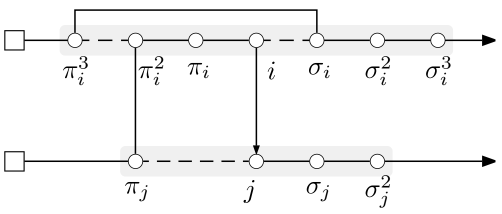

Figure 17 **A 3OEX application induced by move generator (i,j) relocating path $(\pi_i^2 - i)$ between π_j and j. Some SMDs involving vertices in the gray area require an update to their δ-tag after the move execution.**

- (v_1, v_2) is inserted into the heap $\mathcal{H}$ if $(v_1, v_2) \notin \mathcal{H}$ and $\delta(v_1, v_2) < 0$;
- the heap property is checked and possibly restored if $(v_1, v_2) \in \mathcal{H}$ and $\delta(v_1, v_2) < 0$;
- finally, (v_1, v_2) is ignored if $(v_1, v_2) \notin \mathcal{H}$ and $\delta(v_1, v_2) \geq 0$.

Since different sparsification rules may refer to the same move generators, a timestamp associated with each move generator (i,j) can be used to avoid evaluating them more than once, both in the initialization and in the update stages. Note that also when using a single sparsification rule r, a double evaluation may occur when $i, j \in A$ and $T_\ell = (i,j)$ is such that $\ell \in L(T_r, i) \wedge p_{ri\ell} < \gamma_i$ and $\ell \in L(T_r, j) \wedge p_{rj\ell} < \gamma_j$.

A.2.0.1. *Restricted Update for Asymmetric Neighborhoods.* The δ-tag update of move generators involving a vertex $i \in A$ for a local search operator defining an asymmetric neighborhoods may be restricted from $\{(i, v_2), (v_1, i) : v_1, v_2 \in V\} \cap T^\gamma$ to only one between $\{(i, v_2) : v_2 \in V\} \cap T^\gamma$ and $\{(v_1, i) : v_1 \in V\} \cap T^\gamma$. As an example, consider the 3OEX application shown in Figure 17. The set of affected vertices is $A = \{\pi_i^3, \pi_i^2, \pi_i, i, \sigma_i, \sigma_i^2, \sigma_i^3, \pi_j, j, \sigma_j, \sigma_j^2\}$. However, not all move generators $\{(i,j),(j,i) : i \in A, j \in V\} \cap T^\gamma$ have to be updated. For example, considering vertex π_i^3, move generators $(\pi_i^3, j), j \in V$ require an update since the successor of π_i^3 changes after the move execution, however, move generators $(j, \pi_i^3), j \in V$ do not, in fact, the predecessor of π_i^3 remains the same. For operator 3OEX and ignoring the current sparsification level, the total number of move generators requiring an update after a 3OEX application can be reduced of about 36%.

Finally, we refer the reader to Section A.3 of the Appendix for the operator-dependant definitions of the feasibility check, the assembly of the list A of vertices, the restricted update and the execution stage.

A.2.1. Dynamic Vertex-wise Move Generators for SMD-based Local Search Operators. Vertex-wise management of move generators requires a little extra care for the SMD update stage to be correctly performed. To highlight this, consider a scenario in which at the beginning of a neighborhood exploration for a solution S, a vertex j, is currently marked as cached for S, that is $j \in \bar{V}_S$. An illustrative example is shown in Figure 18, representing a portion of an instance with six customers together with a number of move generators depicted as lines ending with little circles. In particular, for a move generator (v_1, v_2), a full circle near to v_1 means that the move generator is currently active in v_1, i.e. $p_{rv_1\ell} \leq \gamma_{v_1}$ where ℓ is the index of $(v_1, v_2)_\ell$ in $L(T)$, while an empty circle represents the opposite, i.e. $p_{rv_1\ell} > \gamma_{v_1}$. In the figure, (i,j) is active in j but not in i. Finally, the grayed area identifies the set $\bar{V}_S$ of currently cached vertices for S.

During the SMD initialization stage, move generators involving vertices in $\bar{V}_S$ are considered to be inserted into the heap data structure $\mathcal{H}$. Suppose that, because inducing an improving move and currently active in j, move generator (i,j), together with other improving move generators including (i,v), is inserted into

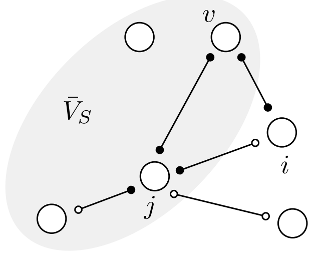

Figure 18 **A portion of an instance containing six customers (circles) and five move generators (lines). A move generator $(v_1, v_2)_\ell$ active in v_1, i.e. $p_{rv_1\ell} \leq \gamma_{v_1}$, is represented with a full circle near to v_1, whereas an empty circle denotes the opposite, i.e. $p_{rv_1\ell} > \gamma_{v_1}$. As an example (i,j) is active in j but not in i. The direction of move generators is not shown because not relevant.**

$\mathcal{H}$. During the SMD search stage, move generator (i, v) is found feasible before the evaluation of (i, j). The move induced by (i, v) is then applied and a number of affected vertices A may be such that $i \in A$ but $j \notin A$. Note that i shares (i, j) with j but (i, j) is not currently active in i because of the sparsification factor γ_i. The SMD update stage requires that, from each vertex $v \in A$ active move generators are updated. *Should (i, j) still be updated even if not active in i?* The answer is yes. Being (i, j) active in j, it may be, as in this scenario, already into the heap $\mathcal{H}$ and possibly be extracted in future search stages. In fact, being i among the affected vertices A because of the application of (i, v), the δ-tag of any move generator involving a vertex $v \in A$ requires an update, and hence (i, j) does. On the other hand, if (i, j) were not active in both j and i, updating it after (i, v) is not required because it would have never being inserted into $\mathcal{H}$.

The dynamic management of vertex-wise move generators may thus require the update of move generators that are not active in one of the affected vertices but only active in the other endpoint that may not be in the list of vertices affected by the move application. A possible implementation uses two additional flags per move generator (i, j) storing whether it is active in i and/or in j. During the SMD update stage the flags are checked to identify whether an update is required.

Finally, this works correctly under the assumption that the sparsification vector $\boldsymbol{\gamma}$ is not changed during a neighborhood exploration.

A.3. SMD Implementation Details of Local Search Operators

In the following, we provide a detailed description of the implementation details for the local search operators used in FILO. In particular, we detail the operator-dependant procedures to be defined when applying a move induced by a move generator (i, j) within an SMD-based operator. To better accomplish this, we introduce few additional notation elements. In particular, we denote by π_i^ℓ and σ_i^ℓ the ℓ^{th}- predecessor and successor of vertex $i \in V$ respectively in the solution under examination. We omit the apex when $\ell = 1$. Moreover, we identify with q_i^{up} and q_i^{from} the cumulative load up to and from any customer $i \in V_c$ included, i.e., $q_i^{up} = q_i + q_{\pi_i} + q_{\pi_i^2} + \ldots + q_0$ and $q_i^{from} = q_i + q_{\sigma_i} + q_{\sigma_i^2} + \ldots + q_0$. Finally, in the following paragraphs, a figure is shown for each local search operator highlighting the move induced by a move generator (i, j) and the set of vertices affected by its application (grayed area). Note that the move generator direction does not necessarily reflect the crossing direction in the resulting route. Finally, as defined in Section 2.2, path is used to refer to a contiguous sequence of vertices belonging to a route, and head and tail are used to denote a path belonging respectively to the initial and final part of a route.

A.3.1. TWOPT. Replace a path of vertices with its reverse.

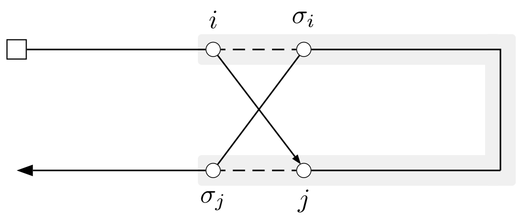

- Type: symmetric.
- Pre-processing: none.
- Cost computation: $\delta_{ij} = -c_{i\sigma_i} + c_{ij} - c_{j\sigma_j} + c_{\sigma_i\sigma_j}$.
- Feasibility Check: $r_i = r_j$.
- Update List: all vertices between i and σ_j, for which successors and predecessors change after the move application.
- Execution: reverse the path between σ_i and j included.

A.3.2. SPLIT. Replace the tail of route r_i with the reversed head of route r_j and replace the head of route r_j with the reversed tail of route r_i.

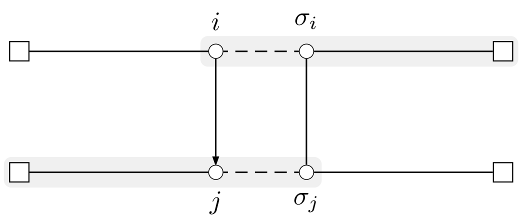

- Type: symmetric.
- Pre-processing: compute q_i^{up} and q_i^{from} for any customer $i \in V_c$.
- Cost Computation: $\delta_{ij} = -c_{i\sigma_i} + c_{ij} - c_{j\sigma_j} + c_{\sigma_i\sigma_j}$.
- Feasibility Check: $(r_i \neq r_j) \wedge (q_i^{up} + q_j^{up} \leq Q) \wedge (q_{\sigma_j}^{from} + q_{\sigma_i}^{from} \leq Q)$.
- Update List: all vertices from i to the depot and from the depot to σ_j, for which successors and predecessors change after the move application.
- Execution: replace (i, σ_i) and (j, σ_j) with (i, j) and (σ_i, σ_j) and reverse paths from depot to j and from σ_i to depot. Update the cumulative load q_v^{up} and q_v^{from} for customers v belonging to r_i and r_j, if not empty.

A.3.3. TAILS. Swap the tails of two different routes.

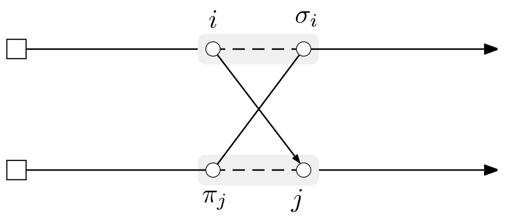

- Type: asymmetric.
- Pre-processing: compute $q_i^{up}(i)$ and q_i^{from} for any customer $i \in V_c$.
- Cost Computation: $\delta_{ij} = -c_{i\sigma_i} + c_{ij} - c_{j\pi_j} + c_{\pi_j\sigma_i}$.
- Feasibility Check: $(r_i \neq r_j) \wedge (q_i^{up} + q_j^{from} \leq Q) \wedge (q_{\pi_j}^{up} + q_{\sigma_i}^{from} \leq Q)$.
- Update List: i, σ_i, j and π_j.
  The update can be restricted to move generators $\{(i,v), (v,\sigma_i), (v,j), (\pi_j, v) : v \in V\} \cap T^\gamma$.
- Execution: replace (i, σ_i) and (π_j, j) with (i, j) and (π_j, σ_i). Update the cumulative load q_v^{up} and q_v^{from} for customers v belonging to r_i and r_j, if not empty.

A.3.4. n0EX with $n \geq 1$. Relocate a path of n vertices within the same or into a different route.

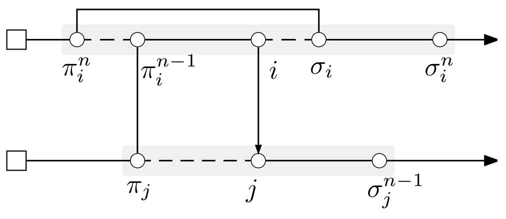

- Type: asymmetric.
- Pre-processing: none.
- Cost Computation: $\delta_{ij} = -c_{\pi_i^n \pi_i^{n-1}} - c_{i\sigma_i} - c_{j\pi_j} + c_{\pi_i^n \sigma_i} + c_{\pi_j \pi_i^{n-1}} + c_{ij}$.
- Feasibility Check: logical disjunction of

— $(r_i = r_j) \wedge \bigwedge_{\ell=1}^{n-1}(j \neq \pi_i^\ell) \wedge (j \neq \sigma_i)$.
When $r_i = r_j$ and $\bigvee_{\ell=1}^{n-1} j = \pi_i^\ell$, the path to relocate overlaps with the destination position.
When $r_i = r_j$ and $j = \sigma_i$, the move does nothing but the δ_{ij} computation is not correct.
— $(r_i \neq r_j) \wedge (i \neq 0) \wedge \bigwedge_{\ell=1}^{n-1}(\pi_i^\ell \neq 0) \wedge (q_{r_j} + q_i + \sum_{\ell=1}^{n-1} q_{\pi_i^\ell} \leq Q)$.
The condition makes sure the depot is not relocated and the capacity constraint of the target route is respected.

- Update List: $\bigcup_{\ell=1}^{n} \pi_i^\ell \cup i \cup \bigcup_{\ell=1}^{n} \sigma_i^\ell \cup \pi_j \cup j \cup \bigcup_{\ell=1}^{n-1} \sigma_j^\ell$.
The update can be restricted to move generators
— $\{(\pi_i^n, v), (\pi_i^{n-1}, v), (v, \pi_i^{n-1}) : v \in V\} \cap T^\gamma$;
— $\{(\pi_i^\ell, v) : \ell = n-2, \dots, 1 \text{ and } v \in V\} \cap T^\gamma$;
— $\{(i, v) : v \in V\} \cap T^\gamma$;
— if $n = 1$ include $\{(v, i) : v \in V\} \cap T^\gamma$;
— $\{(\sigma_i, v), (v, \sigma_i) : v \in V\} \cap T^\gamma$;
— $\{(\sigma_i^\ell, v) : \ell = 2, \dots, n \text{ and } v \in V\} \cap T^\gamma$;
— $\{(\pi_j, v) : v \in V\} \cap T^\gamma$;
— $\{(j, v), (v, j) : v \in V\} \cap T^\gamma$;
— $\{(\sigma_j^\ell, v) : \ell = 1, \dots, n-1 \text{ and } v \in V\} \cap T^\gamma$.
- Execution: replace $(\pi_i^n, \pi_i^{n-1}), (i, \sigma_i)$ and (j, π_j) with $(\pi_i^n, \sigma_i), (\pi_i^{n-1}, \pi_j)$ and (i, j).

A.3.5. *n*0REX with $n \geq 2$. Relocate a reversed path of n vertices within the same or into a different route.

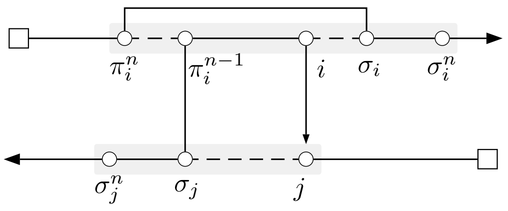

- Type: asymmetric.
- Pre-processing: none.
- Cost Computation: $\delta_{ij} = -c_{\pi_i^n \pi_i^{n-1}} - c_{i\sigma_i} - c_{j\sigma_j} + c_{\pi_i^n \sigma_i} + c_{\sigma_j \pi_i^{n-1}} + c_{ij}$.
- Feasibility Check: logical disjunction of
— $(r_i = r_j) \wedge \bigwedge_{\ell=1}^{n}(j \neq \pi_i^\ell)$.
When $r_i = r_j$ and $\bigvee_{\ell=1}^{n-1} j = \pi_i^\ell$, the path to relocate overlaps with the destination position.
When $r_i = r_j$ and $j = \pi_i^n$, the move could be reduced to a TWOPT induced by move generator (j, i) but would require a special handling in this context.
— $(r_i \neq r_j) \wedge (i \neq 0) \wedge \bigwedge_{\ell=1}^{n-1}(\pi_i^\ell \neq 0) \wedge (q_{r_j} + q_i + \sum_{\ell=1}^{n-1} q_{\pi_i^\ell} \leq Q)$.
The condition makes sure the depot is not relocated and the capacity constraint of the target route is respected.
- Update List: $\bigcup_{\ell=1}^{n} \pi_i^\ell \cup i \cup \bigcup_{\ell=1}^{n} \sigma_i^\ell \cup j \cup \bigcup_{\ell=1}^{n} \sigma_j^\ell$.
The update can be restricted to move generators
— $\{(\pi_i^\ell, v), (\pi_i^\ell, v), (i, v), (v, i) : \ell = n, \dots, 1 \text{ and } v \in V\} \cap T^\gamma$;
— $\{(\sigma_i^\ell, v), (\sigma_j^\ell, v) : \ell = 1, \dots, n \text{ and } v \in V\} \cap T^\gamma$;
— $\{(j, v), (v, j) : v \in V\} \cap T^\gamma$.
- Execution: replace $(\pi_i^n, \pi_i^{n-1}), (i, \sigma_i)$ and (j, σ_j) with $(\pi_i^n, \sigma_i), (\pi_i^{n-1}, \sigma_j)$ and (i, j).

A.3.6. *nm*EX with $1 \leq m \leq n$. Swap a path of n vertices with a path of m vertices within the same or between different routes.

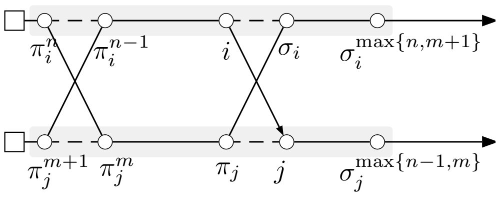

- Type: asymmetric.
- Pre-processing: none.
- Cost Computation: $\delta_{ij} = -c_{\pi_i^n \pi_i^{n-1}} - c_{i\sigma_i} - c_{\pi_j^{m+1}\pi_j^m} - c_{j\pi_j} + c_{\pi_i^n \pi_j^m} + c_{\pi_j \sigma_i} + c_{\pi_j^{m+1}\pi_i^{n-1}} + c_{ij}$.
- Feasibility Check: logical disjunction of
  — $(r_i = r_j) \wedge \bigwedge_{\ell=1}^{n-1}(j \neq \pi_i^\ell) \wedge \bigwedge_{\ell=1}^{m+1}(j \neq \sigma_i^\ell)$.
  When $r_i = r_j$ and $\bigvee_{\ell=1}^{m} j = \sigma_i^\ell \vee \bigvee_{\ell=1}^{n-2} j = \pi_i^\ell$, the paths overlap.
  When $r_i = r_j$ and $j = \sigma_i^{m+1}$, the move could be reduced to a m0EX induced by move generator (σ_i, π_i^{n-1}) or to a n0EX induced by move generator (i,j) but would require a special handling in this context.
  When $r_i = r_j$ and $j = \pi_i^{n-1}$, vertex j is at the same time part of the path to move and destination of the movement.
  — $(r_i \neq r_j) \wedge (i \neq 0) \wedge \bigwedge_{\ell=1}^{n-1}(\pi_i^\ell \neq 0) \wedge \bigwedge_{\ell=1}^{m}(\pi_j^\ell \neq 0) \wedge (q_{r_j} + q_i + \sum_{\ell=1}^{n-1} q_{\pi_i^\ell} - \sum_{\ell=1}^{m} q_{\pi_j^\ell} \leq Q) \wedge (q_{r_i} - q_i - \sum_{\ell=1}^{n-1} q_{\pi_i^\ell} + \sum_{\ell=1}^{m} q_{\pi_j^\ell} \leq Q)$.
  The condition makes sure the depot is not relocated and the capacity constraints are not violated.
- Update List: $\bigcup_{\ell=1}^{n} \pi_i^\ell \cup i \cup \bigcup_{\ell=1}^{\max\{n,m+1\}} \sigma_i^\ell \cup \bigcup_{\ell=1}^{m+1} \pi_j^\ell \cup j \cup \bigcup_{\ell=1}^{\max\{n-1,m\}} \sigma_j^\ell$.
  The update can be restricted to move generators
  — $\{(\pi_i^n, v) : v \in V\} \cap T^\gamma$;
  — $\{(\pi_i^\ell, v) : \ell = n-1, \ldots, 1 \text{ and } v \in V\} \cap T^\gamma$;
  — $\{(v, \pi_i^\ell) : \ell = n-1, \ldots, n-1-m \text{ and } v \in V\} \cap T^\gamma$;
  — $\{(i, v) : v \in V\} \cap T^\gamma$;
  — if $n - m < 2$ include $\{(v, i) : v \in V\} \cap T^\gamma$;
  — $\{(\sigma_i, v), (v, \sigma_i) : v \in V\} \cap T^\gamma$;
  — $\{(\sigma_i^\ell, v) : \ell = 2, \ldots, n \text{ and } v \in V\} \cap T^\gamma$;
  — $\{(v, \sigma_i^\ell) : \ell = 2, \ldots, m+1 \text{ and } v \in V\} \cap T^\gamma$;
  — $\{(\pi_j^{m+1}, v) : v \in V\} \cap T^\gamma$;
  — $\{(\pi_j^\ell, v), (v, \pi_j^\ell) : \ell = m, \ldots, 1 \text{ and } v \in V\} \cap T^\gamma$;
  — $\{(j, v), (v, j) : v \in V\} \cap T^\gamma$
  — $\{(\sigma_j^\ell, v) : \ell = 1, \ldots, n-1 \text{ and } v \in V\} \cap T^\gamma$;
  — $\{(v, \sigma_j^\ell) : \ell = 1, \ldots, m \text{ and } v \in V\} \cap T^\gamma$.
- Execution: replace (π_i^n, π_i^{n-1}), (i, σ_i), (π_j^{m+1}, π_j^m) and (j, π_j) with (π_i^n, π_j^m), $(\pi_i^{n-1}, \pi_j^{m+1})$, (π_j, σ_i) and (i, j).

A.3.7. *nm*REX (and *nm*REX*) with $1 \leq m \leq n$. Swap a reversed path of n vertices with a path of m vertices within the same or between different routes (nmREX). If $m \geq 2$, we consider an additional variant that also reverses the path of m vertices (nmREX*).

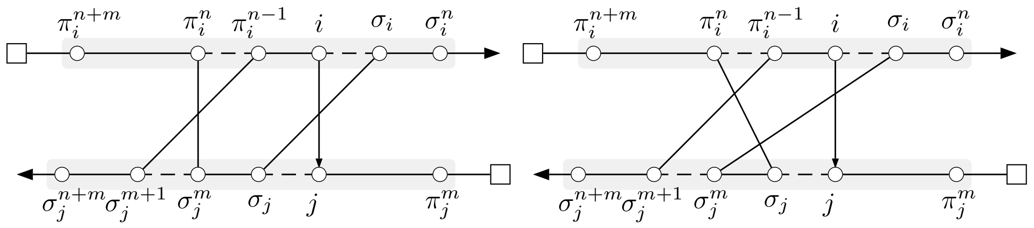

- Type: asymmetric.
- Pre-processing: none.
- Cost Computation:

— nmREX*: $\delta_{ij} = -c_{\pi_i^n \pi_i^{n-1}} - c_{i\sigma_i} - c_{j\sigma_j} - c_{\sigma_j^m \sigma_j^{m+1}} + c_{\pi_i^n \sigma_j^m} + c_{\pi_i^{n-1}\sigma_j^{m+1}} + c_{\sigma_j \sigma_i} + c_{ij}$.
— nmREX: $\delta_{ij} = -c_{\pi_i^n \pi_i^{n-1}} - c_{i\sigma_i} - c_{j\sigma_j} - c_{\sigma_j^m \sigma_j^{m+1}} + c_{\pi_i^n \sigma_j} + c_{\pi_i^{n-1}\sigma_j^{m+1}} + c_{\sigma_j^m \sigma_i} + c_{ij}$.

- Feasibility Check: logical disjunction of
  — $(r_i = r_j) \wedge \bigwedge_{\ell=1}^{n+m} (j \neq \pi_i^\ell)$.
  When $r_i = r_j$ and $\bigvee_{\ell=1}^{n+m-1} j = \sigma_i^\ell$, the paths overlap.
  When $r_i = r_j$ and $j = \sigma_i^{m+n}$
    * nmREX*: the move could be reduced to a TWOPT induced by move generator (j, i);
    * nmREX: the move could be reduced to a n0REX induced by move generator (i, j);
  but, in both cases, this would require a special handling.
  — $(r_i \neq r_j) \wedge (i \neq 0) \wedge \bigwedge_{\ell=1}^{n-1} (\pi_i^\ell \neq 0) \wedge \bigwedge_{\ell=1}^{m} (\sigma_j^\ell \neq 0) \wedge (q_{r_j} + q_i + \sum_{\ell=1}^{n-1} q_{\pi_i^\ell} - \sum_{\ell=1}^{m} q_{\sigma_j^\ell} \leq Q) \wedge (q_{r_i} - q_i - \sum_{\ell=1}^{n-1} q_{\pi_i^\ell} + \sum_{\ell=1}^{m} q_{\sigma_j^\ell} \leq Q)$.
  The condition makes sure the depot is not relocated and the capacity constraints are not violated.
- Update List: $\bigcup_{\ell=1}^{n+m} \pi_i^\ell \cup i \cup \bigcup_{\ell=1}^{n} \sigma_i^\ell \cup \bigcup_{\ell=1}^{m} \pi_j^\ell \cup j \cup \bigcup_{\ell=1}^{n+m} \sigma_j^\ell$.
  The update can be restricted to move generators
  — $\{(v, \pi_i^\ell) : \ell = n+m, \ldots, n+1 \text{ and } v \in V\} \cap T^\gamma$;
  — $\{(\pi_i^\ell, v), (v, \pi_i^\ell) : \ell = n, \ldots, 1 \text{ and } v \in V\} \cap T^\gamma$;
  — $\{(i, v), (v, i) : v \in V\} \cap T^\gamma$;
  — $\{(\sigma_i^\ell, v) : \ell = 1, \ldots, n \text{ and } v \in V\} \cap T^\gamma$;
  — $\{(\sigma_j^\ell, v) : \ell = n+m, \ldots, m+1 \text{ and } v \in V\} \cap T^\gamma$;
  — $\{(\sigma_j^\ell, v), (v, \sigma_j^\ell) : \ell = m, \ldots, 1 \text{ and } v \in V\} \cap T^\gamma$;
  — $\{(j, v), (v, j) : v \in V\} \cap T^\gamma$;
  — $\{(v, \pi_j^\ell) : \ell = 1, \ldots, m \text{ and } v \in V\} \cap T^\gamma$.
- Execution:
  — nmREX*: Replace $(\pi_i^n, \pi_i^{n-1}), (i, \sigma_i), (j, \sigma_j)$ and $(\sigma_j^m, \sigma_j^{m+1})$ with $(\pi_i^n, \sigma_j^m), (\pi_i^{n-1}, \sigma_j^{m+1}), (\sigma_j, \sigma_i)$ and (i, j). Reverse the paths between $\pi^n - 1$ and i and the path between σ_j and σ_j^m.
  — nmREX: Replace $(\pi_i^n, \pi_i^{n-1}), (i, \sigma_i), (j, \sigma_j)$ and $(\sigma_j^m, \sigma_j^{m+1})$ with $(\pi_i^n, \sigma_j), (\pi_i^{n-1}, \sigma_j^{m+1}), (\sigma_j^m, \sigma_i)$ and (i, j). Reverse the path between $\pi^n - 1$ and i.

A.3.8. EJCH. Perform a sequence of 10EX applications.

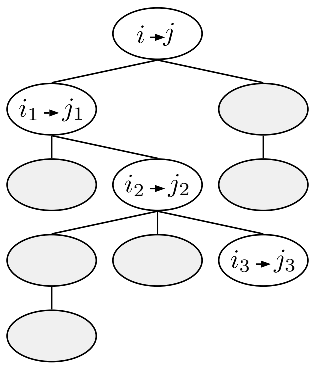

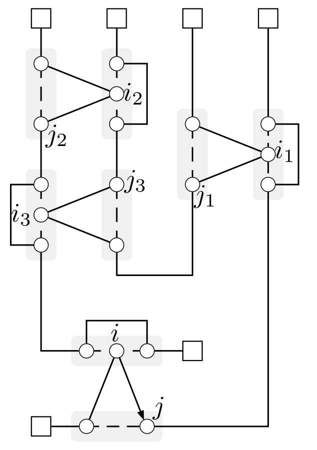

- Type: asymmetric.
- Pre-processing: none.
- Cost Computation: the same as for the 10EX operator.
- Feasibility Check: a tree of nodes associated with 10EX moves is generated by using (i, j) as tree root. A path from the tree root (i, j) to any other node in the tree is a sequence of 10EX moves. Every sequence s stores a number of state variables defining the effect of its application on the current solution. The goal of the feasibility check is to find a sequence whose application generates a feasible and improving solution. In particular, each sequence s contains

—the modified loads q_r^s for each route r affected by 10EX moves of s;
—the variation of the objective function δ_s due to the application of 10EX moves of s;
—a set $\mathcal{F}_i^s$ storing customers that cannot be relocated because already involved in previous relocate actions within s. More precisely, their successors or predecessors have changed due to previous 10EX moves of s but the current structure of the solution does not reflect those changes. Note, in fact, that during the feasibility check we are only simulating the 10EX effects to find a feasible and improving sequence without really changing the solution;
—finally, a set $\mathcal{F}_j^s$ storing customers that cannot be the target of a relocate action because already involved in previous relocate actions within s. More precisely, their predecessors have changed due to previous 10EX moves of s but, as described above, the current structure of the solution does not reflect those changes.

Note that a different handling without $\mathcal{F}_i^s$ and $\mathcal{F}_j^s$ would require to keep a copy of the solution, on which 10EX moves have been applied, for each tree node associated with a sequence s.

A sequence s of 10EX moves generating a cost variation δ_s to the objective function, ending with a move (i_n, j_n) that relocates customer $i_n \in V_c$ from route r_{i_n} to route r_{j_n} before vertex $j_n \in V$ is extended by scanning all customers i_{n+1} belonging to $r_{j_n} = r_{i_{n+1}}$ that satisfy the following joint conditions:

—$q^s_{r_{i_{n+1}}} - q_{i_{n+1}} \leq Q$.
The removal of i_{n+1} restores the feasibility of route $r_{i_{n+1}}$ that was violated by the previous insertion of j_n.
—$i_{n+1} \notin \mathcal{F}_i^s$.
Customer i_{n+1} can be relocated.

Every customer i_{n+1} satisfying the previous conditions is considered as the new starting point for a 10EX for which a potential endpoint is generated by scanning the currently active move generators T^γ that have i_{n+1} as the object of the relocation, i.e., $\{(i_{n+1}, j_{n+1}), j_{n+1} \in V_c\} \cap T^\gamma$. A customer $j_{n+1} \in V_c$ belonging to route $r_{j_{n+1}}$ is selected to be the target of the relocation if it satisfies the following joint conditions:

—$j_{n+1} \neq 0$.
The depot alone does not allow to identify a specific route.
—$r_{i_{n+1}} \neq r_{j_{n+1}}$.
Customer i_{n+1} is relocated into a route different from the origin one.
—$\delta_s + \delta_{i_{n+1}j_{n+1}} < 0$.
Sequence s still provides an improvement to the objective function.
—$j_{n+1} \notin \mathcal{F}_j^s$.
Customer j_{n+1} can be target of a relocation.

Every customer j_{n+1} satisfying the previous conditions is considered as an endpoint for the (i_{n+1}, j_{n+1}) 10EX move and a new tree node s', son of the current one s, is created. State variables of s' are defined as follows:

—$q^{s'}_{r_{i_{n+1}}} = q^s_{r_{i_{n+1}}} - q_{i_{n+1}}$;
—$q^{s'}_{r_{j_{n+1}}} = q^s_{r_{j_{n+1}}} + q_{j_{n+1}}$;
—$\delta_{s'} = \delta_s + \delta_{i_{n+1}j_{n+1}}$;
—$\mathcal{F}_i^{s'} = \mathcal{F}_i^s \cup \{\pi_{i_{n+1}}, i_{n+1}, \sigma_{i_{n+1}}, \pi_{j_{n+1}}, j_{n+1}\}$;
—$\mathcal{F}_j^{s'} = \mathcal{F}_j^s \cup \{i_{n+1}, \sigma_{i_{n+1}}, j_{n+1}\}$.

The tree frontier is explored by following a best-δ-first strategy, that is, the sequence providing the greatest improvement is always extended first. This is obtained by using an additional heap data structure managing the tree nodes. As can be inferred by the above description, sequences are not limited in depth and the same route can be accessed by a 10EX move more than once. A limit is however imposed on the total maximum number of explored tree nodes which in the proposed implementation is $n_{EC} = 25$. Finally, the feasibility check step ends as soon as a feasible sequence is found, i.e., the last 10EX move does not violate the capacity of the target route, or the maximum number of tree nodes is explored.

- Update List: $\mathcal{F}_i^{s^*}$ with s^* a feasible improving sequence.
For each 10EX (i, j) move generator composing the sequence s^*, the update can be restricted to move generators $\{(\pi_i, v), (i, v), (v, i), (\sigma_i, v), (v, \sigma_i), (j, v), (v, j), (\pi_j, v) : v \in V\} \cap T^\gamma$

- Execution: execute the 10EX moves of a feasible sequence. Note that, due to the restrictions imposed during the sequence space exploration, the order in which moves are executed does not affect the final result.

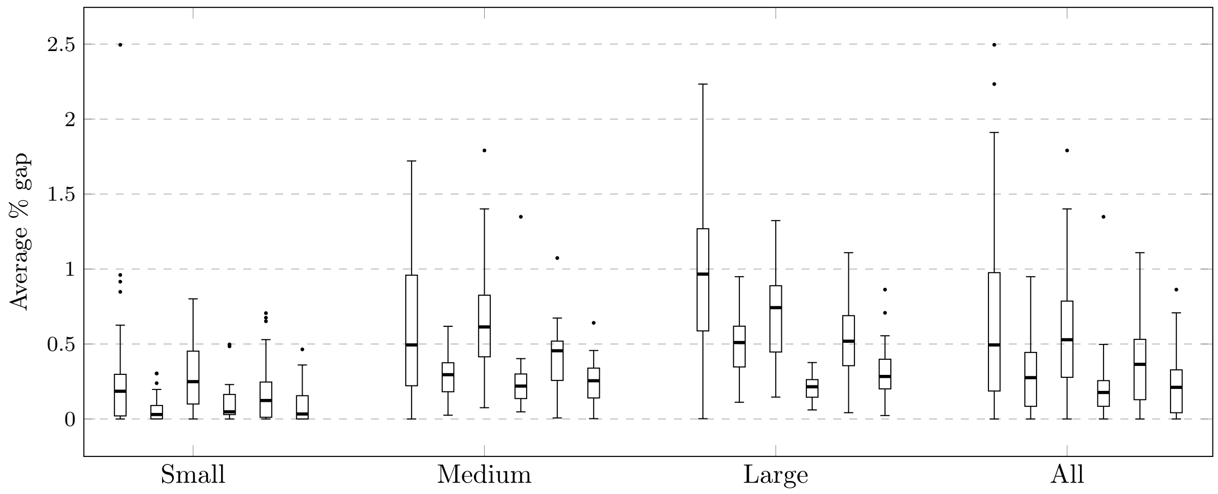

Figure 19 Comparison of average gaps obtained by algorithms on the 𝕏 dataset. For each group, boxplots, from left to right, are associated with: ILS-SP, HGSADC, KGLS, SISR, FILO, and FILO (long).

Appendix B: Computational details for 𝕏 instances

Detailed results about computations on the 𝕏 dataset can be found in Tables 9 – 11 and Figure 19. Moreover, to better assess whether results obtained by FILO are statistically different with respect to competing algorithms, we followed the procedure used in Christiaens and Vanden Berghe (2020). In particular, we conducted a one-tailed Wilcoxon signed-rand test (Wilcoxon (1945)) in which we consider a null hypothesis H_0

$$H_0 : \textsc{AverageCost}(FILO) = \textsc{AverageCost}(X)$$

and an alternative hypothesis H_1

$$H_1 : \textsc{AverageCost}(FILO) > \textsc{AverageCost}(X)$$

where X can be ILS-SP, HGSADC, KGLS, and SISR. We tested the above hypotheses on small, medium, large and over all the instances. The p-values associated with the tested hypothesis are shown in Table 8 (left). The p-values for a similar analysis, in which we compared FILO (long) with competing methods is shown in Table 8 (right).

A hypothesis is rejected when its associated p-value is greater than a significance level α. Failing to reject H_0 means that the average results of the two compared methods are not statistically different. On the other hand, when H_0 is rejected, the average results obtained by the methods are statistically different and the alternative hypothesis H_1 can be tested to find whether the average results obtained by FILO are statistically greater than those of the competing method. Rejecting H_1 implies that FILO performs better than the competing method.

When performing multiple comparisons involving the same data, the probability of erroneously rejecting a null hypothesis increases. To control these errors, the significance level α is typically adjusted to lower values. Bonferroni correction (Dunn (1961)) is a simple method used to adjust α when performing multiple comparisons. In particular, given n comparisons, the significance level is set to α/n. In our case, for each FILO configuration, we tested a total number of $n = 8$ hypotheses corresponding to the partitioning of instances (Small, Medium, Large, and All) and to the two hypotheses (H_0 and H_1). Thus, by assuming an initial significance level $\alpha_0 = 0.025$, the adjusted value becomes $\alpha = \alpha_0/8 = 0.003125$.

As can ben seen from Table 8 (left)

- FILO performs better than ILS-SP on large instances and on all the 𝕏 dataset, and it has a similar performance on small and medium instances;
- FILO has a similar performance compared to HGSADC on large instances and on the whole 𝕏 dataset, however, HGSADC performs better on small and medium instances;
- FILO performs better than KGLS on medium and large instances, as well as on all the 𝕏 dataset, and it has a similar performance on small instances;

Table 8 Computations on the $\mathbb{X}$ dataset: p-values for FILO on the left and FILO (long) on the right.

	Small					Small			
	ILS-SP	HGSADC	KGLS	SISR		ILS-SP	HGSADC	KGLS	SISR
H_0	0.309491	**0.000273**	0.020427	0.064141	H_0	**0.000273**	0.808654	**0.000140**	0.130121
H_1	0.154746	0.999876	0.010214	0.969381	H_1	**0.000136**	0.404327	**0.000070**	0.065061
	Similar	Worse	Similar	Similar		Better	Similar	Better	Similar
	Medium					Medium			
	ILS-SP	HGSADC	KGLS	SISR		ILS-SP	HGSADC	KGLS	SISR
H_0	0.071754	**0.001737**	**0.000000**	**0.000066**	H_0	**0.001057**	0.046584	**0.000000**	0.346122
H_1	0.035877	0.999183	**0.000000**	0.999970	H_1	**0.000528**	0.023292	**0.000000**	0.830925
	Similar	Worse	Better	Worse		Better	Similar	Better	Similar
	Large					Large			
	ILS-SP	HGSADC	KGLS	SISR		ILS-SP	HGSADC	KGLS	SISR
H_0	**0.000335**	1.000000	**0.000234**	**0.000000**	H_0	**0.000000**	**0.000837**	**0.000000**	**0.002227**
H_1	**0.000167**	0.503678	**0.000117**	1.000000	H_1	**0.000000**	**0.000419**	**0.000000**	0.998963
	Better	Similar	Better	Worse		Better	Better	Better	Worse
	All					All			
	ILS-SP	HGSADC	KGLS	SISR		ILS-SP	HGSADC	KGLS	SISR
H_0	**0.000036**	0.007739	**0.000000**	**0.000000**	H_0	**0.000000**	**0.000111**	**0.000000**	0.065432
H_1	**0.000018**	0.996173	**0.000000**	1.000000	H_1	**0.000000**	**0.000056**	**0.000000**	0.967546
	Better	Similar	Better	Worse		Better	Better	Better	Similar

p-values in bold are associated with rejected hypothesis when $\alpha = 0.003125$.
The last row of each group contains a p-value interpretation when $\alpha = 0.003125$. In particular, FILO is not statistically different from the competing method when H_0 cannot be rejected (Similar), FILO is statistically better when both H_0 and H_1 are rejected (Better), and, finally, FILO is statistically worse when H_0 is rejected and H_1 is not rejected (Worse).

- finally, FILO has a similar performance compared to SISR on small instances, however, SISR performs better on medium, large and on all the $\mathbb{X}$ dataset.

Table 8 (right) shows a similar analysis comparing FILO (long) with the other methods. In particular,

- FILO (long) performs better than ILS-SP on all partitions of instances;
- FILO (long) performs better than HGSADC on large and on all the $\mathbb{X}$ dataset, and it has a similar performance on small and medium instances;
- FILO (long) performs better than KGLS an all partitions of instances;
- finally, FILO has a similar performance compared to SISR on small, medium and on the whole $\mathbb{X}$ dataset, however, SISR performs better on large instances.

Table 9 **Computations on small-sized $\mathbb{X}$ instances.**

		ILS-SP		HGSADC		KGLS		SISR		FILO				FILO (long)			
ID	BKS	Avg	$\hat{t}^1$	Avg	$\hat{t}^1$	Avg	$\hat{t}$	Avg	$\hat{t}$	Best	Avg	Worst	t	Best	Avg	Worst	t
X-n101-k25	27591	0.00	0.06–0.07	0.00	0.85–0.91	0.21	2.69	0.00	0.58	0.00	0.00	0.22	1.10	0.00	0.00	0.00	11.89
X-n106-k14	26362	0.05	1.22–1.31	0.08	2.43–2.61	0.19	2.83	0.07	0.95	0.00	0.06	0.11	1.82	0.00	0.02	0.08	19.64
X-n110-k13	14971	0.00	0.12–0.13	0.00	0.97–1.04	0.00	2.94	0.00	0.73	0.00	0.00	0.00	1.63	0.00	0.00	0.00	16.43
X-n115-k10	12747	0.00	0.12–0.13	0.00	1.09–1.17	0.00	3.07	0.00	0.15	0.00	0.00	0.00	1.65	0.00	0.00	0.00	16.94
X-n120-k6	13332	0.04	1.03–1.11	0.00	1.40–1.50	0.00	3.21	0.00	1.16	0.00	0.00	0.00	1.74	0.00	0.00	0.00	18.36
X-n125-k30	55539	0.24	0.85–0.91	0.01	1.64–1.76	0.47	3.34	0.03	2.25	0.00	0.53	1.37	1.24	0.00	0.16	0.61	11.75
X-n129-k18	28940	0.20	1.15–1.24	0.03	1.64–1.76	0.11	3.45	0.03	1.09	0.00	0.06	0.19	1.58	0.00	0.03	0.05	17.72
X-n134-k13	10916	0.29	1.28–1.37	0.17	2.01–2.15	0.00	3.58	0.22	2.04	0.00	0.15	0.30	1.58	0.00	0.06	0.16	16.81
X-n139-k10	13590	0.10	0.97–1.04	0.00	1.40–1.50	0.00	3.72	0.04	1.45	0.00	0.00	0.00	1.98	0.00	0.00	0.00	21.84
X-n143-k7	15700	0.29	0.97–1.04	0.00	1.88–2.02	0.18	3.83	0.04	1.53	0.15	0.17	0.43	1.55	0.00	0.14	0.17	17.78
X-n148-k46	43448	0.01	0.49–0.52	0.00	1.95–2.09	0.35	3.96	0.05	2.04	0.00	0.12	0.35	1.36	0.00	0.01	0.33	15.10
X-n153-k22	21220	0.85	0.30–0.33	0.03	3.34–3.59	0.80	4.10	0.04	4.07	0.02	0.22	0.69	1.66	0.02	0.05	0.34	15.30
X-n157-k13	16876	0.00	0.49–0.52	0.00	1.95–2.09	0.00	4.20	0.02	2.69	0.00	0.00	0.00	2.57	0.00	0.00	0.00	28.74
X-n162-k11	14138	0.16	0.30–0.33	0.02	2.01–2.15	0.06	4.34	0.14	2.47	0.02	0.18	0.23	1.82	0.00	0.09	0.18	18.95
X-n167-k10	20557	0.25	0.55–0.59	0.03	2.25–2.41	0.16	4.47	0.02	2.33	0.00	0.05	0.17	1.91	0.00	0.00	0.02	20.19
X-n172-k51	45607	0.02	0.36–0.39	0.00	2.31–2.48	0.44	4.61	0.03	3.85	0.00	0.01	0.14	1.15	0.00	0.00	0.00	12.65
X-n176-k26	47812	0.92	0.67–0.72	0.30	4.62–4.96	0.39	4.71	0.08	3.78	0.00	0.65	1.25	1.35	0.00	0.19	1.13	14.28
X-n181-k23	25569	0.01	0.97–1.04	0.09	3.83–4.11	0.23	4.85	0.04	4.00	0.00	0.02	0.10	2.22	0.00	0.00	0.01	23.70
X-n186-k15	24145	0.17	1.03–1.11	0.01	3.59–3.85	0.20	4.98	0.14	2.91	0.01	0.10	0.30	1.55	0.00	0.04	0.21	15.94
X-n190-k8	16980	0.96	1.28–1.37	0.05	7.36–7.90	0.33	5.09	0.03	6.62	0.00	0.09	0.44	1.80	0.00	0.02	0.05	18.47
X-n195-k51	44225	0.02	0.55–0.59	0.04	3.71–3.98	0.49	5.23	0.17	4.44	0.00	0.18	0.53	1.25	0.00	0.06	0.26	12.03
X-n200-k36	58578	0.20	4.56–4.89	0.08	4.86–5.22	0.29	5.36	0.10	4.87	0.18	0.68	1.91	1.32	0.08	0.36	0.51	16.17
X-n204-k19	19565	0.31	0.67–0.72	0.03	3.22–3.46	0.52	5.47	0.50	3.56	0.00	0.13	0.70	1.41	0.00	0.01	0.12	14.90
X-n209-k16	30656	0.36	2.31–2.48	0.08	5.23–5.61	0.27	5.60	0.04	4.36	0.00	0.12	0.27	1.31	0.00	0.05	0.12	13.70
X-n214-k11	10856	2.50	1.40–1.50	0.20	6.20–6.66	0.67	5.74	0.48	6.33	0.13	0.43	1.11	1.37	0.04	0.23	0.93	14.22
X-n219-k73	117595	0.00	0.49–0.52	0.01	4.68–5.02	0.09	5.87	0.05	5.82	0.00	0.00	0.01	4.94	0.00	0.00	0.00	54.01
X-n223-k34	40437	0.24	5.17–5.55	0.15	5.05–5.42	0.63	5.98	0.23	5.53	0.08	0.28	0.66	1.22	0.00	0.16	0.27	12.84
X-n228-k23	25742	0.21	1.46–1.57	0.14	5.96–6.39	0.34	6.12	0.19	7.64	0.03	0.21	0.45	1.33	0.00	0.16	0.25	13.84
X-n233-k16	19230	0.55	1.82–1.96	0.30	4.13–4.44	0.58	6.25	0.21	5.89	0.16	0.42	0.71	1.56	0.00	0.30	0.54	17.24
X-n237-k14	27042	0.14	2.13–2.28	0.09	5.41–5.81	0.38	6.36	0.18	5.24	0.00	0.03	0.50	2.13	0.00	0.01	0.16	23.67
X-n242-k48	82751	0.15	10.82–11.61	0.24	7.54–8.09	0.47	6.49	0.16	7.20	0.09	0.31	0.58	1.51	0.00	0.16	0.39	16.81
X-n247-k50	37274	0.63	1.28–1.37	0.03	12.40–13.31	0.17	6.63	0.13	13.38	0.06	0.71	1.30	1.56	0.00	0.46	1.05	16.08
Mean		0.31	1.46 – 1.57	0.07	3.65 – 3.92	0.28	4.66	0.11	3.78	0.03	0.18	0.47	1.69	0.00	0.09	0.25	18.06

[1] computed by considering the range of single-thread rating of compatible CPUs.

Table 10 **Computations on medium-sized $\mathbb{X}$ instances.**

		ILS-SP		HGSADC		KGLS		SISR		FILO				FILO (long)			
ID	BKS	Avg	$\hat{t}^1$	Avg	$\hat{t}^1$	Avg	$\hat{t}$	Avg	$\hat{t}$	Best	Avg	Worst	t	Best	Avg	Worst	t
X-n251-k28	38684	0.40	6.57–7.05	0.29	7.11–7.63	0.60	6.74	0.28	7.13	0.17	0.36	0.66	1.57	0.00	0.25	0.38	17.38
X-n256-k16	18839	0.24	1.22–1.31	0.22	3.95–4.24	0.32	6.87	0.26	8.36	0.22	0.22	0.23	2.13	0.22	0.22	0.22	23.80
X-n261-k13	26558	1.17	4.07–4.37	0.27	7.72–8.29	0.55	7.00	0.32	8.58	0.17	0.48	1.27	1.56	0.01	0.31	0.50	16.98
X-n266-k58	75478	0.11	6.08–6.53	0.37	13.01–13.96	0.65	7.14	0.19	7.86	0.18	0.51	0.87	1.80	0.07	0.38	0.57	20.67
X-n270-k35	35291	0.21	5.53–5.94	0.22	6.81–7.31	0.46	7.25	0.20	8.29	0.05	0.26	0.44	1.40	0.05	0.15	0.27	14.17
X-n275-k28	21245	0.05	2.19–2.35	0.17	7.29–7.83	0.26	7.38	0.11	9.67	0.00	0.08	0.37	1.87	0.00	0.02	0.39	20.23
X-n280-k17	33503	0.80	5.84–6.26	0.31	11.61–12.46	0.61	7.52	0.37	12.87	0.05	0.46	0.76	1.47	0.04	0.36	0.52	15.52
X-n284-k15	20215	1.16	5.23–5.61	0.35	12.10–12.99	0.86	7.62	0.35	11.13	0.15	0.53	1.03	1.58	0.06	0.26	0.53	15.51
X-n289-k60	95151	0.31	9.79–10.51	0.33	12.95–13.90	0.77	7.76	0.21	10.40	0.31	0.60	0.86	1.77	0.24	0.40	0.61	20.07
X-n294-k50	47161	0.20	7.54–8.09	0.21	8.94–9.59	0.61	7.89	0.24	10.69	0.14	0.32	0.59	1.12	0.12	0.23	0.35	11.80
X-n298-k31	34231	0.37	4.19–4.50	0.18	6.63–7.11	0.30	8.00	0.13	10.55	0.00	0.27	0.46	1.18	0.01	0.19	0.31	12.36
X-n303-k21	21738	0.73	8.63–9.27	0.52	10.52–11.29	0.64	8.14	0.18	12.58	0.21	0.45	0.89	1.23	0.09	0.33	0.66	11.91
X-n308-k13	25859	0.94	5.77–6.20	0.14	9.30–9.98	0.82	8.27	1.35	18.69	0.01	0.51	1.83	1.62	0.02	0.46	1.42	18.27
X-n313-k71	94044	0.27	10.64–11.42	0.24	13.62–14.62	0.85	8.41	0.15	13.75	0.29	0.52	0.81	1.39	0.15	0.32	0.57	15.23
X-n317-k53	78355	0.00	5.23–5.61	0.04	13.62–14.62	0.08	8.51	0.05	16.00	0.00	0.01	0.04	3.02	0.00	0.00	0.01	31.68
X-n322-k28	29834	0.53	8.94–9.59	0.41	9.24–9.92	0.68	8.65	0.31	12.29	0.25	0.48	0.88	1.25	0.05	0.34	0.54	13.19
X-n327-k20	27532	1.02	11.61–12.46	0.35	11.06–11.88	0.44	8.78	0.36	15.71	0.17	0.47	0.81	1.71	0.09	0.29	0.55	19.83
X-n331-k15	31102	0.43	9.54–10.24	0.19	14.83–15.92	0.13	8.89	0.08	14.84	0.00	0.02	0.30	2.00	0.00	0.00	0.01	21.59
X-n336-k84	139111	0.25	13.01–13.96	0.30	23.10–24.80	1.40	9.03	0.19	16.58	0.36	0.61	0.93	1.41	0.19	0.38	0.55	13.80
X-n344-k43	42050	0.56	13.74–14.75	0.38	13.19–14.16	0.83	9.24	0.26	15.64	0.28	0.58	0.80	1.35	0.03	0.33	0.56	12.67
X-n351-k40	25896	0.98	15.32–16.44	0.46	20.49–21.99	1.03	9.43	0.33	19.27	0.33	0.67	1.03	1.36	0.26	0.45	0.72	13.06
X-n359-k29	51505	1.11	29.73–31.91	0.42	21.21–22.77	0.94	9.64	0.14	16.80	0.16	0.48	0.85	1.51	0.00	0.24	0.45	16.30
X-n367-k17	22814	0.83	7.96–8.55	0.11	13.37–14.36	0.69	9.86	0.09	26.26	0.00	0.19	0.68	1.65	0.00	0.04	0.15	17.03
X-n376-k94	147713	0.00	4.32–4.63	0.03	17.20–18.47	0.11	10.10	0.05	23.28	0.00	0.01	0.03	4.17	0.00	0.01	0.03	43.35
X-n384-k52	65940	0.66	20.97–22.51	0.50	24.44–26.23	0.70	10.32	0.25	18.84	0.19	0.46	0.74	1.71	0.13	0.27	0.51	18.01
X-n393-k38	38260	0.52	12.64–13.57	0.30	17.39–18.66	0.32	10.56	0.35	22.11	0.10	0.29	0.61	1.41	0.03	0.12	0.37	14.97
X-n401-k29	66187	0.80	36.72–39.41	0.27	30.09–32.30	0.58	10.78	0.09	27.64	0.09	0.22	0.44	1.98	0.02	0.10	0.20	19.96
X-n411-k19	19712	1.23	14.47–15.53	0.16	21.09–22.64	1.79	11.05	0.29	42.48	0.22	0.52	1.49	1.82	0.24	0.37	0.84	18.87
X-n420-k130	107798	0.04	13.49–14.49	0.12	32.34–34.71	0.51	11.29	0.08	34.84	0.08	0.25	0.50	1.16	0.04	0.14	0.26	11.29
X-n429-k61	65467	0.43	23.22–24.93	0.28	25.23–27.08	0.54	11.53	0.19	25.46	0.19	0.39	0.75	1.40	0.01	0.19	0.33	14.55
X-n439-k37	36391	0.14	24.07–25.84	0.17	20.97–22.51	0.31	11.80	0.23	30.62	0.01	0.09	0.25	1.64	0.01	0.02	0.10	17.74
X-n449-k29	55254	1.72	36.41–39.09	0.54	39.45–42.35	0.89	12.07	0.28	27.64	0.34	0.62	1.02	1.46	0.18	0.34	0.67	15.14
X-n459-k26	24145	1.31	36.84–39.54	0.53	26.02–27.93	0.39	12.34	0.40	41.10	0.09	0.31	0.86	1.57	0.00	0.21	0.39	16.51
X-n469-k138	221824	0.16	22.07–23.69	0.36	52.70–56.57	0.73	12.61	0.18	34.91	0.73	1.07	1.36	1.62	0.47	0.64	0.80	16.03
X-n480-k70	89449	0.47	30.64–32.89	0.35	40.73–43.72	0.58	12.90	0.12	36.73	0.15	0.36	0.55	1.63	0.02	0.21	0.41	17.09
X-n491-k59	66487	1.11	31.73–34.06	0.62	43.71–46.92	1.16	13.20	0.24	37.39	0.29	0.53	0.84	1.40	0.12	0.32	0.50	13.88
Mean		0.59	14.05 – 15.09	0.30	18.42 – 19.77	0.64	9.40	0.25	19.64	0.17	0.39	0.75	1.66	0.08	0.25	0.45	17.51

[1] computed by considering the range of single-thread rating of compatible CPUs.

Table 11 **Computations on large-sized $\mathbb{X}$ instances.**

		ILS-SP		HGSADC		KGLS		SISR		FILO				FILO (long)			
ID	BKS	Avg	$\hat{t}$[1]	Avg	$\hat{t}$[1]	Avg	$\hat{t}$	Avg	$\hat{t}$	Best	Avg	Worst	t	Best	Avg	Worst	t
X-n502-k39	69226	0.17	49.12–52.72	0.15	38.66–41.50	0.15	13.50	0.07	44.30	0.00	0.04	0.10	2.52	0.00	0.03	0.07	25.92
X-n513-k21	24201	0.96	21.28–22.84	0.40	20.12–21.60	0.36	13.79	0.38	56.08	0.06	0.35	0.86	1.84	0.00	0.15	0.40	19.54
X-n524-k153	154593	0.27	16.60–17.81	0.25	49.06–52.66	0.48	14.09	0.14	110.12	0.08	0.50	0.99	1.38	0.04	0.24	0.56	13.68
X-n536-k96	94868	0.88	37.75–40.52	0.49	65.35–70.15	1.06	14.41	0.32	54.33	0.71	0.83	1.00	1.58	0.53	0.71	0.83	16.02
X-n548-k50	86700	0.20	38.90–41.76	0.34	51.18–54.94	0.25	14.74	0.11	46.91	0.00	0.10	0.25	1.86	0.00	0.05	0.13	19.60
X-n561-k42	42717	0.97	41.88–44.96	0.35	36.84–39.54	0.64	15.09	0.35	53.68	0.21	0.43	0.74	1.32	0.08	0.29	0.54	13.49
X-n573-k30	50673	0.99	68.08–73.08	0.48	114.40–122.80	0.68	15.41	0.26	82.19	0.22	0.37	0.66	1.91	0.15	0.25	0.38	20.00
X-n586-k159	190316	0.32	47.72–51.22	0.27	106.56–114.39	0.41	15.76	0.15	62.77	0.45	0.70	0.98	1.62	0.22	0.37	0.63	16.39
X-n599-k92	108451	0.86	44.38–47.63	0.57	76.53–82.15	0.87	16.11	0.22	54.84	0.30	0.51	0.74	1.68	0.19	0.30	0.45	17.58
X-n613-k62	59545	1.51	45.47–48.81	0.70	71.30–76.54	0.93	16.49	0.31	64.08	0.39	0.67	1.11	1.16	0.06	0.40	0.76	11.35
X-n627-k43	62173	1.18	98.90–106.16	0.56	145.71–156.41	0.71	16.87	0.23	64.95	0.17	0.34	0.54	1.80	0.09	0.20	0.41	18.65
X-n641-k35	63705	1.41	85.35–91.61	0.76	96.53–103.62	0.52	17.24	0.23	67.28	0.13	0.38	0.66	1.88	0.11	0.22	0.45	19.10
X-n655-k131	106780	0.00	28.69–30.80	0.11	91.49–98.20	0.18	17.62	0.06	79.72	0.01	0.04	0.08	3.23	0.00	0.02	0.05	33.44
X-n670-k130	146332	0.92	37.20–39.93	0.61	160.54–172.33	1.00	18.02	0.27	144.67	0.66	1.11	1.70	1.42	0.43	0.86	1.24	14.16
X-n685-k75	68225	1.12	44.86–48.16	0.63	95.25–102.25	1.03	18.43	0.21	98.27	0.44	0.63	0.88	1.42	0.16	0.43	0.67	13.65
X-n701-k44	81923	1.37	127.72–137.09	0.69	153.91–165.22	0.77	18.86	0.17	89.10	0.36	0.53	0.69	1.57	0.06	0.28	0.51	15.91
X-n716-k35	43387	1.81	137.26–147.34	0.59	160.66–172.46	0.89	19.26	0.22	115.14	0.49	0.70	1.06	1.67	0.14	0.28	0.50	17.14
X-n733-k159	136190	0.63	67.84–72.82	0.29	148.63–159.54	0.86	19.72	0.15	104.16	0.18	0.36	0.48	1.26	0.09	0.21	0.31	12.84
X-n749-k98	77314	1.24	77.32–83.00	0.71	190.81–204.82	1.32	20.15	0.25	106.41	0.54	0.71	0.88	1.45	0.28	0.42	0.63	13.90
X-n766-k71	114456	1.12	147.17–157.97	0.60	232.82–249.91	0.84	20.61	0.27	126.85	0.46	0.68	1.07	1.59	0.24	0.43	0.76	15.76
X-n783-k48	72394	1.84	143.16–153.67	0.85	163.94–175.98	0.89	21.07	0.37	123.80	0.34	0.61	0.87	1.75	0.18	0.35	0.57	18.54
X-n801-k40	73331	0.92	262.97–282.28	0.55	175.80–188.71	0.26	21.55	0.14	99.72	0.02	0.23	0.41	1.80	-0.02	0.11	0.26	18.28
X-n819-k171	158121	0.82	90.51–97.16	0.49	227.53–244.24	0.89	22.04	0.19	125.47	0.65	0.84	1.05	1.39	0.44	0.56	0.67	14.31
X-n837-k142	193737	0.67	105.28–113.02	0.38	281.69–302.38	0.76	22.52	0.12	121.32	0.37	0.53	0.70	1.78	0.21	0.31	0.42	18.57
X-n856-k95	88990	0.32	93.43–100.29	0.28	175.31–188.19	0.34	23.03	0.16	116.38	0.02	0.14	0.28	1.76	-0.00	0.06	0.16	18.00
X-n876-k59	99303	1.12	248.80–267.07	0.59	301.14–323.26	0.95	23.57	0.18	158.13	0.32	0.47	0.63	1.74	0.15	0.26	0.38	17.46
X-n895-k37	53928	1.91	249.35–267.66	0.95	195.68–210.05	0.73	24.09	0.29	154.56	0.33	0.58	0.94	1.77	0.02	0.26	0.55	17.93
X-n916-k207	329179	0.54	137.44–147.53	0.31	340.90–365.93	0.58	24.65	0.10	156.60	0.50	0.70	0.85	1.75	0.17	0.39	0.55	18.98
X-n936-k151	132812	1.29	123.10–132.13	0.53	323.09–346.81	0.87	25.19	0.23	300.18	0.39	0.91	1.38	1.32	0.24	0.50	0.79	12.70
X-n957-k87	85469	0.55	189.17–203.06	0.41	263.15–282.47	0.34	25.76	0.18	147.22	0.04	0.14	0.24	1.86	0.00	0.09	0.20	18.93
X-n979-k58	118988	1.06	417.73–448.41	0.43	336.76–361.49	0.63	26.35	0.11	201.19	0.26	0.37	1.02	2.36	0.12	0.23	0.35	23.76
X-n1001-k43	72369	2.23	481.93–517.32	0.81	333.72–358.23	0.95	26.94	0.22	206.79	0.41	0.65	0.83	1.65	0.15	0.33	0.53	16.40
Mean		0.98	118.95 – 127.68	0.50	163.28 – 175.27	0.69	19.47	0.21	110.54	0.30	0.50	0.77	1.72	0.14	0.30	0.49	17.56

[1] computed by considering the range of single-thread rating of compatible CPUs.
New best solutions: (X-n801-k40, 73313);(X-n856-k95, 88989)

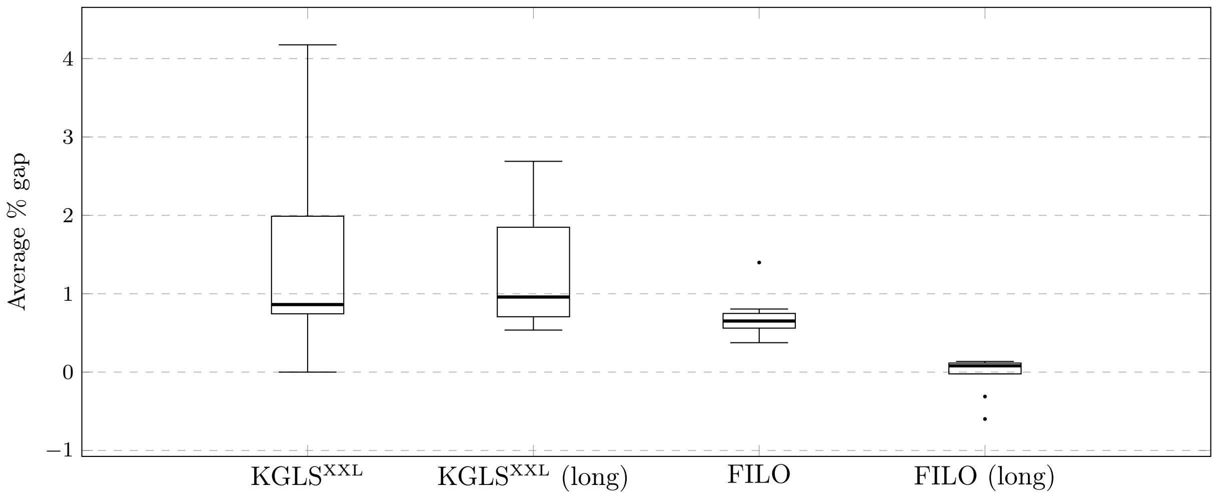

Figure 20 **Comparison of average gaps obtained by algorithms on the $\mathbb{B}$ dataset.**

Table 12 **Computations on the $\mathbb{B}$ dataset: p-values for FILO on the left and for FILO (long) on the right.**

	KGLS$^{\text{XXL}}$	KGLS$^{\text{XXL}}$ (long)
H_0	**0.001953**	0.037109
H_1	**0.000977**	0.018555
	Better	Similar

	KGLS$^{\text{XXL}}$	KGLS$^{\text{XXL}}$ (long)
H_0	**0.001953**	**0.001953**
H_1	**0.000977**	**0.000977**
	Better	Better

p-values in bold are associated with rejected hypothesis when $\alpha = 0.0125$.
The last row contains a p-value interpretation when $\alpha = 0.0125$. In particular, FILO is not statistically different from the competing method when H_0 cannot be rejected (Similar), FILO is statistically better when both H_0 and H_1 are rejected (Better), and, finally, FILO is statistically worse when H_0 is rejected and H_1 is not rejected (Worse).

Appendix C: Computational details for very large-scale instances

This section contains computational details associated with large-scale datasets. In particular, Figures 20, 21 and 22 show by means of boxplots the average gaps obtained by algorithms on the $\mathbb{B}$, $\mathbb{K}$, and $\mathbb{Z}$ dataset, respectively. Average solution values are analyzed by conducting analysis similar to those for the $\mathbb{X}$ dataset of Section B. In particular, the null hypothesis H_0 and the alternative hypothesis H_1 are the same. However, contrarily to previous analysis, we did not partition dataset instances in smaller groups. Thus the total number of analysis performed for each dataset is $n = 2$, one for each hypothesis. The initial confidence level $\alpha_0 = 0.025$ is thus adjusted through the Bonferroni correction to $\alpha = 0.025/2 = 0.0125$. Tables 12 and 13 shows the p-values associated with the $\mathbb{B}$ and $\mathbb{K}$ datasets, respectively. Finally, due to the very limited number of instances of the $\mathbb{Z}$ dataset, the Wilcoxon signed-rank test cannot be used because it cannot give a significant result.

As can be seen from Table 12

- FILO performs better than KGLS$^{\text{XXL}}$ and it has a performance similar to that of KGLS$^{\text{XXL}}$ (long);
- FILO (long) performs better than KGLS$^{\text{XXL}}$ and KGLS$^{\text{XXL}}$ (long).

As can be seen from Table 13, both FILO and FILO (long) performs better than KGLS$^{\text{XXL}}$ and KGLS$^{\text{XXL}}$ (long).

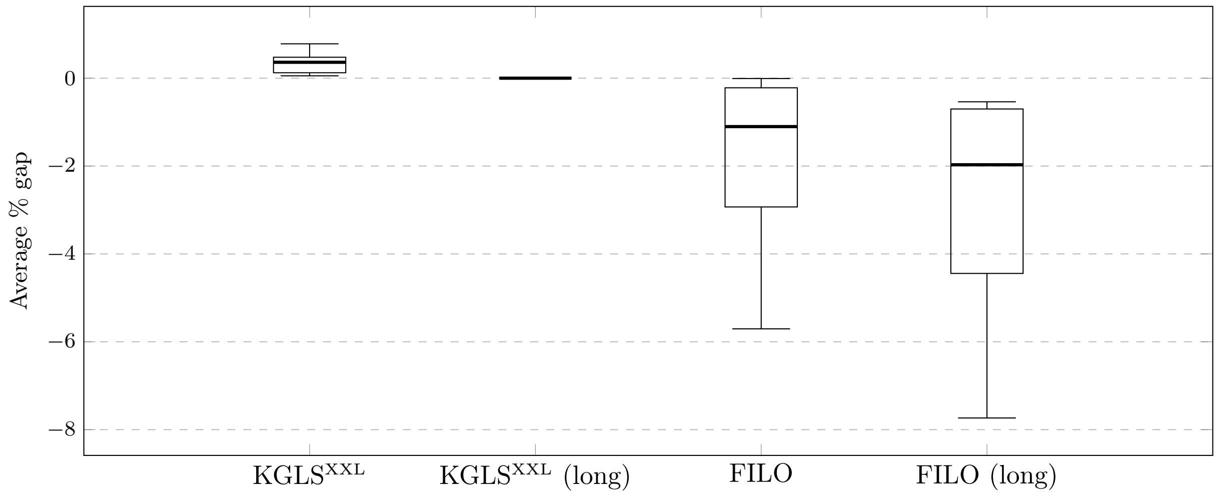

Figure 21 Comparison of average gaps obtained by algorithms on the $\mathbb{K}$ dataset.

Table 13 Computations on the $\mathbb{K}$ dataset: p-values for FILO on the left and for FILO (long) on the right.

	KGLS^{XXL}	KGLS^{XXL} (long)
H_0	**0.0078125**	**0.0078125**
H_1	**0.00390625**	**0.00390625**
	Better	Better

	KGLS^{XXL}	KGLS^{XXL} (long)
H_0	**0.0078125**	**0.0078125**
H_1	**0.00390625**	**0.00390625**
	Better	Better

p-values in bold are associated with rejected hypothesis when $\alpha = 0.0125$.
The last row contains a p-value interpretation when $\alpha = 0.0125$. In particular, FILO is not statistically different from the competing method when H_0 cannot be rejected (Similar), FILO is statistically better when both H_0 and H_1 are rejected (Better), and, finally, FILO is statistically worse when H_0 is rejected and H_1 is not rejected (Worse).

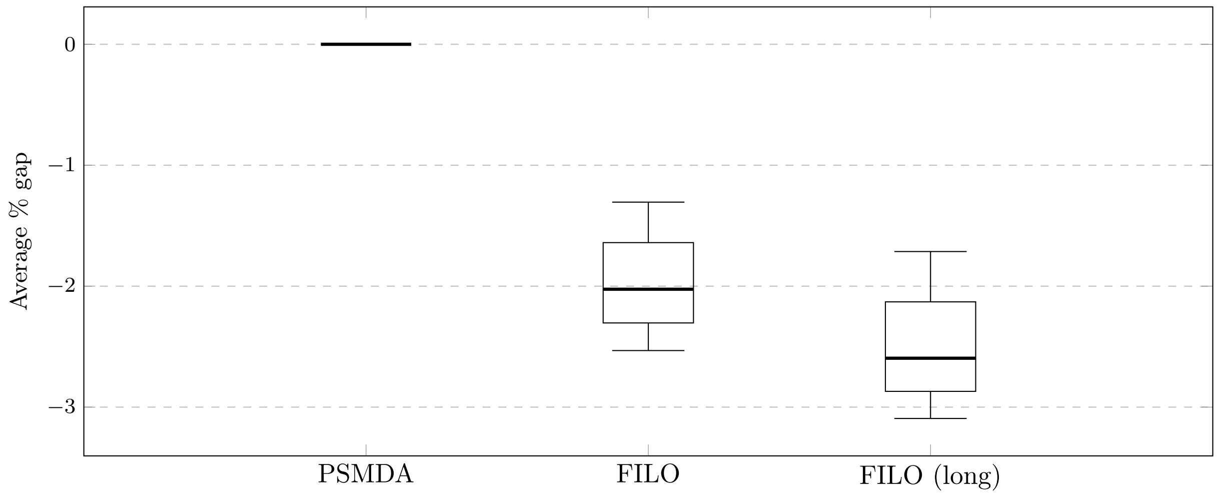

Figure 22 Comparison of average gaps obtained by algorithms on the $\mathbb{Z}$ dataset.

References

Accorsi L, Vigo D, 2020 *A hybrid metaheuristic for single truck and trailer routing problems. Transportation Science* 0(Available Online):null, URL `http://dx.doi.org/10.1287/trsc.2019.0943`.

Arnold F, Gendreau M, Sörensen K, 2019 *Efficiently solving very large-scale routing problems. Computers & Operations Research* 107:32 – 42, URL `http://dx.doi.org/10.1016/j.cor.2019.03.006`.

Arnold F, Sörensen K, 2019 *Knowledge-guided local search for the vehicle routing problem. Computers & Operations Research* 105:32 – 46, URL `http://dx.doi.org/10.1016/j.cor.2019.01.002`.

Beek O, Raa B, Dullaert W, Vigo D, 2018 *An efficient implementation of a static move descriptor-based local search heuristic. Computers & Operations Research* 94:1 – 10, URL `http://dx.doi.org/https://doi.org/10.1016/j.cor.2018.01.006`.

Bergstra J, Bengio Y, 2012 *Random search for hyper-parameter optimization. Journal of Machine Learning Research* 13(10):281–305, URL `http://jmlr.org/papers/v13/bergstra12a.html`.

Christiaens J, Vanden Berghe G, 2020 *Slack induction by string removals for vehicle routing problems. Transportation Science* 54(2):417–433, URL `http://dx.doi.org/10.1287/trsc.2019.0914`.

Clarke G, Wright JW, 1964 *Scheduling of vehicles from a central depot to a number of delivery points. Operations Research* 12(4):568–581, URL `http://dx.doi.org/10.1287/opre.12.4.568`.

CVRPLIB, 2020 *Capacitated vehicle routing problem library.* URL `http://vrp.galgos.inf.puc-rio.br/index.php/en/`, visited on 2020-07-19.

Duarte A, Sánchez-Oro J, Mladenović N, Todosijević R, 2018 *Variable Neighborhood Descent*, 341–367 (Cham: Springer International Publishing), ISBN 978-3-319-07124-4, URL `http://dx.doi.org/10.1007/978-3-319-07124-4_9`.

Dunn OJ, 1961 *Multiple comparisons among means. Journal of the American Statistical Association* 56(293):52–64, URL `http://www.jstor.org/stable/2282330`.

Etiemble D, 2018 *45-year cpu evolution: one law and two equations.*

Frank E, Hall MA, Witten IH, 2016 *The WEKA Workbench. Online Appendix for "Data Mining: Practical Machine Learning Tools and Techniques"* (Morgan Kaufmann), 4 edition.

Glover F, 1989 *Tabu search—part i. ORSA Journal on Computing* 1(3):190–206, URL `http://dx.doi.org/10.1287/ijoc.1.3.190`.

Glover F, 1996 *Ejection chains, reference structures and alternating path methods for traveling salesman problems. Discrete Applied Mathematics* 65(1):223 – 253, URL `http://dx.doi.org/10.1016/0166-218X(94)00037-E`, first International Colloquium on Graphs and Optimization.

Helsgaun K, 2017 *An Extension of the Lin-Kernighan-Helsgaun TSP Solver for Constrained Traveling Salesman and Vehicle Routing Problems: Technical report* (Roskilde Universitet).

Irnich S, Funke B, Grünert T, 2006 *Sequential search and its application to vehicle-routing problems. Computers & Operations Research* 33(8):2405 – 2429, URL `http://dx.doi.org/10.1016/j.cor.2005.02.020`.

Johnson DS, 1999 *A theoretician's guide to the experimental analysis of algorithms. Data Structures, Near Neighbor Searches, and Methodology.*

Kirkpatrick S, Gelatt CD, Vecchi MP, 1983 *Optimization by simulated annealing. Science* 220(4598):671–680, URL `http://dx.doi.org/10.1126/science.220.4598.671`.

Kytöjoki J, Nuortio T, Bräysy O, Gendreau M, 2007 *An efficient variable neighborhood search heuristic for very large scale vehicle routing problems. Computers & Operations Research* 34(9):2743 – 2757, URL `http://dx.doi.org/10.1016/j.cor.2005.10.010`.

Lourenço HR, Martin OC, Stützle T, 2003 *Iterated Local Search*, 320–353 (Boston, MA: Springer US), ISBN 978-0-306-48056-0, URL `http://dx.doi.org/10.1007/0-306-48056-5_11`.

Martello S, Toth P, 1990 *Knapsack Problems: Algorithms and Computer Implementations* (USA: John Wiley & Sons, Inc.), ISBN 0471924202.

Matsumoto M, Nishimura T, 1998 *Mersenne twister: A 623-dimensionally equidistributed uniform pseudo-random number generator. ACM Trans. Model. Comput. Simul.* 8(1):3–30, URL `http://dx.doi.org/10.1145/272991.272995`.

Mladenović N, Hansen P, 1997 *Variable neighborhood search. Computers & Operations Research* 24(11):1097 – 1100, URL `http://dx.doi.org/https://doi.org/10.1016/S0305-0548(97)00031-2`.

PassMark® Software, 2020 *Professional cpu benchmarks.* URL `https://www.passmark.com/index.html`, visited on 2020-07-19.

R Core Team, 2020 *R: A Language and Environment for Statistical Computing.* R Foundation for Statistical Computing, Vienna, Austria, URL `https://www.R-project.org/`.

Reinelt G, Rinaldi G, 1994 *The traveling salesman problem.*

Schneider M, Schwahn F, Vigo D, 2017 *Designing granular solution methods for routing problems with time windows. European Journal of Operational Research* 263(2):493–509, URL `http://dx.doi.org/10.1016/j.ejor.2017.04.059`.

Schrimpf G, Schneider J, Stamm-Wilbrandt H, Dueck G, 2000 *Record breaking optimization results using the ruin and recreate principle. J. Comput. Phys.* 159(2):139–171, URL `http://dx.doi.org/10.1006/jcph.1999.6413`.

Subramanian A, Uchoa E, Ochi LS, 2013 *A hybrid algorithm for a class of vehicle routing problems. Computers & OR* 40(10):2519 – 2531, URL `http://dx.doi.org/10.1016/j.cor.2013.01.013`.

Taillard É, Badeau P, Gendreau M, Guertin F, Potvin JY, 1997 *A tabu search heuristic for the vehicle routing problem with soft time windows. Transportation Science* 31(2):170–186, URL `http://dx.doi.org/10.1287/trsc.31.2.170`.

Toth P, Vigo D, 2003 *The granular tabu search and its application to the vehicle-routing problem. INFORMS Journal on Computing* 15(4):333–346, URL `http://dx.doi.org/10.1287/ijoc.15.4.333.24890`.

Uchoa E, Pecin D, Pessoa A, Poggi M, Vidal T, Subramanian A, 2017 *New benchmark instances for the capacitated vehicle routing problem. European Journal of Operational Research* 257(3):845 – 858, URL `http://dx.doi.org/10.1016/j.ejor.2016.08.012`.

Vidal T, Crainic TG, Gendreau M, Lahrichi N, Rei W, 2012 *A hybrid genetic algorithm for multidepot and periodic vehicle routing problems. Operations Research* 60(3):611–624, URL `http://dx.doi.org/10.1287/opre.1120.1048`.

Voudouris C, Tsang E, 1999 *Guided local search and its application to the traveling salesman problem. European Journal of Operational Research* 113(2):469 – 499, URL `http://dx.doi.org/10.1016/S0377-2217(98)00099-X`.

Wilcoxon F, 1945 *Individual comparisons by ranking methods. Biometrics Bulletin* 1(6):80–83, URL `http://www.jstor.org/stable/3001968`.

Zachariadis EE, Kiranoudis CT, 2010 *A strategy for reducing the computational complexity of local search-based methods for the vehicle routing problem. Comput. Oper. Res.* 37(12):2089–2105, URL `http://dx.doi.org/10.1016/j.cor.2010.02.009`.